The oceanographic tower *Acqua Alta*: more than a quarter of a century of activity

L. CAVALERI (*)
Istituto Studio Dinamica Grandi Masse - S. Polo 1364, Venezia, Italy

(ricevuto il 3 Giugno 1998; approvato il 21 Luglio 1998)

Summary. — This paper summarizes the relevant research activities that have been carried out on board of the oceanographic tower during more than a quarter of a century of its active life. There is no special event that has triggered this paper, but the conviction that the amount of researches and results, still already published in the specialized magazines, deserves a summarizing and compact presentation. In this way it is possible to appreciate the frequent interaction among the different branches of the marine researches, and to realize how a single relevant result is always the final product of a large number of previous advances. Still with a predominance of the physical aspect, the paper covers many subjects of the marine research, moving from biology and chemistry to the physics of the atmosphere and the ocean. The location of the tower is in the Adriatic Sea, 15 km off the coast of the Venice lagoon. The limited depth (16 m) excludes any consideration of the deep water processes in the oceans, but provides the rare possibility of combining fundamental research and intensive practical applications of the obtained results. Expectably, the presence of Venice, prime reason for the existence of the tower, has been a catalyst in this direction.

PACS 92.10.Hm – Surface waves, tides and sea level.

1. – Introduction

The history of Venice has been a continuous interaction with the sea and with its never ending activity. It has been a story of love, the town taking full advantage of its position to expand its power, and also a story of fight, because of the permanent menace of disruption of the fragile environment in which Venice is located. The most widely known problem, the periodic floods due to storm surges in the Northern Adriatic Sea, has been enhanced during this century by the steadily rising sea level and by the now halted sinking of the town due to human activities. A full account of the problem is found in Ansa Dossier (1996).

The big flood of November 1966 triggered a wave of global interest and the founding of the Istituto per lo Studio della Dinamica delle Grandi Masse (ISDGM,

(*) E-mail: gigi@isdgm.ve.cnr.it

literally Institute for the Study of the Dynamics of Large Masses), of the Italian National Research Council, with the aim of studying the hydraulic and geological problems of the area. The best symbol of the institute is the oceanographic tower that was soon acquired for open sea measurements. Located 15 km off the coast, it represents well the interaction with nature, fighting for survival in the harsh open sea environment, but blending with it for continuous and extensive measurement campaigns.

Today, after more than 25 years of continuous and growing activity, it is worthwhile to frame the situation, summarizing the results so far obtained, listing the present activities and the prospects for the immediate future.

The on board measurements and campaigns cover many aspects of meteorology and oceanography, that are dealt with in different sections. First (sect. **2**) I provide the base for the following discussion with a compact description of the tower, of its mechanical structure, and of the related logistics. The on board instruments are described in sect. **3**. We turn then to practical results. In sect. **4** I briefly list the subjects and how they are dealt with. Section **5** is devoted to biology, sect. **6** to the carbon cycle in the water column, sect. **7** to the atmosphere, sect. **8** to wind, an obvious focus of interest. The two following sections cover two subjects of strong relevance, namely tides and surges, and wind waves. Section **11** is devoted to sediment transport, sect. **12** to remote sensing, a subject of ever growing interest. In sect. **13** I describe the main ongoing activities. The final section **14** provides information on the management of the tower. In this respect I will be extremely grateful to anyone who, on the base of a similar experience or simple intuition, will provide useful comments and suggestions.

2. – The oceanographic tower

The tower was designed and put into position free of charge by Micoperi, a very qualified company in the field of offshore structures. Its position is shown in fig. 1. It is

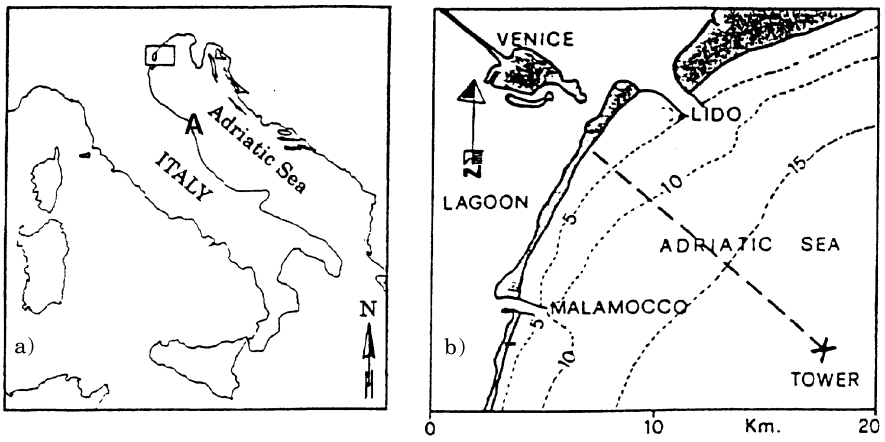

Fig. 1. – a) The Adriatic Sea. Its dimensions are about 700×200 km^2. The small rectangle marks the area enlarged in b). A indicates the position of Ancona. The tower is about 15 km off the coast. Three inlets connect the sea with the lagoon, Lido, Malamocco and Chioggia, the southernest one, not shown in the figure.

located 15 km off the coast of the Venice lagoon. The local depth is 16 m. The isobaths are more or less parallel to the coast, with an average transversal gradient of 1/1000. The bottom is a mixture of sand and silt. According to the hydrographic maps available at the time of construction, the tower should have been on the top of a sand bank. However, when putting the tower into position, we soon discovered that sand banks are a rather erratic feature of the bottom. As a consequence, the upper structure is two metres closer to the sea surface than originally planned. While this has made practically not usable the first floor (see below for a more detailed description), it turned out, with later experience, to be a very positive fact, because the flat bottom in the immediate neighbouring area avoids unwanted local modifications of the undisturbed sea conditions.

The tower is basically composed of two parts, the submerged part, with limited protrusion above the surface, designed to stand the violence of the sea, and the upper working and living quarters. The submerged part, called template, is basically composed of four 0.60 m diameter, almost vertical, steel cyclinders, converging upwards, 12.5 mm thick, about 20 m long, connected by an intricate system of smaller tubes to make a very rigid and solid structure. Figure 2 provides a side view of the tower. The four cylinders are located at the corners of a square, its side slowly increasing with depth (5 m at the top end, 7.3 m at the bottom).

Once the template was placed into position, four smaller cylinders were sliced inside the larger ones and hammered for 22 m into the bottom. The space between each couple of cylinders was then filled with liquid concrete, and the two cylinders welded together at the upper end. The protruding sections of the inner cylinders were then cut at their upper level, to act as horizontal support for the upper section, then firmly welded to the template.

An overall view of the tower is given in fig 3. The upper structure is made of three floors and a terrace. The lower floor, only 4.2 m off the sea surface for the reason explained above, is too often smashed by waves to be of any use for long-term activity. Apart from hosting some instruments, it acts mainly as deposit of well tied carpentry material.

About two metres above, the second floor hosts the power generators, a small workshop and the battery compartment. The third floor, 9.3 m off the sea surface, hosts the living quarters, made of a $4.8 \times 4.8\ m^2$ living room, including a $1 \times 2\ m^2$ bathroom, plus a $3 \times 2\ m^2$ kitchen and a $2 \times 2\ m^2$ instrument room. Both the second and the third floor are surrounded by a 1.3 m wide walking platform.

The four corners of the tower point to the four cardinal points. Two horizontal extensions protrude from the South-East and North-East sides, used to deploy instruments away from the basic frame. The North-East extension hosts also a laboratory.

The upper terrace, 12.3 m off the surface, spans $5 \times 7\ m^2$, plus a 1.3 m extension of three of its four sides. A $3\ m^3$ water container stands at its centre. An 8 m long lowerable meteorological mast is located at the South corner. A wind power generator is located at the opposite corner. The West corner has been expanded into a $3 \times 3\ m^2$ platform in connection with the calibration of the ERS-1 altimeter (ESA, 1993).

Close to the sea surface, two horizontal $2 \times 1\ m^2$ platforms, at different heights, on both the North-West and South-West side, allow disembarkement also with relatively rough sea. The access to the first floor is by ladder, while all the other floors are connected by stairs.

Protection against the corrosion of the submerged part is obtained with sacrificial anods welded to the submerged template. Distributed with an average distance of 5-6 m,

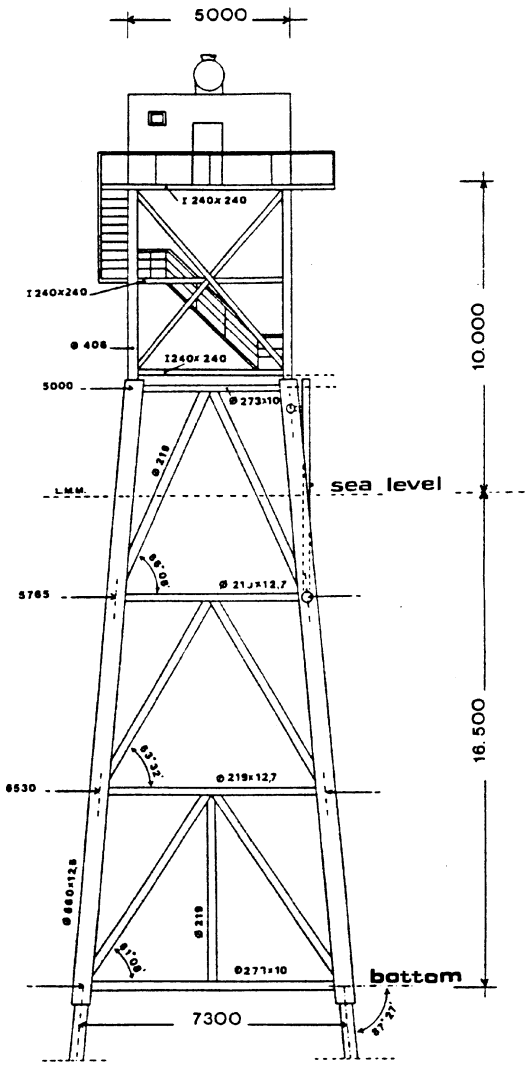

Fig. 2. – The original basic structure of the oceanographic tower. The poles penetrate for 22 m into the bottom.

they have given very positive results. A recent inspection has revealed lack of corrosion also at the connections between the different tubes, the most crucial part of the structure. The corrosion can be very active in the splashing zone because of the continuous presence of oxygen due to breaking waves and exposure to atmosphere. In this area an effective protection has been achieved covering the sand blasted surfaces with an epoxy resin. Direct inspection has recently revealed the underlying surface as shiny as 25 years ago.

The electrical system includes two power generators, 30 and 15 kVA, respectively, with energy supply at 380, 220 and 125 VAC (50 Hz). The generators are encased within fully sound proof covers. A large battery storage (3000 Ah) provides 12 and 24 VDC.

Fig. 3. – The oceanographic tower "*Acqua Alta*" seen from the South.

Goods, up to 500 kg, are lifted on board by means of two electrical winches. However, when the sea is rough and at least for light items, we have found it preferable to act by hand.

The tower can host up to five persons, including one or two responsible persons, for an unlimited period of time. A larger number is acceptable during the day.

3. – Instruments

An overall view of the tower is given in fig. 3. On describing the on board instruments, it is convenient to distinguish between the permanent and the temporary ones. Permanent are the instruments that are or have been continuously at work, independent of any specific campaign. The temporary ones are connected to specific projects.

The basic set includes a full meteorological station with the addition of some marine instruments. The measured quantities include:

- wind (speed and direction),
- solar radiation,
- humidity,
- air temperature,
- rain,
- water temperature (two levels),
- tide,
- wind waves.

The station has been working since 1992. Initiated as a cooperative effort between the institute and ENEL (the Italian National Electricity Company), it passed in 1997 under the responsibility of ISDGM. Since 1998 it has been handled together with the Istituto Idrografico e Mareografico (Hydrographic and Tidal Institute) of Venice, a branch of Servizi Tecnici Nazionali (National Technical Services). The data are recorded on board with different sampling rate, according to the parameters. They are displayed on board and transmitted to land by modem for permanent recording. The wave signal is taken from a parallel independent system that stores on board the output of three pressure transducers placed on three legs of the tower. This system has been operational since 1978.

An old fashion propeller anemometer, with continuous graphic recording, is the best source of information for guessing the immediate weather changes. Also, as better explained in subsect. 8˙4, it provides quite a bit of information on the turbulence of the surface boundary layer.

Two tide gauges are installed on the tower. Both are of the conventional well type, even if with different filtering characteristics (see subsect. **9**˙1).

Besides the instruments connected to the activities of the institute, the tower hosts, under contract, also a number of instruments belonging to other organizations. Consorzio Venezia Nuova, the consortium in charge of designing the planned barrages at the inlets of the lagoon and of the main maritime works in the area, runs its own meteo-oceanographic station. The Centro Previsioni e Segnalazioni Maree (the Tidal Forecast and Warning Centre) of the Venetian authority records and telemeters to land in real time data about wind and tide.

Temporary instruments, too many to be listed, are implicitly mentioned in the following sections along with the obtained results.

4. – Presentation of results

In the following sections I describe the main activities that have been carried out on board and the related results. As mentioned in the previous section, apart from the permanent ones, a large variety of temporary instruments has been used for the different researches. Where necessary, they are briefly described in the relevant section.

This paper covers only a part of all the measurements carried out on board. Activities of pure local interest and without a technical significance have been ignored. The focus is on results and conclusions that are relevant for the area and/or of interest for other researches.

The detailed splitting of the subjects in sections and subsections is:

1. Introduction
2. The oceanographic tower
3. Instruments
4. Presentation of results
5. Biology
   5·1. Fouling
      5·1.1. Distribution of size
      5·1.2. Influence of depth and support material
      5·1.3. Pollution
   5·2. Benthos
6. Carbon cycle and particulate flux in the water column
7. Atmosphere
   7·1. Local circulation
   7·2. CO_2 air-sea exchange
   7·3. Trend analysis of wet deposition samples
8. Wind
   8·1. Sea climatology from coastal stations
   8·2. Validation of meteorological models
   8·3. Extreme and climatological analysis
   8·4. Gustiness
9. Tides and surges
   9·1. A fast response tide gauge
   9·2. Storm surge modelling
   9·3. Set-up
10. Wind waves
   10·1. Long-term measurements
   10·2. Wave kinematics
      10·2.1. Attenuation with depth
      10·2.2. Reynolds stresses
   10·3. Measurement of directional spectra
   10·4. White capping
   10·5. Long-term hindcast
   10·6. Extreme wave heights in the Northern Adriatic Sea
   10·7. Coupled models
   10·8. Calibration of ECMWF wind
   10·9. Bottom friction
   10·10. Wind gustiness—effects on ocean modelling
   10·11. Refraction modelling
      10·11.1. VENICE—a ray wave model
      10·11.2. Wave refraction in front of the Venetian littoral
   10·12. Evaluation of the wave conditions at the coast
      10·12.1. Sensitivity of the wave conditions to the different physical processes
      10·12.2. Nonlinear shoaling
   10.13. Design wave height at the barrages of the lagoon
      10·13.1. Short waves
      10·13.2. Long waves
   10·14. Wave forecast in the Adriatic Sea
11. Sediment transport
   11·1. Coastal transport

12. Remote sensing
12·1. The calibration of optical measurements
12·2. The calibration of the ERS-1 radar altimeter
12·2.1. The tower position
12·2.2. The absolute calibration
12·3. Wind measurement by scatterometer
12·4. Surface stresses derived from SAR images
13. Ongoing activities
14. Management
Acknowledgements
References

In the interdisciplinary science of the sea it is not possible to split neatly the various researches among the different official branches. Many, if not most, researches imply different know-how and their results are of interest to different fields. In the following each result is discussed in the relevant section. If the whole cannot be logically splitted, it is dealt with in the section of the dominant subject.

5. – Biology

5·1. *Fouling.* – Marine fouling is a serious problem for marine instruments. However, it can be, expecially mussels, a wealth for biologists. Mussels, the most common sessile marine organism on the submerged structures in the temperate seas, are extremely sensitive to the characteristics of the environment and, as such, very good indicators of its quality.

The tower was put into position in March 1970. The first biological settling took place almost immediately, and by the following summer fouling was actively growing on all the submerged surfaces (including instruments). The Northern Adriatic Sea, and in particular the area around the tower, is relatively shallow (see fig. 1), and consequently very sensitive to the variations of temperature of the atmosphere. While the temperature of the upper layers of the northern part varies between 13 °C in winter and 23 °C in summer (see, *e.g.*, Malanotte Rizzoli and Bergamasco, 1983), close to coast the variations are larger because of the shallower water, hence of the reduced thermal capacity. At the tower the temperature drops to 5 °C in winter and raises to 24 °C in summer. The consequences are an evident yearly cycle in the local marine life, the growth being concentrated between March, when the settling of the new elements takes place, till October or November, depending on the season. After an initial faster growth, the average rate is between 1 and 2 cm per year.

Apart from their growing on all the available surfaces, the mussels create another indirect problem. The tower is not permanently manned, the percentage of working days on board being presently close to 50% (including holidays). When the tower is empty of persons and the mussels are grown enough, the fishermen active in the area come and harvest them. Unluckily, they use very effective, but rudimentary, methods that cause also a complete smash of the instruments eventually clamped to the submerged tower elements.

5·1.1. Distribution of size. With the settling of the larvae in spring and with a clear yearly cycle, the distribution of size in the mussel population shows well defined peaks, corresponding to the average growth rate and to the period of establishment

(Dalla Venezia, 1976, 1979, 1981). The size is found to vary with depth (the dominant factor) and with the orientation of the supporting surface. It increases moving downwards from the sea surface, reaching a maximum at about nine metres of depth. The smaller size in the upper few metres is associated to the exposure to breaking waves and frequent harvesting by occasional divers. With increasing depth the mussels must compete with other species for survival, particularly oysters.

The presence of mussels stops at 12–14 m of depth, just off the bottom. This is associated to a permanent layer of cold water, the thermocline never lowering below this depth. Because its maximum depth increases with the bottom depth, the lowest layer at which mussels are found varies from place to place, according of course also to the local environmental conditions. About 100 km to the South, where several gas extraction rigs are located and the depth is 30 m, the mussels are found well below the 20 m line.

The sensitivity to the conditions of the environment, together with their abundance and relatively fast growth rate, makes the mussels very good indicators of the history of recent past (order of years). Mussels retrieved in 1978 from an artificial submerged barrier in front of Ancona (Dalla Venezia, 1979; see fig. 1 for its location), with a local depth comparable to that at the tower, showed clearly a two year old frequency peak in their distribution, while there was no trace of settling in the two following springs. This was not the case at the tower. While a detailed analysis was not carried out, this result indicates that in 1977 and 1978 the conditions off Ancona were not favourable to new settlings. Specific reasons may be traced back to oceanographic conditions or pollution level (see the next section for related sensitivity of mussels). The area of Ancona, South of the Po exit, the major Italian river, can be strongly affected by the river outflow. The details of the local circulation (see Malanotte Rizzoli and Bergamasco, 1983) depend on several factors, including the distribution of salinity and temperature in the sea, the volume and temperature of the outflow and the overall meteorological conditions. Accordingly, the conditions at the coast vary substantially, depending on the Po water flowing outside, off the coast, or bending clockwise, bordering the coast while moving South. Whichever the specific cause, it is clear that mussels, and fouling in general, can act as reliable indicators of the recent history of the environment.

5·1.2. Influence of depth and support material. An extensive experiment was carried out to quantify the settling time of fouling and the dependence on depth of its characteristics (Montanari *et al.*, 1991). Three series of panels, each held by a suitable steel frame, were placed and firmly blocked at three different depths on the South-West side of the tower. The upper panel was just below the surface, the second at 6.5 m, the third one at 12.3 m of depth. On each frame 16 panels of fiber-cement ($30 \times 30 \times 0.4$ cm) were left into position for 3, 6, 9 and 12 months. The aim was to quantify the growing rate for later comparison with anti-fouling experiments, for commercial purposes and for similar problems on the legs of the many gas extraction rigs in the area in front of Ravenna, about 100 km South of Venice.

Notwithstanding the limited differences, substantially different results were found at the different depths. Close to the surface and on the intermediate panels, after 12 months mussels (*Mytilus galloprovincialis*) dominate the local fouling population. However, this situation is reached via different paths. At the surface the first colonists are algae and barnacles (*Balanus amphitrite*), then larger barnacles and small mussels, the latter ones taking over after the ninth month. At 6.5 m of depth the first

settlement is by serpulids (mainly *Pomatoceros Triquetor*). The bivalves step in only after the sixth month, to dominate the local population at the end of the first year.

The situation changes approaching the bottom, *i.e.* the cold water below the thermocline. With the gradual warming of the upper layers in spring, the thermocline gradually moves from the surface downwards. Many years of diving have shown that the depth reached along the season varies, as expected, in connection with the outer climate. In any case, the closer to bottom is the support surface, the less the local fouling is exposed to relatively warm temperatures, and the less is consequently its growing. Because serpulids are better fit for lower temperatures, they dominate the population on the 12.3 m panel, mussels being present only with a small size limited population.

Given the above, and the fact that the depth of the thermocline varies from place to place, in connection also with the local bathymetry, it is not surprising that the characteristics and distribution of fouling show similar variations.

The support surface affects the colonization with its mechanical (rough, shiny, etc.) and chemical characteristics. Shiny, very smooth surfaces oppose the colonization by bivalves. However, this is only delayed, as in a short while barnacles and serpulids provide a convenient substratum for the following mussels.

Also antifouling painting is not a complete deterrent. Sacrificial elements, that die on the poisoning surface, provide nevertheless in due time a sufficient substratum for a following active population. The advantage is that a thick cover of fouling is reached in longer times, with a consequent economic advantage if a periodic cleaning is required.

The only submerged part of the tower really free of mussels are the sacrificial anods (see subsect. 5·2). Apart from any chemical consideration, the gradual peeling of the surface due to corrosion excludes any possibility of colonization.

5·1.3. Pollution. In contrast to vertebrates, which possess enzymes capable to metabolize hydrocarbons, bivalves do not metabolize significant quantities of these compounds (Lee *et al.*, 1972a, b; Burns, 1976), and therefore they act as accumulators. Turning this negative fact into a useful tool, bivalves, and more commonly mussels, are used as pollution indicators, expecially when, as in the case of the Venice lagoon, there is a reference station close by, the tower, where water is comparatively clean.

In a series of papers (Fossato and Siviero, 1974; Fossato and Dolci, 1976, 1977; Fossato *et al.*, 1979; Nasci *et al.*, 1989) the level of pollution by aliphatic hydrocarbons and polycyclic aromatic hydrocarbons (PAH, a large class containing numerous compounds having carcinogenic properties) has been studied by comparing the pollution content of mussels sampled throughout the year from different zones of the lagoon and from the tower.

Focusing, in particular, on 3,4-benzopyrene (BaP) and perylene (Pe), for which a relatively simple method of analysis exists, the highest concentrations have been found close to the actual sources, namely the industrial area, the town of Venice and the fishing harbour of Chioggia, at the southern end of the lagoon. Values of dry weight (see Fossato *et al.*, 1979, for the technical details) as high as 327 μg/kg for BaP and 71 μg/kg for Pe were measured, compared to minimal values of 12.0 and 1.5 respectively. Note that these values should not be considered as representative of not polluted conditions, because of the local redistribution by wind, current, tides and waves to adjacent areas.

As expected, the level of contamination decreases steadily with the distance from the sources. The aliphatic pollution is more probably of anthropogenic origin, whereas

Bap and Pe contamination are likely derived from the combustion of fossil fuels and other organic material.

To estimate the limits of such a monitoring scheme, it is essential to know how rapidly the mussels respond to a change in the environmental level of pollution. An interesting study along this line has been carried out by Tiozzo (1998), who has analysed the reaction of mussels to a variation in the concentration of heavy metals. Using as reference mussels from the ISDGM tower, Tiozzo has at first studied the content of metals by analysing samples from the interior of the lagoon, at the border of the channel leading to the industrial area, and from one of the exits to the sea. The elements analysed include Mn, Fe, Zn, Cu, Cr, Pb. Expectably, for most metals higher concentrations have been found inside the lagoon, closer to their respective sources. No significant difference has been found for Cr and Zn between the three sample locations. Note that Cu and Cd are more scarce in areas characterized by strong hydrodynamical activity (*e.g.* the three entrances to the lagoon), because their presence is associated to very small particles, easily kept in suspension by an energetic current.

After determining the original characteristics, a representative sample of the mussels from the tower, including elements of different sizes, hence ages, was transplanted inside the lagoon and monitored for three months. Using a careful statistical analysis, Tiozzo (1998) was able to isolate the consequences associated to the different metal contents from other factors, the main one being the age of the mussels, and their consequently different methabolic level.

All the transplanted mussels showed a drastic increase of their rate of growth, likely associated to the larger amount of food available. Apart from this, for all the metals with a higher content inside the lagoon, there was an expected increase within the mussel tissues, also when normalized with respect to the size of the animal. However, the content c reached after two months was higher than c_0, the level found in the residual elements. During the third month c started decreasing, gradually approaching the equilibrium level. The overshoot was present also for the metals, like Cr and Zn, for which the c at the tower equals the c_0 at the location inside the lagoon.

The explanation is likely associated to the different eutrophic and pollution levels in the two environments. Moved to an area, the lagoon, with a larger availability of metals and food, the mussels seem to increase so much their rate of accumulation, that they overshoot the equilibrium level, before slowing down and returning gradually to c_0. Note, however, that the response time seems to depend not only on the kind of pollutant, but also on the local physical conditions. In a direct experiment Dunn and Stich (1976) reported a biological half-life of more than two weeks that, together with the above results, justifies the seasonal cycle found for the content of some pollutants in the tissues of mussels (the maxima for BaP and Pe occur in January, the minima in May and July). At the same time, working in cold water, hence at a lower level of biological activity, Riget *et al.* (1997) reported a response time up to one or two years. In this case the approach to the equilibrium is likely to be simply asymptotic, without any overshoot.

Dalla Venezia *et al.* (1982) found that the mussels survive well in an environment with salinity between 20 and 50%. Limited shifts below or above these limits cause an immediate drastic decay of the population.

The traditional approach described above considers mussels as indicators of the pollution level in a given environment. More recently, the need has arisen for the evaluation of the possible biological impact. This has led to the development of tecniques, defined as stress- or biomarkers, to measure the changes and the eventual

damages in the different organisms at the biochemical, histochemical and physiological level, as derived from the exposure to xenobiotices. The enzymatic and citological methods have proven particularly promising. In this respect the definition of different indices of stress that can objectively be derived from the analysis of the organisms is noteworthy. In all these studies the mussels from the tower act as references elements for clean water. Reference works on this subjects are Dalla Venezia *et al.* (1994), Livingstone *et al.* (1995), Pipe *et al.* (1995), Widdows and Nasci (1998).

5·2. *Benthos.* – Benthos, the biota living at direct contact with the sea bottom, is interesting not only for the dynamical interaction with the above column of water, but also, and probably more, for the marine life that develops in it. Out of the extreme variety that we find in this environment, the tiny foraminifera, the one-cellular protozoans with a mainly calcareous test, deserve particular attention for a unique characteristic. Small enough not to be destroyed by the continuous action of the above water before being imbedded in the lower bottom layers, they retain in themselves a tremendous amount of information about the environment in which they lived. Taking advantage of their abundance in the world, they are the most widely used fossils to obtain information about the marine paleoenvironment they lived in. For this reason during the last thirty or fourty years much effort has been addressed to establish which of the various marine parameters are most effective in determining their distribution.

In the early stages much attention was given to depth, developing the concept of isobathial species. In the 1970s the characteristics of the water masses, as salinity, temperature, nutrients, etc., were believed to be the dominant factor, while in the 1980s the attention was focused on the overall availability of "food" connected to their biological productivity.

The availability of the tower in the middle of an environment suitable for their growth offers the possibility of exploiting this information. In this subsection I report an attempt to find a relationship between their characteristics and those of the environment in which they live.

To obtain direct evidence of the relationship between the benthic foraminifera and the characteristics of the water masses interacting with them, a long-term research has been undertaken by Morisieri (1997). During the period from February 1991 to January 1995 a sequence of measurement campaigns, one every two months, was done on the oceanographic tower. Each campaign lasted 48 hours (four tidal cycles). Beside collecting a sample of the bottom sediments, a number of marine parameters were measured at frequent intervals. These included water salinity, conductivity, temperature, oxygen content, redox potential and *p*H. Water samples taken close to the bottom were analysed for their content of iron, organic carbon, solphates, clorurs, orthophosphates, nitrates. The duration of four tidal cycles aimed at averaging out the eventual influence of the tidal phase on the measured parameters.

After the collection, the sediments were treated with Rose Bengal to highlight the presence of protoplasm, then washed and treated with carbon tetraclorur to separate the organic and lithic components. The obtained condensed matter was fully analysed for living foraminifera (64 species were recognized), while for total assemblage a microsplitter was used to obtain sample fraction with at least one thousand individuals (88 species recognized). The content of living foraminifera in the 25 samples varied from 26 to 257 individuals.

The, still preliminary, analysis of this large data set has provided clear evidence of an irregular seasonality (see fig. 4). The key factor conditioning the characteristics of

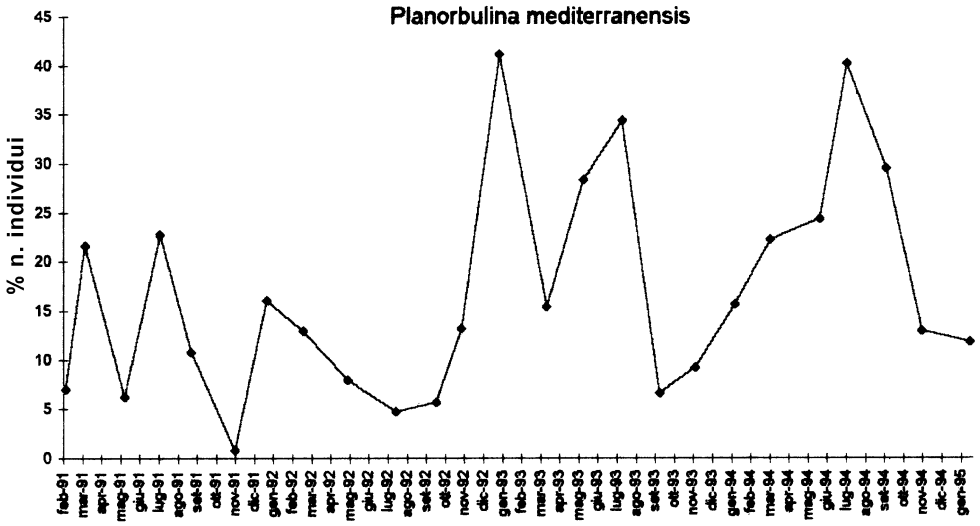

Fig. 4. – Percentage of *Planorbulina mediterranensis* in living foraminifera. Period from February 1991 to January 1995 (after Morisieri, 1997).

the benthic foraminifera seems to be the availability of nutrients. An interesting aspect has been the evidence for survival competition between different species.

6. – Carbon cycle and particulate flux in the water column

Organic carbon is a strong index of the biological activity in the sea, and it is therefore of interest to quantify its cycle in an area. The Northern Adriatic Sea is characterized by enhanced biological activity, due to its hydrological features and the extended river runoff. Besides, the limited depth (see fig. 1) and the ample variations in thermal conditions lead to strong local variations.

An important fraction of the organic carbon content is associated to the suspended phase. Therefore, a method for monitoring its spatial and temporal distribution is by means of sediment traps, that collect the downward vertical flux of particulate, and by a periodic retrieval with subsequent analysis in the laboratory. A full description of the methodology is given by Giani *et al.* (1998).

Sediment traps have been used in the past in the Northern Adriatic Sea, placed at different well chosen locations, so as to monitor different conditions, depending on the various factors that affect both the carbon distribution and the sediment flux. Boldrin (1998) gives a full account of the measurements and the related results.

The particulate organic carbon derives basically from three different sources: the local biological production, advection of water with different characteristics, and the resuspension of bottom sediment fine fractions by hydraulic forcing.

Granted an horizontal spatial diversity, at each location there is also a marked variability in carbon content along the vertical. Typically, higher concentrations are found in the upper layers where the productivity processes are more active. Lower concentrations in the lower layers are justified by the biological consumption along the water column, at its maximum during the active summer months.

This typical distribution is strongly affected, certainly in quantitative terms, by the hydrological factors mentioned above. Strong outflow from close-by rivers, particularly just after a period of heavy rain, brings with it large contents of sediments and carbon associated with them (particulate organic carbon, POC). The less saline, hence lighter, riverine waters flow in the upper layers, modifying the local characteristics. In the Northern Adriatic Sea (see fig. 1a) the by far major source is the Po River, whose discharge in fall can increase up to $3000\ m^3/s$. In these conditions the POC concentration in the diluted coastal waters can be down to 15% of the annual average concentration found in the river itself ($200 \pm 100\ \mu mol/dm^3$ in the lower Po). At the same time the suspended matter is enriched in the organic carbon fraction with respect to the river water, indicating the important contribution of marine organic carbon production, especially in surface water.

The stratification of the marine waters is one of the most effective causes of the diversification of the biological production along the vertical. Apart from areas affected by river outflows, there is a strong periodic stratification connected to the yearly thermal cycle. In winter the cooling of the upper layer leads to a general mixing of the water column, favoured also by the frequent and violent storms that affect the area. During spring and throughout summer the warming at the sea surface produces a warm layer of increasing depth, down to a few metres off the bottom in the coastal area, and down to 15-20 m in the more offshore zone, where the depth goes up to 25-30 m. This stratification is very effective and highly stable, strongly conditioning the vertical distribution of the biological activity, and consequently the carbon content, with higher production in the warm upper layers.

The stratification affects the biological activity also through the oxygen content. In the summer months the cold bottom layers, below the thermocline, are virtually cut off of any oxygen supply and the local life has to rely on the gradually diminishing local oxygen content, down to 20% of its saturation value. In some extreme cases, when a prolonged calm season made the thermocline last till late November (1977 was a remarkable and dramatic case), the bottom layers were virtually devoided of oxygen, with a distributed death of the local fauna. These conditions persist till when the cooling of the surface and the first severe winter storm mix the water column, destroying the barrier of the thermocline.

Heavy waves at the surface imply an intense orbital motion also in the lower layers, hence a stirring and resuspension of the bottom sediments in the coastal waters (see subsect. **10**·2 and sect. **11**). In turn, this affects the transparency of the water column also well off the area of influence of the turbid river water. While the euphotic zone, defined as the one where the radiant flux is at least 1% of its surface value, normally extends till the bottom in the summer months, after the first winter storms the zone is limited to 10-15 m of depth.

Obviously, this affects the local biological activity and also the composition of the particulate. This is mainly clay, with an increasing percentage of carbonates while approaching the bottom. The latter is typically around 40%, but it can go up to 50% after a storm, approaching the 53% value that characterises the local sediments.

Following the above argument, it is obvious that the resuspension, redistribution and then the sedimentation of the particulate are strictly related to the meteo-oceanographic conditions that typify the area in a certain period. Figure 5 shows the time history of the total sediment flux, measured two metres off the bottom, at the oceanographic tower, where the depth is 16 m. The various peaks are concentrated in the winter months. The winter of 1993-94 is particularly remarkable for its strong

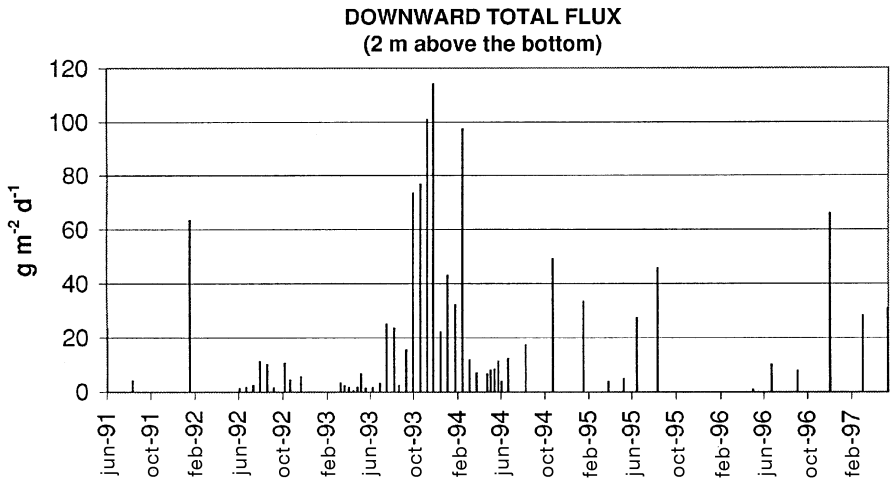

Fig. 5. – Total downward flux of suspended particulate, measured two metres off the bottom, at the oceanographic tower. See fig. 1 for its position (S. Rabitti, personal communication, 1998).

activity. It is interesting to relate fig. 5 with the time series of the wave conditions at the same location (the recording system is described in subsect. **10**˙1). There is a close relationship between the downward flux and the average wave energy in a certain period, even if the sparse sampling shown in fig. 5 impedes a case by case correspondence. It is worthwhile to point out that, even with the same wave height, different kinds of storms act in a different way on the bottom sediments. The long waves due to sirocco (a discussion on the local wave climatology is given in subsect. **10**˙5) are much more effective in stirring the bottom than the often higher, but shorter, bora waves. The sirocco waves can move the sediments down to a surprising depth. Evidence of wave action, supported by simple calculations, has been found down to 30 m of depth. Exceptional storms in the Northern Adriatic Sea are estimated to act effectively on the bottom till depths of 40 m.

The combined action of seasonality, river outflows and storms leads to a large variability of the vertical flux. Different time scales are present. The stirring of the bottom material is a practically immediate reaction to the forcing of the storm. The residence time of the suspended particles, once the forcing is over, varies with their size, from a few hours for the coarse size till the order of weeks for the very fine ones. The river outflow has a seasonal cycle associated to the melting of snow in the mountains and an irregular one linked to the occasional rainy periods, with a response time of the order of days and an extension of the same order of magnitude. Finally, we have the large seasonal thermal cycle with the formation of the thermocline.

All this implies, in a coastal area or a small enclosed basin as the Northern Adriatic Sea, a marked spatial and temporal variability of the content and production of organic carbon. An overall budget for the three basic situations, riverine outflows, coastal area and offshore zone, is given by Boldrin (1998), as shown in fig. 6. In front of the Po River exit (station S1 in the figure) the primary production (PP) is high during the summer months (3000 mg C $m^{-2} d^{-1}$), mostly concentrated in the upper layer. The C export

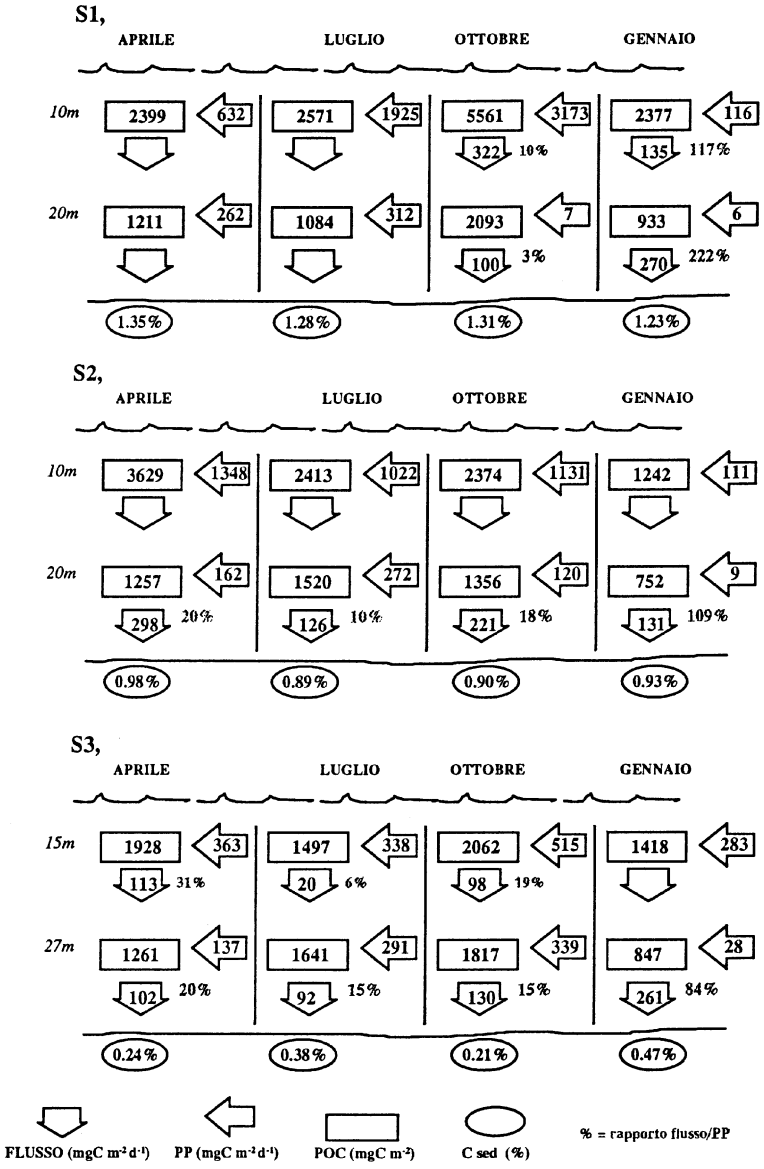

Fig. 6. – Overall integrated balance for organic carbon at S1) riverine outflow area, S2) coastal zone, S3) offshore area. Two layers are considered at each zone. PP=primary production, POC=concentration of particulate organic carbon, Csed=content of carbon in the sediments. %=ration flux/PP (after Boldrin, 1998).

from this layer is a small fraction ($\simeq 10\%$) of the local production, and an even smaller percentage reaches the bottom, indicating an active local consumption. During the winter months most carbon derives from lateral advection and resuspension of

sediments. In the coastal zone (S2 in the figure), off the influence of the Po River, the C production is about three times lower, still mostly concentrated in the upper layer, with a limited fraction (10-20%) reaching the bottom. In winter production and export compensate each other.

The conditions change substantially moving offshore (S3 in the figure). The overall PP is about 50% of the coastal zone, with half of it happening in the lower layer. During the active summer months almost the whole carbon production is locally consumed, particularly close to the surface. In winter the local PP is much larger than at the coastal stations, but with a limited consumption, so that almost the whole C production is deposited at the bottom.

Schemes similar to fig. 6, but for nitrogen and phosphorus, can be found in Boldrin (1998). In general, their flux is smaller than for carbon, mainly for the higher consumption all along the water column.

7. – Atmosphere

7·1. *Local circulation.* – The combination in the Venice area of mainland, coastal lagoon, sea and a relatively close mountain range (the Alps) leads to a peculiar atmospheric environment, whose behaviour is partially different from the one typical of coastal zones. An extensive combination of measurements at several locations, including the ISDGM tower (Camuffo *et al.*, 1979; Camuffo, 1981), have been used to characterize the local circulation, as represented in fig. 7. While the most frequent daytime wind is from SSE, almost perpendicular to the local coastline (see fig. 1b), the night wind flows at cross angle with this direction. The daily wind is clearly associated to the sea breeze, connected to the different daily variation of temperature of sea and land. The nightly NE breeze requires a more complex explanation.

The origin of the nocturnal flow is found in the pressure field induced by horizontal temperature gradients associated to unequal nocturnal cooling of the Alps and adjacent low-lying regions (both land and sea). Whereas, because of the different thermal capacity, the air density is continuously changing on the mainland, the lines of equal pressure tend to follow the coast. This effect is illustrated in fig. 8 with the mean isallobaric pattern found during the early evening hours in summer, when it reaches its maximum value. During periods of near calm synoptic circulation, the isallobaric wind originates in the Alps as a katabatic flow that, forced also by the Coriolis effect, becomes parallel to the isallobars, and thus to the coastline.

Note that the pattern described is critically associated to the local geographic distribution. In the Venetian area it is due to both 1) the very strong isallobaric gradient which always stays in the same direction, so that the surface isobaric pattern deepens more and more, with the isopleths parallel to the coast, 2) the actual distance between the Alps and the sea, that allows the flow to take the observed north-easterly direction, consistent with the geostrophic approximation.

The vertical structure of the nocturnal wind has been investigated with repeated measurements by tracked pilot balloons, monostatic acoustic sounders (Sodar) and slow-rate-of-rise radiosondes. The nocturnal flow starts at 150 m height and at about 18 UTC in summer months, expanding upwards and downwards (till the surface), reaching a maximum height of 500 m and a maximum speed of 6 m/s at 200 m height.

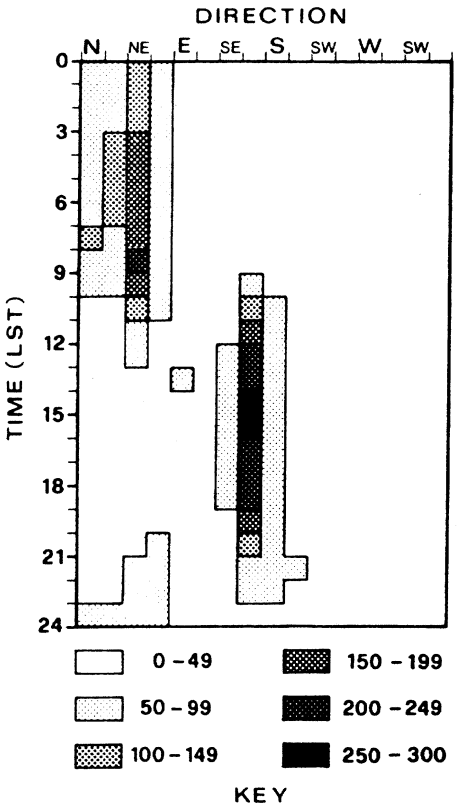

Fig. 7. – Hourly distribution of wind direction in Venice during May to October. The numbers indicate the total cases that occurred during a 4 year period (after Camuffo *et al.*, 1979).

7·2. CO_2 *air-sea exchange.* – Within the present attention to the steady increase of carbon dioxide in the atmosphere, there is a strong interest for the role of the ocean to act as possible sink of CO_2. At given time and location the exchange of CO_2 between air and sea depends basically on the related Δp, *i.e.* on the difference of the partial pressure in the ocean and in the atmosphere (Δp is defined as $pCO_2(\text{sea}) - pCO_2(\text{air})$). The flow is obviously in the direction of the negative gradient.

The solubility of CO_2, hence its partial pressure, in water depends on its salinity and temperature. The actual exchange then depends on a number of other factors, the main ones being the local wind and wave conditions. It follows that the air-sea exchange of carbon dioxide shows a strong spatial and temporal variability. It is therefore of interest to carry out repeated measurements at different locations 1) to characterize the capability of the various areas to act as source or sink of CO_2, 2) to relate, in the longer terms, the actual exchange to specific meteo-oceanographic conditions. Given the ever growing quantitative knowledge of the physical characteristics of the oceans, this would then allow to extend worldwide a reliable estimate of the CO_2 exchange.

With this in mind, CISE, a company based in Milan, Italy, and commissioned by ENEL (the Italian National Electricity Company), carried out in the second semester of 1995 two measurement campaigns in the Northern Adriatic Sea (see fig. 1), one using

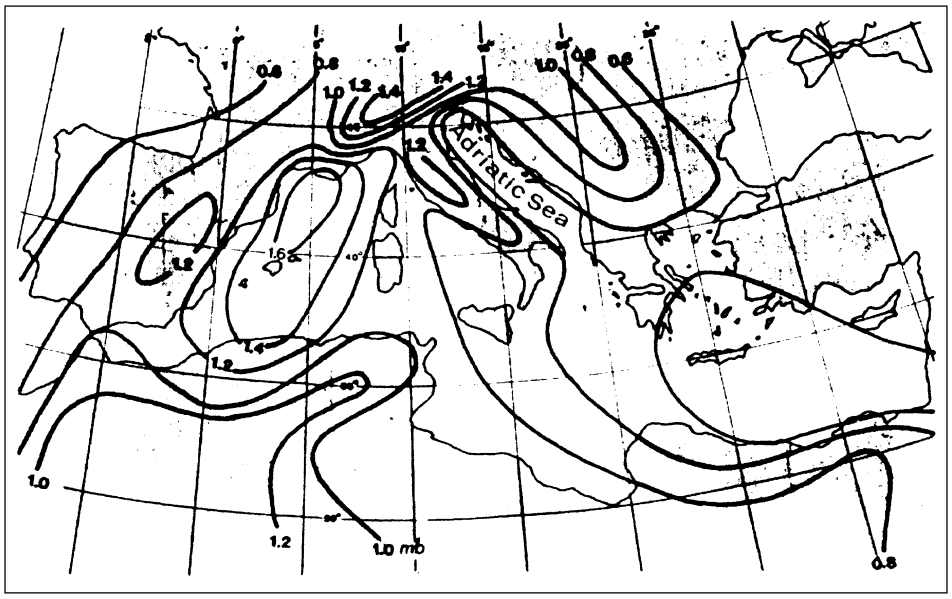

Fig. 8. – Pressure change in mb during summer from 1800 to 2100 GMT (after Reiter, 1971).

a large vessel, the second on the ISDGM tower. The two campaigns aimed at characterizing the local conditions with respect to spatial and temporal variability. Details for the tecnique and the measurements can be found in Ceradini and Meloni (1994).

The basic result of the two campaigns has been that the sea acts locally as a sink, with $\overline{\Delta p} = -42\,\mu$atm ($\overline{p}\,CO_2(\text{air}) = 375\,\mu$atm, $\overline{p}\,CO_2(\text{sea}) = 333\,\mu$atm). The large difference and the marine values higher than usual are probably justified with the geographical characteristics of the Adriatic Sea, enclosed among land areas with an active production of carbon dioxide. However, the surprising result has been the large variability ($\sigma = 8.8\,\mu$atm at the tower) of the sea partial pressure, even at short time interval at the same location. Granted the reliability of the measurements, with errors well below the above σ, Ceradini and Garofalo (1995) looked for possible reasons for the variability. This did not show any correlation with the meteorological and oceanographic conditions. The most likely explanation is the vertical exchange of water masses associated to the gradual cooling of the atmosphere, hence of the upper sea layers. Following the stratification typical of the hot summer months, and the consequent restraint of the biogenic production of CO_2 to the bottom layers, the trigger of vertical instability implies a gradual mixing of the water column, with the consequent time variability experienced during the measurements. While showing clearly how critical these measurements are, these results indicate how careful one must be in extrapolating similar results in space and time.

7·3. *Trend analysis of wet deposition samples.* – The problem of acid rain is well known and must be faced with long-term political decisions at international level. Parallel to the various actions taken to alleviate the problem, a continuous and extended monitoring of the concentration level in the atmosphere is recommended, to

follow the time variations of the pollutants responsible for the acid rain. In this perspective the meteorological station on board of the tower (see sect. **3**) has included for a few years a wet and dry measurement device, *i.e.* an instrument designed to collect separately the rain and the deposition of atmospheric dust. Subsequent chemical analysis provides clear indication of the level of related pollution in the atmosphere. The station on the tower was part of an extended network managed by ENEL (the Italian National Electricity Company). The analysis of the recent years (Novo and Belgiovine, 1996) has shown the existence in Italy, and particularly in its northern part, of a clear trend toward a decrease of the content of sulphate ion in the local rain. This parallels a similar decrease of 9% per year in industrial emission, the effect being more evident in the flat country (Po valley) than in the mountains. There is no similar statistically significant trend in the nitrate ion. The acidity shows a small, but generalized, tendency toward a lower level in most of the Italian territory.

8. – Wind

Wind is one of the most interesting parameters, and the driver of wind waves, the other element of top interest in coastal oceanography. Therefore, it is not surprising that it has received on the tower a lot of attention. Wind instruments provide on board the longest local time series. Besides, in the years a number of different instruments has been put into position, some for devoted campaigns, some for long-term measurements.

In most of the cases the anemometers are or have been put on top of the tower, at different heights above the terrace. In some specific campaigns they have been located at various heights on the vertical of the wave instruments at the extreme of the outgoing platform, protruded towards South-East at the second floor (see fig. 3 and subsect. **10**˙2 for a description of the system). The influence of the tower has been taken into consideration by placing a model of the structure in a wind tunnel, and studying the deformation of the undisturbed flow around it (Cavaleri *et al.*, 1985). Correction coefficients have been obtained to reduce the measurements at the different positions at their undisturbed value.

8˙1. *Sea climatology from coastal stations.* – The knowledge of the wind field, both as synoptic and climatological information, is obviously of strong practical interest. Prior to the existence of devoted satellites, like ERS-1 and ERS-2, the only source of measured data, even if with a debated approximation, were the ships cruising in the area of interest. Even today, when we focus our attention on a basin of limited area, *e.g.* the Adriatic Sea, the amount of data obtained from a specific satellite is far from the quantity required for many practical purposes. The obvious solution are the meteorological models, which are discussed in the following sections. However, as will be shown in detail, the limited basins cause problems also in this field, and often the use of a higher resolution model is required, a luxury that is not easily at disposal.

A commonly used way-out in the past has been to make use of the wind data recorded at the various local meteorological stations, and to extrapolate them to the open sea by means of different practical formulas, mostly derived either empirically or on the base of measurements at a given location. This solution is not without problems. The surface wind field, and more specifically the surface boundary layer, experiences substantial changes when moving from land to sea or viceversa, a consequence of both the different surface roughness and the different air-sea stability conditions. One of

the main problems is the correct evaluation of the influence of the surrounding landscape on the wind measured at a certain location. As the characteristics may, and they usually do, change drastically from place to place, this casts doubts on the use of specific formulas for a general location.

A solution to the last problem is offered by a climatological wind model developed within the EU "European Wind Atlas" project. Granted a detailed description of the orographic and surface characteristics of a certain zone, the model provides the tool for evaluating the structure of the local surface boundary layer, hence a relationship between the wind measured at typically ten metre height and the undisturbed one existing off the surface layer, at a few hundred metres above the surface. A full description of the model is provided by Troen and Petersen (1988).

This model has been applied to the Adriatic Sea, and verified by intercomparing the wind measured at some of the meteorological stations present along the Italian coastline. In particular, Lavagnini *et al.* (1996) have intercompared also the data from the Venice airport and the offshore tower, at about 25 km distance. In Venice, the airport is located at the inner edge of the lagoon. Note that, to transfer the wind information from place to place, the model assumes spatial uniformity in the wind field. Therefore, it can be used either in the absence of relevant gradient in the horizontal direction, or for long-term statistics, when the gradients are more likely to average out in the long term.

While the EU model has worked well from station to station along the coast, also at distances of more than 200 km, there is an evident underestimate when trasferring the data from land to sea. In particular, the results obtained for the tower location, starting from the ones available at the Venice airport, are on the average underestimated by 28% with respect to the ones derived from the local data. This figure has not received a satisfactory explanation. In any case it has been *de facto* accepted and applied to the data from the other coastal stations to derive a statistical wind distribution along the Adriatic Sea. The result is shown in fig. 9, where the horizontal scale gives the distance (see fig. 1) while moving towards South-East, starting from the upper-left end of the basin. The figure shows both the mean wind speed and the scale parameter of the used Weibull distribution (1961) in correspondence of the various stations. There is an evident trend towards higher values in the southern part of the Adriatic Sea. The off-line value at PE (Pescara) reflects the well known fact that the station at Pescara is subjected to very local wind conditions, poorly reflecting the overall field in the surrounding area, and is therefore poorly representative of the offshore conditions.

8·2. *Validation of meteorological models.* – In the previous section I have mentioned the meteorological models as a possible alternative to the lack of wind data in the open sea. As a matter of fact this alternative is nowadays widely used, the surface wind fields being part of the standard output of any meteorological model and, as I will discuss more in detail in sect. **10**, the input to the modelling of wind waves.

The performance of large scale meteorological models on the oceans is rather good. Extended comparisons of the output of the T213 model of the European Centre for Medium-Range Weather Forecasts (ECMWF, Reading, UK) with altimeter measured wind speeds indicate an average difference (altimeter-model) of 0.25 m/s. However, the situation is not so favourable when we focus on smaller or enclosed basins, like the Mediterranean Sea or, to an even smaller scale, the Adriatic Sea. On the other hand, most economical interests are located in the coastal areas, and it is therefore of interest to be able to provide reliable data also in these areas. The classical way out is the use of

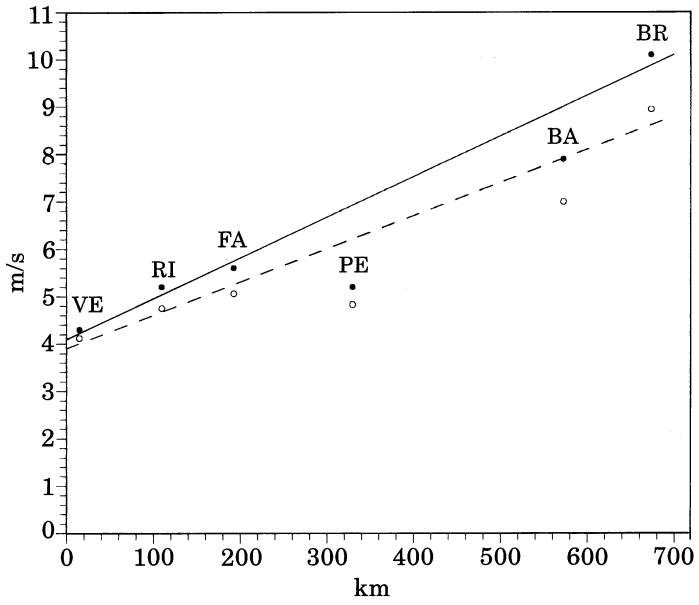

Fig. 9. – Distribution of scale parameter A (continuous line) and mean wind speed U (broken line) along the Adriatic Sea (after Lavagnini *et al.*, 1996).

limited area models (LAM), *i.e.* of models that focus on a limited area, working with higher resolution, using the output of global models as boundary conditions of the area of interest. However, also LAMs do not perform always at the desired level in relatively small basins. A number of effects that do not scale with the basin dimensions, like orographic effects, numerical diffusion (see Cavaleri *et al.*, 1997a) and the transition zone between land and sea, tend to spread their influence on the whole basin, decreasing the quality of the overall surface wind fields. The need for reliable measurements in the open ocean is therefore evident.

The wind data recorded at the tower has been used to validate the results from three different models: LAMBO, T213 and ADRIAWIND. LAMBO (Lazic and Telenta, 1990) is based on the 1980 version of the UB/NMC model, a cooperative product of the University of Beograd and the former National Meteorological Center (now NCEP) of Washington. The model is based on the numerical integration of a set of prognostic primitive equations, plus a full parametrization of the physical processes happening at the scale of the 10-20 km. Wind fields at 20 km resolution have been provided for a few storms by the Servizio Meteorologico Emilia-Romagna (Meteorological Service of Emilia-Romagna, located in Bologna, Italy), where LAMBO is operational for daily forecast for the whole Italy and the surrounding areas (Paccagnella *et al.*, 1992). Comparison with the data measured at the tower and also the use of these data as input to a local wave model (more about this in subsect. **10**·8) have shown that the output of LAMBO in the Adriatic Sea is often underestimated with respect to measured data (Cavaleri *et al.*, 1996a). However, the general meteorological information, and in particular the forecast, of LAMBO appears to be very good, which suggests that the problem can be associated partly to the factors mentioned above, and partly to the parametrization of the surface boundary layer.

Somehow similar results have been obtained for the T213 meteorological model of ECMWF, the one used for daily global forecast from September 1991 till April 1998 (Simmons, 1991). Compared to the tower data, the ECMWF wind speeds are on the average underestimated of about 50%. However, also in this case the overall forecasts are of rather good quality, which suggests that, besides obvious problems of spatial resolution, for possible improvements the attention must be focused also on the near surface atmospheric layers.

If we focus our attention on a specific product, namely the surface wind field, it is possible to approach the problem from a different point of view. Rather than concentrating on highly sophisticated models, we can make use of simpler tools, but with the possibility of tuning the output to the characteristics of a specific area. ADRIAWIND (Bergamasco *et al.*, 1986) is a 2D model that estimates the surface wind fiels starting from the pressure values recorded at the different meteorological stations. After evaluating the associated gradient wind, this is transferred to the surface using empirical rules derived from long-term measurements (Cavaleri *et al.*, 1996b). The basic advantage for our present interest is that the simple structure of the model allows its calibration to a specific area. Making use of the data from the tower and from those from some satellite passages, ADRIAWIND has been tuned to the Adriatic sea, providing very good results. Another advantage with respect to the more complicate models is the very simple input information, *i.e.* the border pressure at some points along the coast. Because this information has been available for quite a while in the past, once the model has been tuned, it is possible to derive the wind field for the corresponding length of time. The wind data at the tower have been available for more than 20 years. A two year section has been used for calibrating the model. Then this has been applied to the remaining section and the output compared with the corresponding tower data. As mentioned above, the results are very good, with a bias of 0.4 m/s and a rms error of 3.5 m/s.

8·3. *Extreme and climatological analysis.* – Extreme values of meteorological parameters, *i.e.* the maximum expectable values of the parameters of interest, in particular of the wind speed, are strongly required for design and safety purposes.

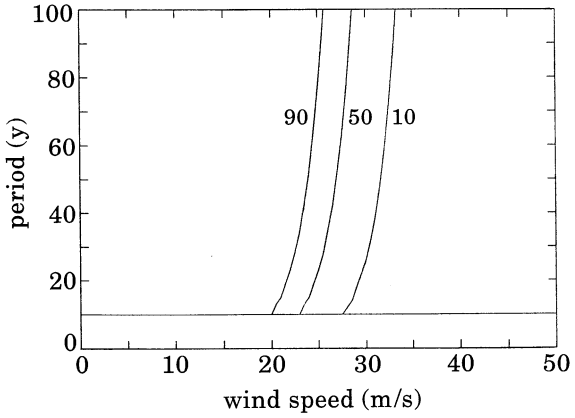

Fig. 10. – Extremes of sirocco wind speed in the Northern Adriatic Sea. The lines show the relationship between wind speed (m/s), exceedance probability (%, specified close to each line) and considered period (years) (after Cavaleri *et al.*, 1996b).

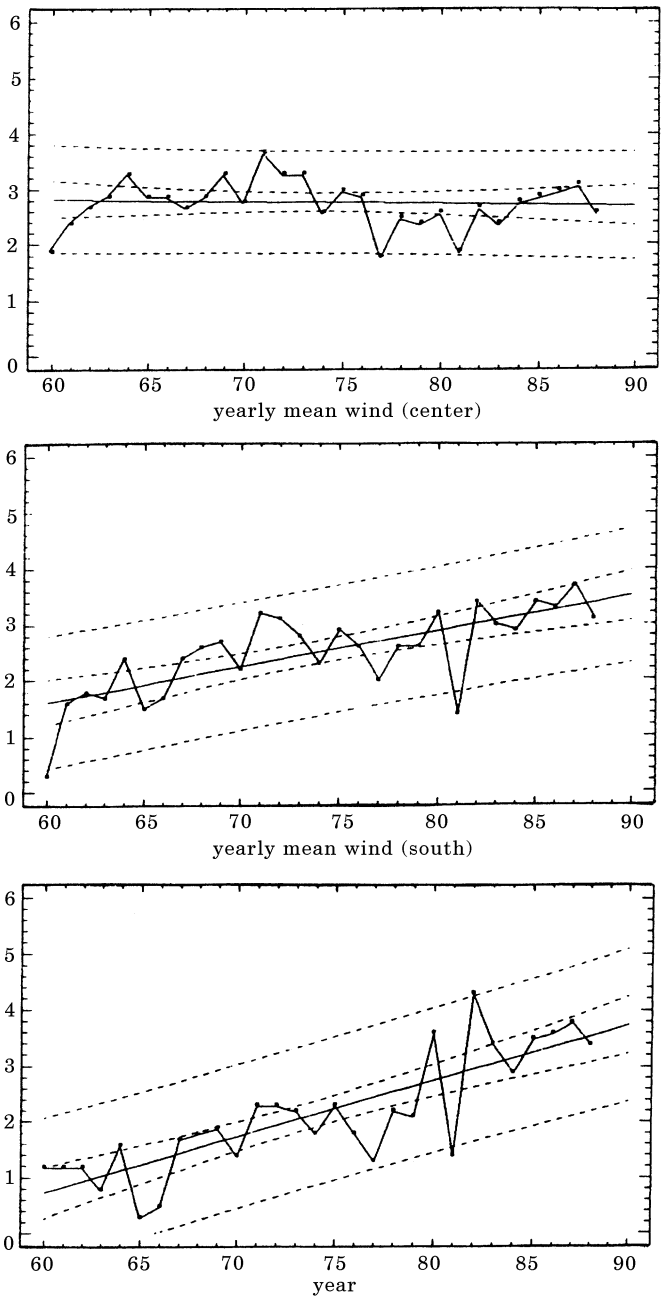

Fig. 11. – The mean value of the wind speed for the different years and, from top to bottom, for the northern, central and southern part of the Adriatic Sea. Vertical scale is in m/s. The broken close lines show the 95% confidence limits of the fit. The far ones show the 95% prediction limits (after Cavaleri *et al.*, 1996b).

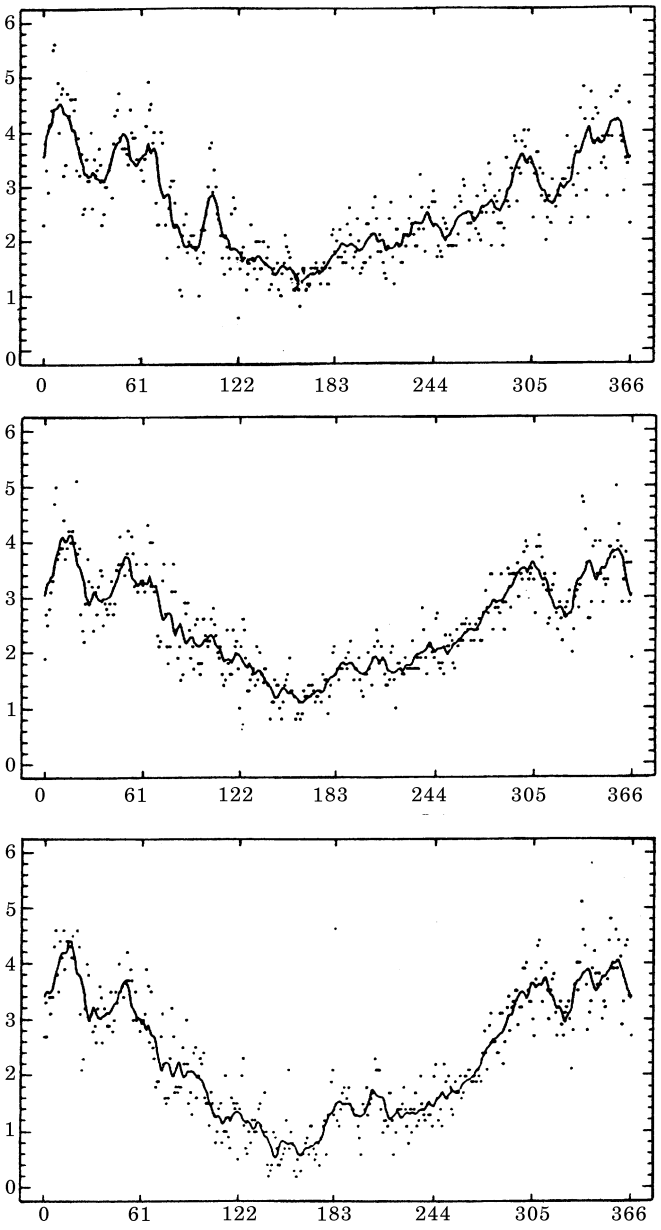

Fig. 12. – The mean wind speed (m/s) for each day of the year and, from top to bottom, for the northern, central and southern part of the Adriatic Sea. The dots show the original data. The continuous lines show the corresponding 21 point running averages (after Cavaleri *et al.*, 1996b).

Reliable estimates can be obtained only from long time series, that for meteorological processes must span tens of years. This is a problem, because the sophisticated 3D model exists with a sufficient resolution only for the very recent past (order of years).

In principle they can be run as hindcast, but the effort required is extremely large, and often the necessary information is not available.

Taking advantage of the simple requirements of the ADRIAWIND model, described in the previous subsection, and of the availability of the necessary information (the atmospheric pressure recorded at the coastal stations), Cavaleri *et al.* (1996b) have extended their hindcast for the Adriatic Sea as far in the past as possible. The limit has been established by the lack of accuracy and reliability of the input data before a certain date. In practice, the hindcast covers the period 1960-1989, the upper date being established by the lack of data from the former Jugoslavia during the war events. In more recent years, as will be shown in detail in subsect. **10**·8, it is preferable to make use of the output of present meteorological models.

The 29 year hindcast allows extensive analysis of extremes and of the local climate. Figure 10 shows the expected extreme values of the wind speed for sirocco storms at the tower location.

The analysis of the wind speed has revealed some interesting features. Cavaleri *et al.* (1996b) have found that the more we move to the South, the more there is an evident trend towards increasing values of the wind speed (see fig. 11). The increase is on the along-axis component, and it implies a growing intensity of the sirocco storms in the lower part of the basin.

Another peculiar characteristic has emerged from the analysis of the variability along the year. For each Julian day the authors have evaluated the average wind speed, from the 8 (synoptic times) $\times$ 29 (years) available fields, further averaging in the northern, central and southern part of the Adriatic Sea. The result is shown in fig. 12, where the continuous line represents a 21 point running average for better identification of the general trend. Apart from the obvious variability with the season, the interesting feature is the clear tendency to higher or lower wind speeds in the various periods of the year. The amplitude of the oscillations is well out of the confidence limits of the estimate, and they represent a physical reality. While this corresponds to the presence of well defined meteorological patterns typical of some periods, it is evident that the probability of higher or lower wind speeds varies also on a time scale much shorter than the seasonal one.

8·4. *Gustiness.* – The perception we have of a wind field by looking at a meteorological map or to the output of a meteorological model, or, alternatively, while being in the middle of a storm, is quite different. Apart from the direct feeling of the speed, perhaps the most striking feature is the, often intense, variability of the field. Figure 13 shows a series of analogue records taken from the ISDGM tower. The different level of gustiness is self-evident.

The level of turbulence in the field appears at all the time and spatial scales. The spectra of extended records taken at the tower and elsewhere show a continuous transition from the micro turbulence till the synoptic variability. Apart from local peculiar conditions, like being on the lee of a prominent orographic feature, the level of turbulence is basically connected to the air-sea stability conditions. The record to the right of fig. 13 has been taken during a severe bora storm, with T_{water} higher than T_{air} by ten degrees or more. In such cases the variability in the field can go up to $\sigma = 0.30$.

The problem is that the related information is seldom available, and even more seldom used by the oceanographers. The consequences are not trivial. As the surface stress on the ocean varies with the square of the wind speed, the average stresses out

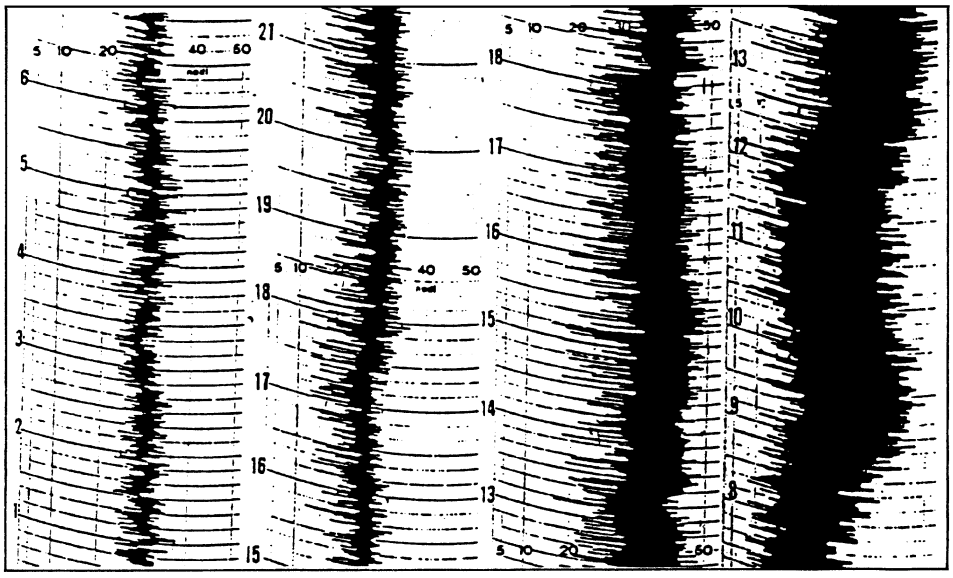

Fig. 13. – Wind records with similar wind speed, but different level of gustiness (after Komen *et al.*, 1994).

of a uniform or turbulent wind do not have the same value. While I discuss in more detail the consequences on wave growth in subsect. **10**·10, it is interesting to analyse the distribution of the number of floods in Venice throughout the year, shown in fig. 14. While the prevalence in fall is connected to the weather pattern that is frequent in this period, the statistical distribution of the forcing function, *i.e.* the sirocco storms in the Adriatic Sea, does not justify the difference with respect to spring (Camuffo 1984). The explanation comes from the air-sea stability conditions that are present in the two

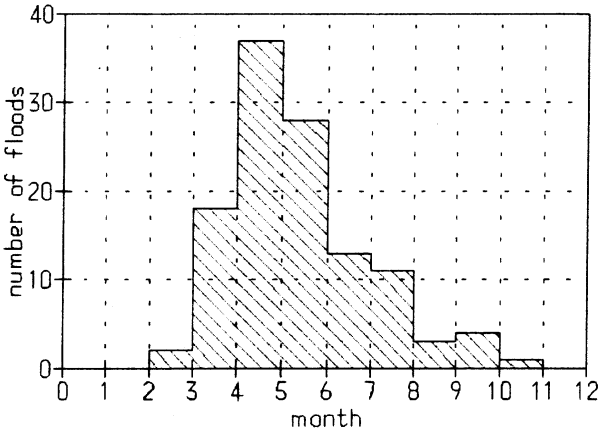

Fig. 14. – Number of floods in Venice throughout the year (beginning in July). Period from 1923 until 1989 (after Camuffo, 1984).

periods. In fall, with still warm water in the sea surface layers, we find an air-water temperature difference up to -12 °C. On the contrary, in spring the conditions are neutral or stable, with $\Delta T_{\text{air-water}} \geq 0$ °C. It follows that in spring the wind is less active and correspondingly smaller is the probability of a flood.

Another consequence of gustiness is the practical impossibility of getting, even theoretically, a "perfect model". With this I mean that, because turbulence is poorly, if even at all, represented in a meteorological model, and because the necessary information is not available, there is no chance that we can reproduce the actual time and space history of the wind field. It is interesting that the theory does not explain levels of turbulence as those seen in fig. 13 (Anton Beljars, personal communication). This implies that, when comparing model *vs.* measured data, what we can aim at is to obtain a zero bias, but always with a variance that cannot be lower than the level of turbulence in the field.

9. – Tides and surges

9·1. *A fast response tide gauge.* – Two tide gauges, of the conventional well type, are operational on the tower, one run by ISDGM, the other one by the Centro Previsioni e Segnalazioni Maree (see sect. **3**). Both the systems have been at work for many years, the ISDGM one having initiated its activity, even if with some blank intervals, back in 1971. While the other gauge is fully authomated (the data are transmitted to land every five minutes), the ISDGM is still operating with ink on paper recording. However, this gauge features some unique characteristics about its filtering capabilities. As better explained better in sect. **10**·2, we needed to know the tidal level with an accuracy of the order of one centimetre. Filtering the waves in shallow water with the conventional squeezing of the small tube out of the well would have introduced delays of the order of ten minutes or more, that, with the local spring tide, would mean errors larger than two or three centimetres. The solution, shown in fig. 15, was to prolong downwards the well with a 5 cm diameter pipe, that is then splitted at the bottom into six diverging 60 m long horizontal pipes of similar diameter. With virtually a zero time constant for any tidal variation, the system filters wind waves in three different ways: by depth, because the signal is taken from the bottom; by spatial average, because the level in the well is the average of those at the six pipe ends; by friction, because of the motion of the water in the pipes. The theory is described in detail by Cavaleri and Curiotto (1979). The overall filtering characteristics are shown in fig. 16. We see that wind waves are filtered always better than 99%, while oscillations with period longer than one minute are practically reproduced in full amplitude.

9·2. *Storm surge modelling.* – Given the frequent floods that affect the town, it is obvious that attention has been focused on a reliable flood warning system. The office in charge is the Centro Previsioni e Segnalazioni Maree (the Tidal Warning and Forecast Centre) of the Venetian authority, that has attacked the problem along two lines: a statistical approach and a deterministic one.

The statistical approach was the first one to become operational more than a decade ago (Canestrelli *et al.*, 1986). It is basically an ARMA model (Box and Jenkins, 1970) that bases the forecast on 50 predictors: the last 30 tidal levels, taken at one hour interval at the location of interest, and 20 atmospheric pressure values recorded at the last five synoptic hours at four Italian stations, one in the Northern, one in the

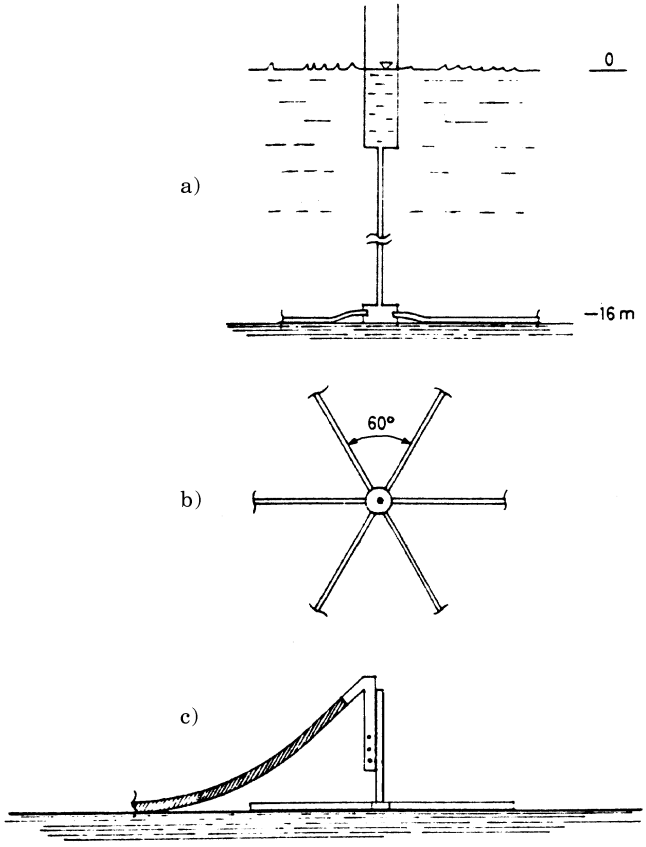

Fig. 15. – a) Lateral scheme of the ISDGM tide gauge. The well continues till the bottom with a pipe, that subdivides into 6 other horizontal pipes. b) Horizontal scheme of the pipes lying on the bottom. They are 60 m long and placed at 60 degrees to each other. c) Outer terminal of one of the horizontal pipes (b)), shadowed in the figure. The vertical tube with its vertical holes avoids the sand filling of the pipe and the dynamical effect of the water motion (after Cavaleri and Curiotto, 1979).

Southern Adriatic, and two on the border of the Tyrrhenian Sea. The first 30 predictors and the local station provide information for the past and the present, hence they allow an extrapolation to the future of the past conditions. The crucial anticipation of the new event is provided by the other three meteorological stations, located in the directions where the meteorological storms responsible for the floods usually come from. The model provides reliable forecasts up to 9 hours in advance, with a rms error less than 10 cm (more or less 10% of the excursion of the local spring tide).

Good for the short term notice, the above system lacks intrinsecally the capability of pushing the forecast further into the future. It is obvious that for this we need to make use of the meteorological forecast. The obvious improvement (Canestrelli and Pastore, 1997) has been to make use of the values of atmospheric pressure forecast for the immediate future, as provided by ECMWF. With this strucure, the 30 tidal predictors provide the information required for extrapolating to the future the memory of the

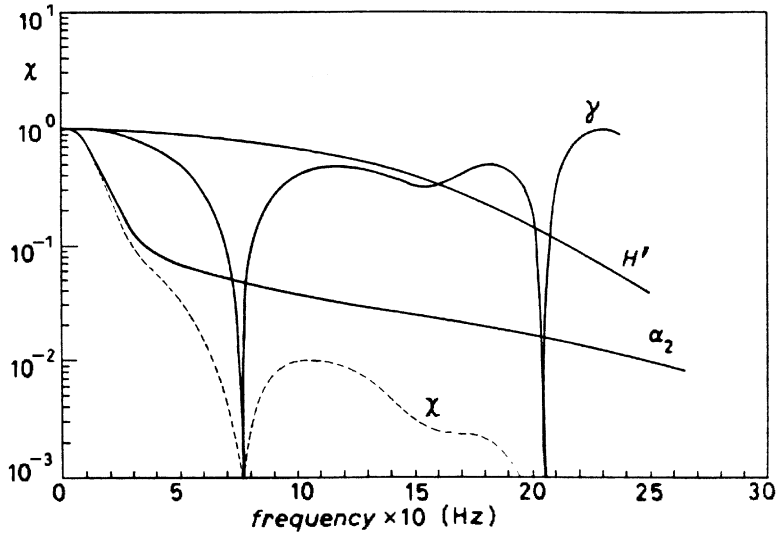

Fig. 16. – Filtering characteristics of the tide gauge shown in fig. 15. α_2 represents the filtering due to the hydrodynamics of the pipes. H' is the attenuation with depth, γ derives from averaging the signal at the 6 vertices of the exagon. χ, product of α_2, H' and γ, is the overall filtering coefficient (after Cavaleri and Curiotto, 1979).

basin for previous events (a seiche can be present in the basin for more than one week), while the forecast pressures take into account, even if in a statistical sense, the forthcoming meteorological events. The model has been tuned with extensive analysis of the recent years. The effective range of forecast has been considerably extended, with a rms error of 14 cm up to 36 hours in advance.

A strong limitation of the statistical approach is that we can expect the model to do a fair job only when the storms are of a "known" type, *i.e.* frequent enough in the past for the model to embed their information in its coefficients. If a "new" type of storm shows up, the statistical model plainly does not know how to interpret it (but it is unaware of its own limitations). An example in this sense is given in the following subsection 9·3.

The drastic solution is to make use of models that reproduce with their equations the physics of the process. They have the further advantages that, once they have been assembled, and given that the physics does not depend on the specific location, they can be readily exported and applied to a new area, without any tuning. In the case of the Adriatic Sea (see Cecconi *et al.*, 1996) the storm surge model has two nested grids, to focus the attention first on the area covering the inlets to the lagoon (see fig. 1), and then on the lagoon itself. The input information is again the forecast produced by ECMWF, but both as surface wind and pressure fields. At 36 hour forecast the model has a rms error of 17 cm.

It is remarkable that a simple statistical model produces somehow better results than a sophisticated storm surge model. Following the argument given above, the choice on which one to use depends on the weight we give to the average error and to the drastic error that can happen once in a while. It is clearly a case of economical and political decision.

While the forecast based on the physical approach can in principle be extended in the future as far as the meteorological forecast is available, there are practical limits based on the decreasing accuracy of the forecast with its range. The problem is enhanced by the limited dimensions of the basin, that make it much more sensitive to meteorological errors in space and time. This is the reason why with both the approaches the operational forecast is limited to 36 hours.

With respect to waves, tidal forecast is more sensitive to timing error in the arrival of a storm. In the Northern Adriatic Sea a storm surge can raise the sea level up to one metre (cases of higher surge have happened, including the historical 4 November 1966). Being of the same order of magnitude as the spring tidal excursion, the actual maximum level reached during an event is crucially dependent on the relative phase between astronomical tide and storm surge. Therefore, it is possible to have a nice surge forecast, perfect in amplitude, but wrong in time, with dramatic results on the overall forecast, which is unluckily the point of relevance and the one to which the final users, the inhabitants of Venice, are sensitive to.

9·3. *Set-up.* – On 22 December 1979 Venice experienced the second ever recorded worst flood. A prolongued sirocco storm led to a very heavy storm surge and, at the same time, to very severe wave conditions in the Northern Adriatic Sea. This was the worst storm within the lifetime of the tower. We do not have any *official* record of the

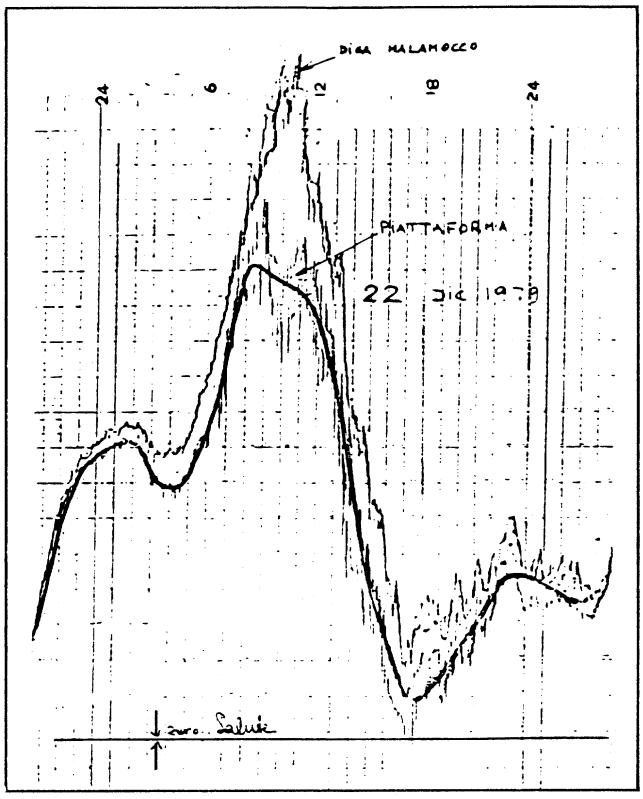

Fig. 17. – The tidal record of 22 December 1979 at the tower (thick line) and at the entrance of the lagoon (upper line). The horizontal spacing is one hour, the vertical one 10 cm.

storm, because the second floor (see fig. 3) was completely destroyed, with consequent loss of power on board. However, we have the evidence of the damage, with H beams broken just below the basement of the third floor, nine metres off the sea surface. Even considering a 1.5 m surge and the high kurtosis of the waves, a conservative estimate is for single wave heights above 11 m.

Of all the instruments on board the only ones that kept working were the two mechanical instruments, *i.e.* the anemometer on the top terrace and the tide gauge on the second floor. Notwithstanding repeated immersions within the wave crests, the latter one survived because of the extreme directionality of the wave field and of its position, shielded by one of the supporting second floor vertical poles. For our present interests the key piece of information was the tidal record, shown in fig. 17, that

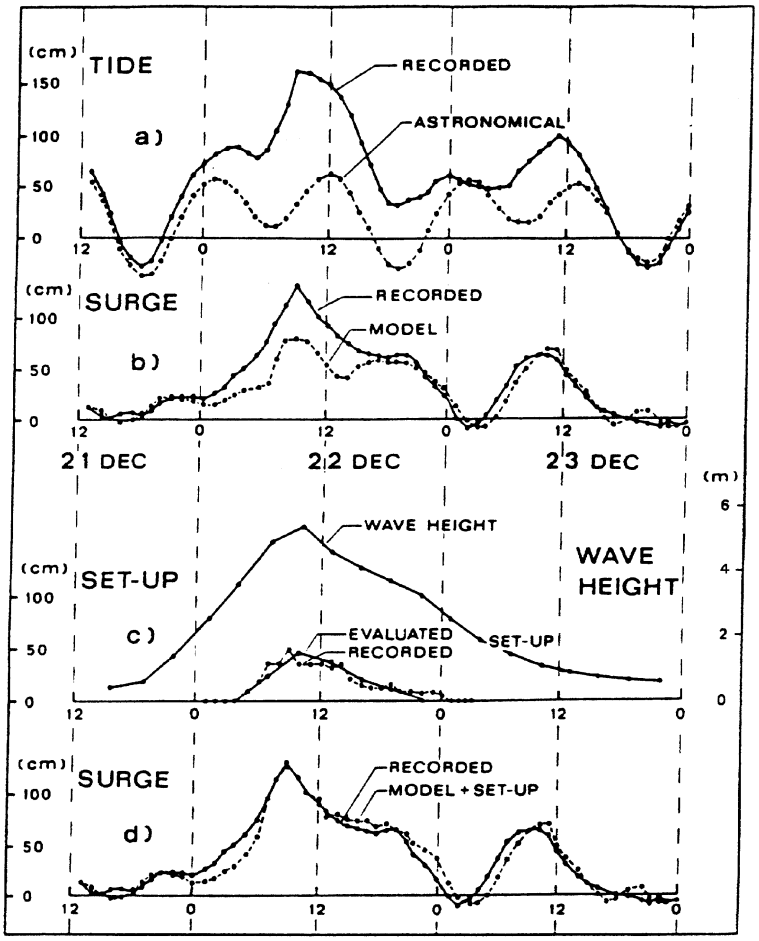

Fig. 18. – a) Recorded and astronomical tide at Venice; b) recorded storm surge level (difference of the two graphs in a) and model prediction; c) wave height at the tower, evaluated and recorded set-up at the harbour entrance; d) recorded storm surge level (same as b)) and corresponding model results (addition of prediction in b) and recorded set-up in c)) (after Cavaleri *et al.*, 1991).

however, turned out to be quite messy and about 40 cm lower than the contemporary record at one of the inlets to the lagoon (see fig. 1b for their respective positions). On top of it, large fast oscillations were superimposed to the average signal. Our first reaction was to assume that the record was faulty, but when an expert (Doug Inman) saw the two records, he immediately identified them as a beautiful example of set-up, the coastal increase of sea level associated to bottom induced breaking of shoaling waves. The key condition for having a tidal difference bewteen the two stations is that the waves experience a substantial breaking before the end of the jetty, where the other tide gauge is located. Having at disposal a unique piece of information, we immediately assembled a set-up model (Bertotti and Cavaleri, 1985; Cavaleri *et al.*, 1991). The full history of the storm, and in particular of the wave conditions at the tower, was estimated using the WAM model (Komen *et al.*, 1994), using as input the wind fields obtained with the ADRIAWIND model, as described in subsect. 8˙2. Starting from the knowledge of the wave conditions and the surface level at the tower, the model estimates the surface profile till the coast. The results at the end of the jetty are shown in fig. 18. Panel a) shows the recorded and the astronomical tide. The difference is due to storm surge. However, panel b) compares the recorded and the modelled values of the surge. There is an evident understimate by the model. Panel c) shows the hindcast wave height at the tower, the evaluated and the recorded difference between the tower and the jetty tide gauges, as derived from fig. 17. Finally, in d) it is shown how the superposition of the set-up level and the storm surge model results lead to the correct figures. Note how the set-up is not correlated with the storm surge, but it is closely linked, because of its physics, to the wave conditions.

The set-up is also the likely explanation for the poor performance of the ARMA model used for tidal forecast during some of the most severe events. As I have mentioned in subsect. **9**˙2, the ARMA model can faithfully reproduce events for which it has a repeatitive previous experience. However, the tide gauges are located at the end of the jetties, which is also the relevant position for determining the tidal level inside the lagoon. We find the set-up at this position only under high wave conditions. A screening of the past records revealed only a limited number of cases when the phenomenon was present. The ARMA model is fitted to the bulk of the data, and consequently the set-up appears as an unknown process, not reproduced by the model. The condition is different in the deterministic approach, where the solution is simply to introduce into the model the proper equations. An example by Lionello (1995) is described in subsect. **10**˙7.

10. – Wind waves

Wind waves are the key parameter of interest in coastal studies. As such, they have received on the tower a lot of attention, both for direct applications in the area and for general scientific studies. Many different kinds of devoted instruments have been put on board, some for long-term measurements, some for specific purposes during devoted campaigns. The overall results are the most prolific source of information from the on board measurements.

An interesting general point about wave measurements from the tower is the problem of possible reflection by the structure. In this respect the mussels mentioned in sect. **5** provide a convenient solution. Acting as sponges, their layer dissipates much

of the energy of impinging waves, avoiding or at least strongly limiting reflection, an unwanted effect during wave measurements. Their effective role has been verified with devoted keen directional measurements (see subsect. **10**·3).

10·1. *Long-term measurements.* – Two authomatic wave recording systems are operational on board. One system is managed by Consorzio Venezia Nuova (see sect. **3**), and has been operated since 1987. The system uses an external acoustic sounder to detect the surface level, and a submerged electromagnetic currentmeter to measure the horizontal orbital motion and to estimate from it the wave direction. The data, sampled at two Hz frequency, are collected for 15 minutes every three hours. The data are both stored on board and transmitted to land in real time. The later analysis is done with the zero crossing method for scalar values (significant wave height H_s, zero crossing period T_z), and by vector analysis of the orbital paths out of the currentmeter for wave direction θ.

The overall system is very robust and technically reliable. However (Cecconi, personal communication), there are occasional problems in the determination of θ, connected to the position of the currentmeter with respect to the tower. The system is located at the East corner of the tower, with the instrument clamped to the corresponding leg at five metres of depth, at the end of a 2 m long supporting arm. A three diameter distance (the leg diameter is 0.60 m) is not sufficient to avoid hydrodynamical interference, but it is enough to reduce it to an acceptable level. The problem arises in severe wave conditions, when the orbital motion, expecially for long sirocco waves, is such to bring till the instrument the vortices that detach from the leg. In these cases the signal is very noisy and poorly informative. The solution is not simple, because for clean data the currentmeter should be located away from any structure and interfering arm. An example is described in subsect. **10**·2. However, a permanent instrument must be firmly held. A solution could be to place it on the bottom, away from the tower. This would strongly reduce the signal because of its attenuation with depth, virtually filtering out all the waves with period below 4–5 s. Besides, this would place the instrument off the vertical of the sounder, with consequently a more problematic analysis. The solution presently considered consists in extending the holding horizontal arm, till at least three metre length, for further reducing the possible interference with the vortex shedding from the leg.

The second system available on board is run by ISDGM and has been operational since 1978. As such this is probably the longest wave time series in Italy, certainly the longest directional one, and one of the longest in the world. The system (Cavaleri *et al.*, 1996c) is composed of three pressure transducers located at about four metre depth on three legs of the tower, at the North, East and South corners. The transducers can be retrieved for inspection and cleaning from the first floor of the tower by means of a double pulley system. The transducers, sturdy and small in diameter (a cylinder 10 cm long, 3 cm diameter), are encased inside a plastic container filled with oil for long-term protection. A soft membrane transmits the pressure signal to the oil, hence to the transducer. Still being within the range of the vortices produces by the legs, the pressure transducers do not suffer from the problems mentioned above, because the pressure signal is much less affected than the velocity field. The vortex signal can eventually introduce a small level of noise into the field, but at a level almost negligible with respect to the robust pressure signal associated to waves.

The transducers are powered only for the necessary period, and the signals recorded for 1024 seconds every three hours, at synoptic times (00, 03, 06, ... UTC). The

full signals are recorded on board for a recently extended period of more than six months. To save memory, the full record is done only when the wave signal is above a certain threshold. A first hand analysis is done on board and telemetered to land as part of the meteo-oceanographic station mentioned in sect. **3**. The full analysis is done on land, after the data retrieval. It was originally done following the classical method of Longuet-Higgins *et al.* (1963), and later according to Kuik *et al.* (1988). The summarizing output parameters are H_s, T_m, T_p (mean and peak period), θ_m (mean direction), the one-dimensional spectrum, plus directional spread, skewness and kurtosis for each frequency.

The results out of the two systems have been intercompared for reciprocal validation. Periods and mean overall directions, when not affected by vortex shedding, agree very well. As H_s, those derived from the pressure transducers are larger than the ones from the eco-sounder by more than 10%. This fact has not yet received a sufficient explanation. One considered possibility is the presence of nonlinearity in the pressure field. However, careful measurements done from the tower in an earlier period (Cavaleri, 1980; the subject is discussed in detail in subsect. **10**˙2) show clearly that, when a certain degree of nonlinearity exists, waves attenuate faster than foreseen by the linear theory, the one used in the analysis of the data. Hence, if present and associated to linear theory, the nonlinearity would act to lower the estimated H_s with respect to the truth. Another possibility is the high frequency tail (for $f > 0.4$ Hz) added to the estimated surface spectrum to close the spectrum in this range. However, the tail does not contain enough energy to justify the difference. Practical tests, including the intercomparison with a third device, are planned to clarify the matter.

10˙2. *Wave kinematics.* – The tower has hosted for many years a sophisticated system to explore the kinematics of wind waves. A sketch of the system is given in fig. 19. Two strongly tensed wires are connected to a heavy ballast on the bottom, and work as guide to a sliding cart holding the main set of instruments. This includes two electromagnetic currentmeters, placed at cross angle to each other, and two pressure transducers at different depths. The horizontal currentmeter, EM1 in the figure, is clamped on an arm that can be rotated to align the instrument in the optimal direction with respect to the incoming waves. The whole provides a quite complete description of the pressure and velocity field under wind waves. The cart can be placed at any depth, controlled by a calibrated wire from the upper deck. The cart is firmly held into position by a lower return wire. Surface profile is measured by a wave staff located on the vertical of the submerged instruments. The symbols for wave velocity components are indicated in the figure. The actual depth was evaluated by combining the known wire length and the reading of the fast response tide gauge described in subsect. **9**˙1. On the whole, the depth was known with an accuracy of 1 cm.

Measurements, with personnel on board, were taken for many years and with very different wave conditions. The analysis was directed towards two main subjects: attenuation with depth and Reynolds stresses.

10˙2.1. Attenuation with depth. The contemporary measurement of the surface profile and of the 3D velocity and pressure fields on the same vertical allowed the experimental verification of the attenuation law with depth. The dynamical effect of water motion on the pressure measured by the transducers was avoided by enclosing them into a soft water filled plastic bag. A full account of the measurements is given by Cavaleri (1980).

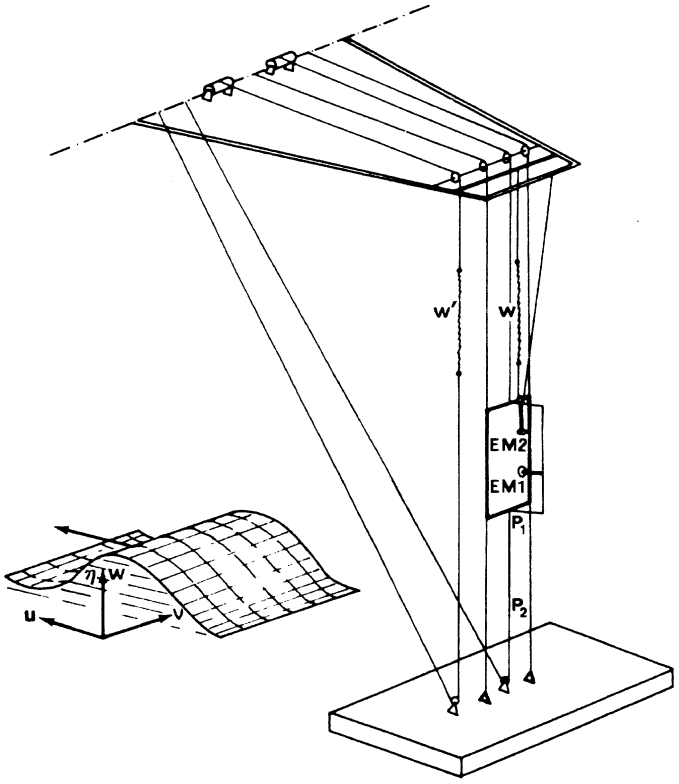

Fig. 19. – Instrumental arrangement to explore the wave kinematics (see fig. 3). Instruments are indicated by W (wave gauge), EM1 and EM2 (electromagnetic currentmeters), and P1 and P2 (pressure transducers). W′ is the reserve position of the wave gauge when the cart is operated very close to the surface (after Cavaleri and Zecchetto, 1987).

The actual attenuation has been obtained by direct comparison of the spectra from the different instruments, and by further comparing with the results from linear theory. All the results are coherent in indicating an attenuation with depth larger than the theoretical one. A summarizing result is given in fig. 20, where we see the ratio between experimental and theoretical attenuation for the various frequencies and for different ranges of depth. Note the very high values of the coherence between the intercompared signals, that excludes any noise in the data. Data with a lower coherence were excluded from the analysis. The overall conclusive results is that waves attenuate faster than suggested by linear theory, the difference increasing with depth. While the behaviour in the high frequency range can be explained on the base of the nonlinear interaction among the different components, no definite explanation has been so far proposed for the larger attenuation on most of the frequency range.

10·2.2. Reynolds stresses. The Reynolds stresses are defined as $P = \varrho\langle uw\rangle$, with ϱ the water density, and u, w, respectively, the horizontal and vertical components of the water motion (see fig. 19 for their definition). P can be interpreted as the average vertical flux of horizontal momentum, and it is strictly connected to the generation of

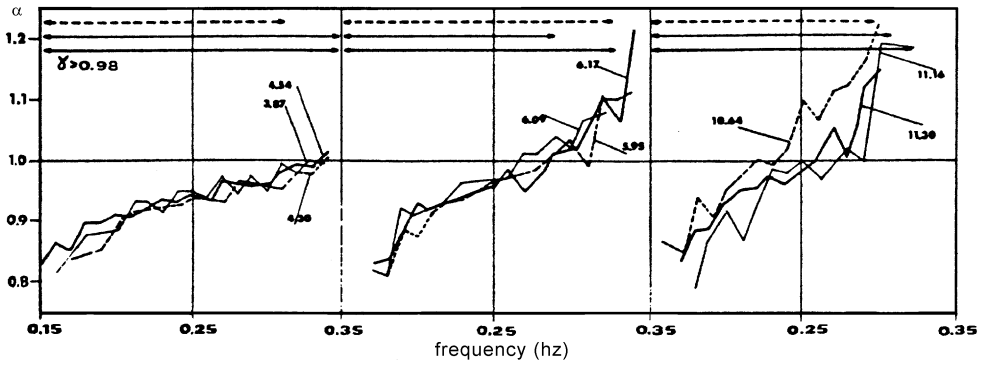

Fig. 20. – Wave attenuation with depth. α is the ratio between the experimental and theoretical values of pressure as a function of frequency. Each line refers to a single record. These are approximately grouped according to the depth of the transducer (in metres). The horizontal segments indicate the frequency range where coherence was greater than 0.99 (after Cavaleri, 1980).

wind waves by wind. Given the wind and wave conditions at certain time and location, the theoretical value of the stresses P_{th} can be established following the theory of Kondo (1975). Conversely, given the local measurements of u and w, we can evaluate the corresponding experimental value P_{exp}. The surprising result, reported by Cavaleri and Zecchetto (1987), is that, under active generation conditions, P_{exp} turns out to be larger by two orders of magnitude. According to linear theory, the u and w components of motion should be orthogonal to each other, which implies the particle orbits to be either circles or ellipses with the longer axis in the horizontal direction. The results of the measurements at the tower are shown in fig. 21a. While the downward transfer of horizontal momentum (necessary for wave growth) implies a certain inclination of the orbits, there is no theoretical explanation for the high inclination shown in the figure. A complete result for one of the many available records is shown in fig. 22.

Considering the phase shift α_{xx} between the different variables, we note that, while the surface profile η and the vertical component of orbital motion w are close to the theoretical 90 degrees, $\alpha_{\eta u}$ shows a very large shift, ranging from 30° at the low

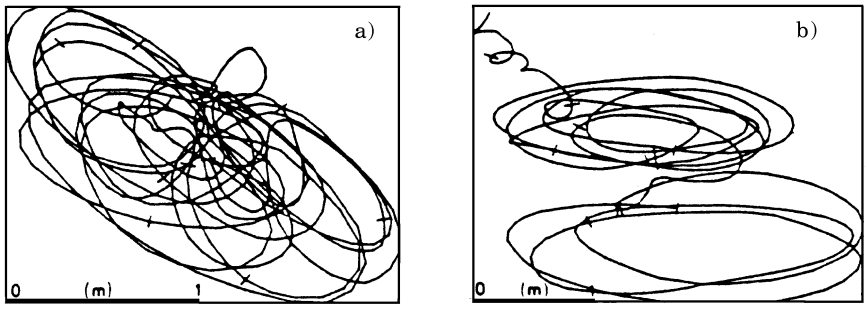

Fig. 21. – Orbital motion during a) wind generation and b) swell conditions (after Cavaleri and Zecchetto, 1987).

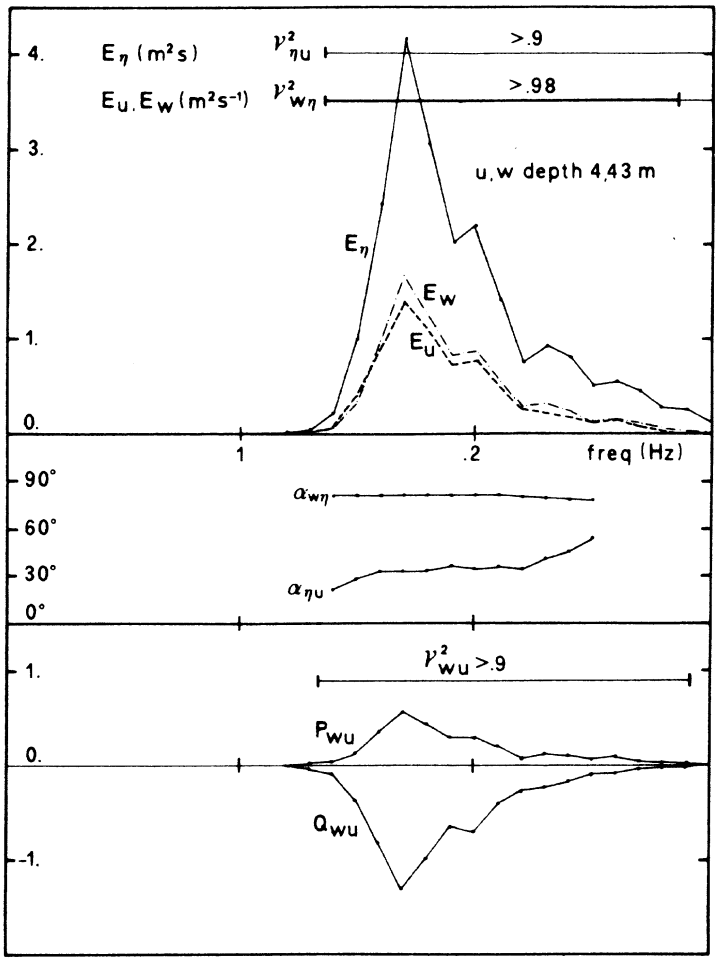

Fig. 22. – Results for a record taken under active generation conditions. E_η, E_u and E_w are spectra of η, u and w (see fig. 19 for their definition), and $\alpha_{\eta,u}$, $\alpha_{w,\eta}$ are the phase of u and w with respect to η. The cospectrum and quadrature spectrum between u and w are shown in the bottom panel. Frequency ranges are indicated where coherence $\gamma^2 > 0.9$. The thicker line means $\gamma^2 > 0.98$ (after Cavaleri and Zecchetto, 1987).

frequency end of the spectrum till 60° in the high frequency tail. The cross spectral values between u and w, in the lowest part of the figure, follow accordingly, with large values of the co-spectrum, consistent with the orbital inclination shown in fig. 21. Note that all the reported results correspond to signals with a square coherence larger than 0.9, which excludes any doubt on possible external reasons for the findings.

Inspection of the original time series is quite enlightening in regard to the time sequence of P. Figure 23 displays a short section of the same record used for the two previous figures. We see clearly that the vertical flux of horizontal momentum, *i.e.* its injection in the lowest layers, does not happen with continuity, but in short bursts associated to the steepest waves. This is reflected in fig. 21a in the different inclination

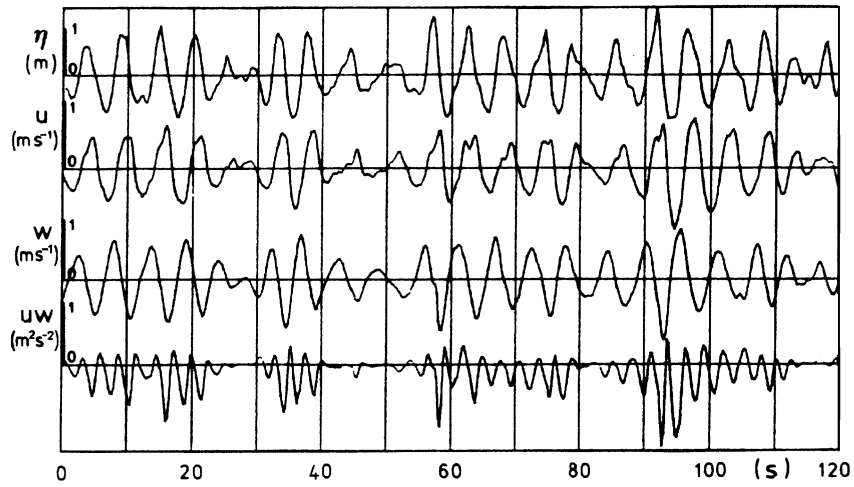

Fig. 23. – A 120 s time sequence of η, u, w and uw from the same record used for fig. 22 (after Cavaleri and Zecchetto, 1987).

of different sections of the orbital trace. More specifically, we can look at the correspondent scatter diagram between $\overline{uw}$ and H_s. Figure 24 shows clearly the relationship between the two quantities.

The results change completely when we consider swell conditions. A remarkable record was obtained in March 1979, when, following an almost four metre peak sirocco storm, a heavy pure swell, gradually decreasing from 3.5 m to low values, lasted for

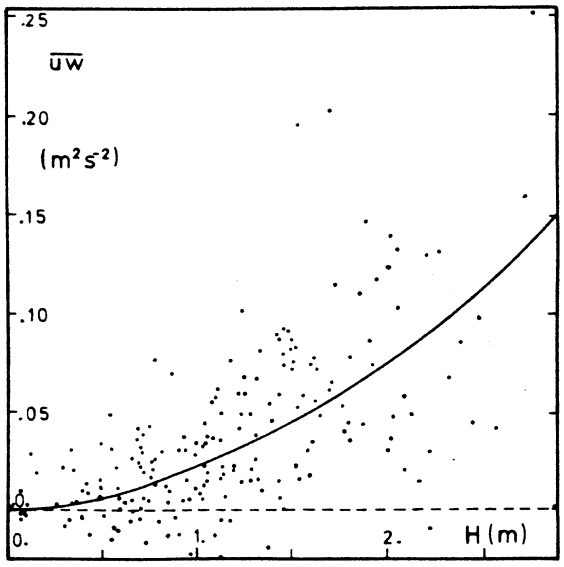

Fig. 24. – Scatter plot of zero-upcrossing waves of height H and average $\overline{uw}$ (see fig. 23). The curve represents the least squares fit of $\overline{uw} = aH^b$ (after Cavaleri and Zecchetto, 1987).

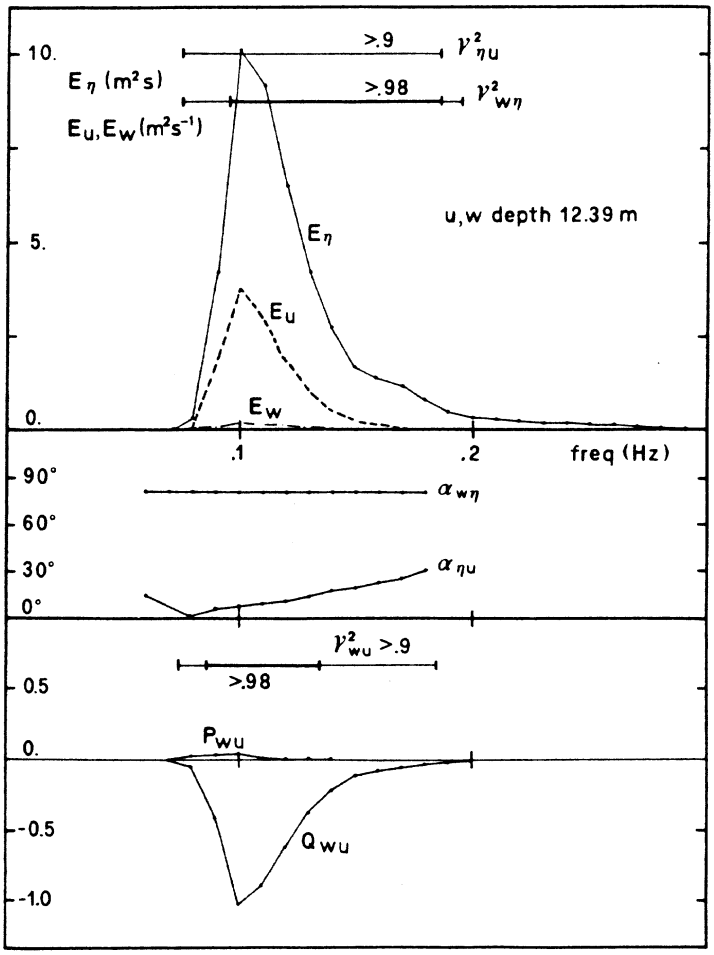

Fig. 25. – As fig. 22, but for a record taken during heavy swell conditions (after Cavaleri and Zecchetto, 1987).

about 12 hours. One example of the corresponding spectra is given in fig. 25. There is some phase shift with respect to theory in the high frequency range, but, when combined with the actual spectral energy, the co-spectrum is virtually nil. The best comparison with the generation conditions is probably given in fig. 21, where panel b) shows the orbits under swell, that contrast markedly with the inclinations present in panel a).

The conclusive result is that, under conditions of active generations, the Reynolds stresses, *i.e.* the input of momentum into the lower layers is much larger than expected by theory, by almost two orders of magnitude. No explanation of this evidence has been given till now. The problem is fully open.

10·3. *Measurement of directional spectra.* – Both the outputs from the wave kinematics system (described in subsect. **10**·2) and the three pressure transducers

fixed at three legs of the tower (subsect. **10**·1) have been used for routine evaluation of the directional distribution of energy in the spectrum. The routine analysis has been done for a long time following the classical method of Longuet-Higgins *et al.* (1963), then substituted by the more recent method by Kuik *et al.* (1988). It should be noted that the above methods do not provide a full directional distribution of energy for each frequency band, but rather some summarizing parameters like mean direction θ_m, directional spread, skewness and kurtosis. The method of Kuik *et al.* (1988) has the advantage of providing also an estimate of the confidence limits of the results.

The results, obtained in all the wave conditions possible in the area, have been used for a long-term validation of the results from both the third generation WAM wave model (Cavaleri *et al.*, 1989) and the first generation model VENICE (Cavaleri and Malanotte Rizzoli, 1981). The former is an advanced third generation wave model widely used, and described in subsect. **10**·5. VENICE is a ray refraction model, including wave generation and dissipation, developed for specific use within limited basins with a shallow bathymetry. In particular, the results from the directional analysis have been used to verify the refraction imbedded into the model.

The capability of measuring the directionality of wind waves is relevant in the Northern Adriatic Sea (fig. 1). When a low pressure centre approaches the area from the West, the typical meteorological situation implies a strong North-East wind in the northern part of the basin and a South-East sirocco in its central and southernest sections. In Venice this situation is named *bora scura* (dark bora), because of the heavy rain that is often associated to it. For our present interests the relevant fact are the cross sea conditions that are present in the northern section, with long waves from South-East and short steep breaking waves from the North-East direction. In these conditions the tower, and the output of the wave models validated through its results, have been the input to all the coastal models studying the local evolution of waves, currents and sea level. In particular, the directional resolution has been a key element in providing the correct input to the set-up model described in subsect. **9**·3.

In some special cases a more sophisticated approach to the evaluation of directional distribution has been used, following the variational method suggested by Long and Hasselmann (1979). Unlike the traditional approach, this method does not imply a drastic smoothing of the directional distribution. It is not used in the routine analysis because of its heavy computational requirements. In particular, starting from the data out of the wave kinematics system, it has been used to verify the lack of any significant reflection from the tower legs, a necessary information for the correct interpretation of the data, particularly about the Reynolds stresses (see subsubsect. **10**·2.2).

10·4. *White capping.* – In the highly studied subject of wind waves, white capping, the surface breaking of waves in deep water, stands as a solitary rock against a full consistent understanding of the process. The strong experimental and theoretical efforts of the 1970s and 1980s led to a wealth of results, enlightening the processes of wave generation, bottom friction, nonlinearities, etc. This led to the formulation of the third generation wave models (WAMDI Group, 1988; Tolman, 1991; Komen *et al.*, 1994, among others), where, however, only the availability of measured data allowed the closure of the problem.

The difficulty of studying the wave breaking stems from the characteristics of the process, that is intermittent, scattered in space, with single events highly concentrated in space and time. The only satisfactory theoretical formulation was given by Hasselmann back in 1974 (see reference) in statistical terms. After a quarter of a

century, no one has been able to suggest something more conclusive, and his formulation is still the one used in present wave modelling. The point is that the Hasselmann formulation, used also in third generation modelling, leaves two constants undefined, which are then established on the base of the overall energy balance in a growing sea (Komen *et al.*, 1994). This approach, still probably the best one presently possible, is not without risk. The expression of breaking considers only the energy present in the one-dimensional frequency spectrum, regardless of its directional distribution, and without consideration of the wind, which whoever has been at sea during a storm realizes as an important factor in establishing the breaking conditions.

It is clear that there is still a lot to do in this direction. As a contribution, Cavaleri and Lionello (1991) have analysed in detail some records from those available from the system described in subsect. **10**·2. Focusing on the surface profile, the related time series, taken at 4 Hz frequency with a resistance wave gauge of one centimeter diameter, have been high pass filtered. The resulting time series and its envelope, shown in fig. 26, have been cross-spectrally analysed *vs.* the original record. The envelope spectrum shows some peaks in the low frequency range, likely connected to wave grouping, plus a peak coincident with that of the dominant field. However, the interesting result is the relative phase between the envelope peak and that of the dominant wave, the former being ahead of about 30 degrees. This locates the short waves just ahead of the crests, a result qualitatively detectable also in the original record.

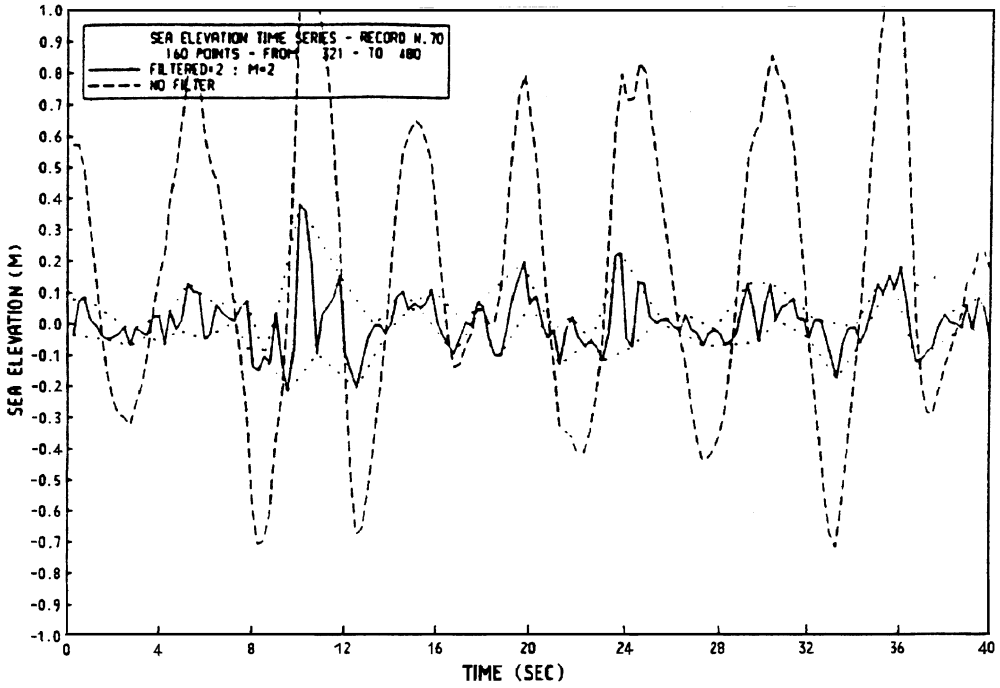

Fig. 26. – Surface profile during active generation conditions. Dashed line = original record, continuous = filtered record, dotted = envelope of filtered record (after Cavaleri and Lionello, 1991).

This result contrasts markedly with those obtained during dominance of swell, *i.e.* in the absence of wind. In these cases, granted the lower level of energy, the above phase shift disappears, with short waves concentrated around the crest of the dominant waves. Two logical possibilities are immediately suggested, one associated to the different level of energy in the two situations, the other one to the absence of wind when in swell conditions. The first hypothesis is immediately discarded when noting that swell can be higher than wind waves (think of the first stages of generation starting from a flat sea). Rather, the relevant factor is the steepness. However, it should be noted that waves in deep water break at a steepness much lower than expected from theory. Waves under active generation conditions have an average slope (H_s/L, with L the wavelength) of about 4%. Besides, steep waves in deep water exist only under the influence of wind. On the whole, everything suggests the relevant role of wind in the process of breaking. However, no sound theory has yet been proposed.

Another series of records taken from the tower (Sturaro, 1994) has shown well the characteristics of breaking. The records have been taken with a very thin resistance gauge and with a high sampling rate (20 Hz). This has allowed the extension of the analysis to a higher frequency range. Till the limits of reliability of the instrument, the spectra have been found to decrease as f^{-4}. However, notwithstanding the useful results, the spectral analysis is not the best tool to study the wave breaking. One of the basic hypothesis for a meaningful spectrum is the stability of the sea conditions during the record. This is exactly the opposite of the breaking, that, as mentioned above, is characterized by intermittency and single events highly concentrated in space and time. A better tool, at least for some aspects of the problem, is provided by the wavelet analysis (see Daubechies, 1992, and Koornwinder, 1993). For our present interest the key characteristic of this tecnique is its capability to analyse very short sections of a record, providing time series of the energy present in each frequency band. The interesting point is that this offers an objective method to identify along a record a breaking event. Weissman *et al.* (1984) have proposed a general method for this. Focusing attention on the energy E in the 6 to 10 Hz frequency band, a breaker is identified when the three following conditions are simultaneously satisfied: 1) E larger than a given threshold, 2) the peak of E happens close to the main crests, 3) $(E - \overline{E}/E_\sigma > 8$, with $\overline{E}$ and E_σ, respectively, mean and variance of the E time series.

A good example of the efficiency of this approach is given in fig. 27. The analysis refers to a section (60 seconds) of a record taken during mild generation conditions and with low wave height ($H_s \simeq 0.4$ m). The time evolution of the energy in the various bands shows continuous variations, with a well defined peak after about 600 units ($\simeq$ 30 s). The peak corresponds to an evident sharp peak in the surface profile (at the bottom in the figure), that we can, also at a qualitative analysis, classify as a likely breaking event. The sharp increase in energy at the various high frequency bands is associated to the grouping of the small waves close to the crest and to the discontinuity that is present here. From the time perspective, this result is confirmed by suitable filtering of the original signal and by its subsequent decomposition into low and high frequency parts, to show clearly the concentration of high frequency components on the large wave crests.

These results are only a hint of the exploration that is still possible and necessary to understand the physics of white capping. However, they are a nice example of the direction in which we have to go. A good understanding of the basic process is a necessary condition before a satisfactory, self-consistent theory can be formulated.

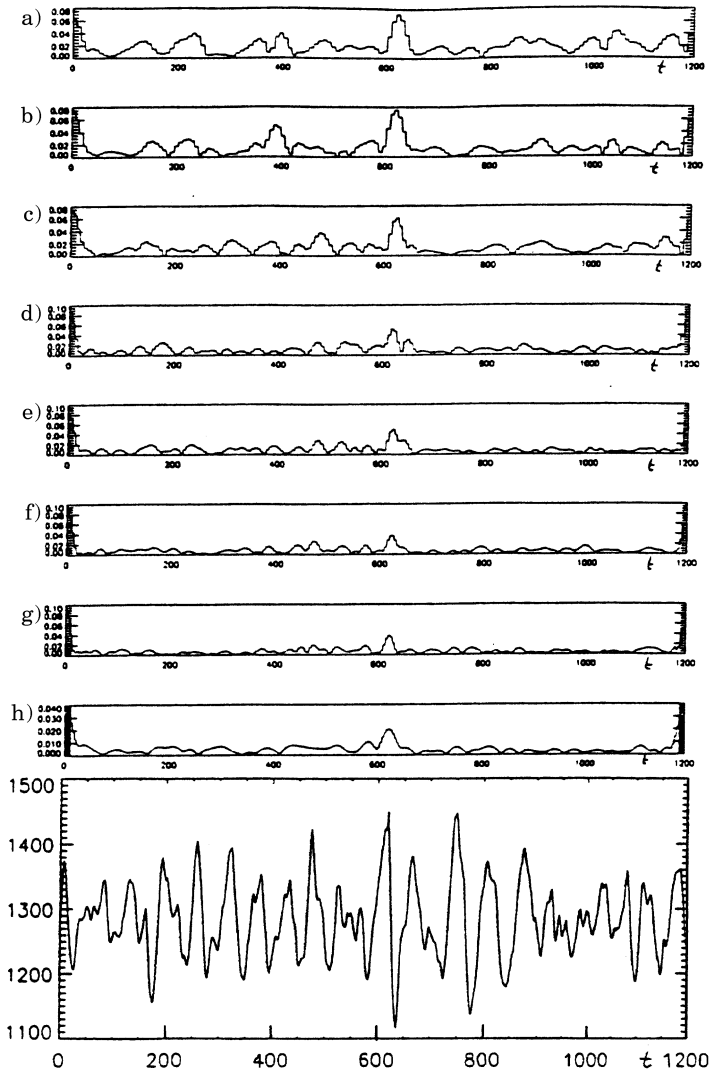

Fig. 27. – Energy content in the various frequency bands during a breaking event. The bottom diagram shows the surface profile. 20 units = 1 s. Vertical scale is in mm. Frequency intervals from top to bottom: a) 4.3–4.8 Hz, b) 4.8–5.3, c) 5.3–5.9, d) 5.9–6.6, e) 6.6–7.3, f) 7.3–8.9, g) 8.9–9.0, h) 9.0–10.0 (after Sturaro, 1994).

10˙5. *Long-term hindcast.* – In subsect. 8˙3 I have described a long-term hindcast of the wind fields on the Adriatic Sea. It was only natural to use this piece of information to carry out a similar hindcast for the wave conditions in the basin. At this aim Bertotti *et al.* (1996) made use of the wave model WAM, an advanced third generation model developed as a cooperative effort by a group of the major experts in the field. The model is amply described in the literature (see the two master references WAMDI Group, 1988; Komen *et al.*, 1994), and implemented on an operational basis at most of

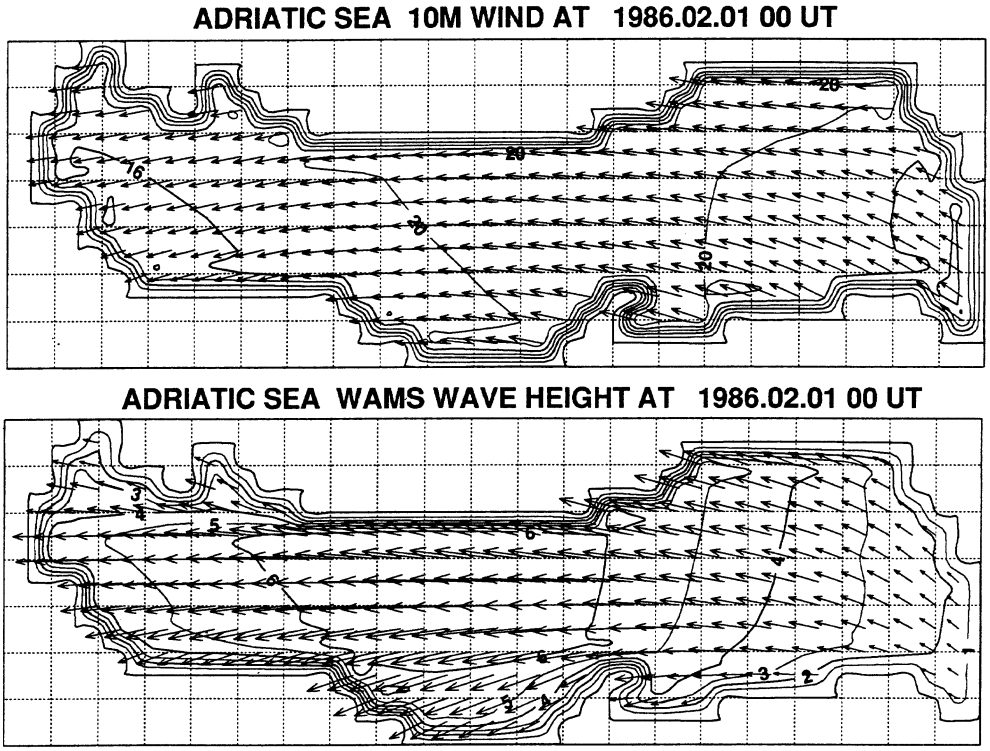

Fig. 28. – Wind and wave fields in the Adriatic Sea at 00 UTC 1 February 1986. Arrows indicate the wind (wave) direction, with a length proportional to the wind speed (wave height). Isolines at 4 m/s and 1 m interval, respectively. The North is to the upper left.

the major meteo-oceanographic centres in the world. On a very essential basis, the model solves on a geographical or Cartesian grid the energy balance equation that determines the energy present at each time and location on all the wave components. The so-called two-dimensional spectrum is discretized into a finite number of components, between 300 and 600, specified in frequency and direction. Given the geometry of the basin (up to the whole world) and the input wind fields, the model provides the time evolution of the spectrum at all the points of the grid. The integration of the spectrum provides more compact information, like the frequency spectrum, the significant wave height H_s, the mean and peak periods T_m, T_p, the mean direction θ_m, etc.

To decrease the overall number of grid points and for a better representation of the coast, the grid has been chosen with 20 km resolution, aligned with the main axis of the basin. The hindcast has been done from January 1980 till December 1989. Figure 28 provides an example of wind and wave fields during a severe sirocco storm.

The results of the hindcast have been validated *vs.* the available wave data recorded at the oceanographic tower (see subsect. **10**˙1). An example is shown in fig. 29, with a 40 day intercomparison, for both wave height and period, between the hindeast and the measured values at the tower location.

The overall resulting scatter diagram is shown in fig. 30. The results are pretty

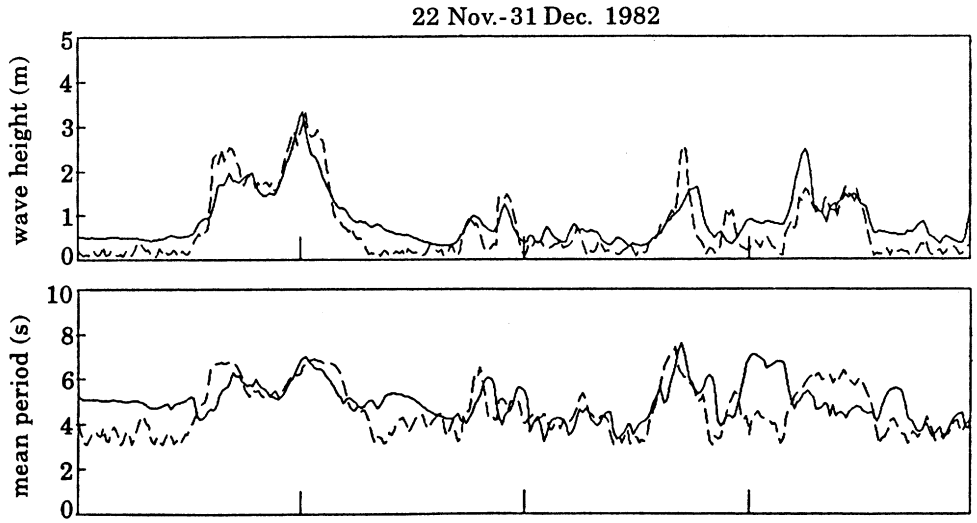

Fig. 29. – A 40 day comparison between modelled (continuous line) and measured (broken line) wave height and mean period at the tower in the Northern Adriatic Sea (see fig. 1 for its location).

good, with a bias of 0.1 m and a rms error of 0.5 m. The validation is twofold. First, it validates the WAM model, but this is no news. More important, it validates at the basin scale the results of the wind hindcast. The key point is that, because of the different structure and the different level of complexity of the physics involved, an advanced

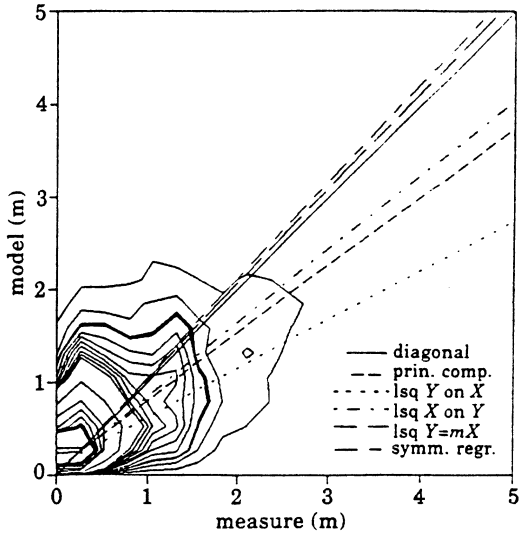

Fig. 30. – Scatter diagram between measured (X, horizontal) and modelled (Y, vertical) wave height in the Northern Adriatic Sea. The straight lines represent different fits to the data. The step between adjacent isolines of density increases towards the peak of the distribution. The two thick isolines include 50% and 90% of the cases, respectively (after Bertotti *et al.*, 1996).

wave model, like WAM, is a much more accurate instrument than a meteorological model. Therefore, when, as in the present case, a hindcast is produced working with a wind and a wave model in series, any drastic error in the final results is likely to be associated to deficiencies in the input wind fields. As a matter of fact (see Komen *et al.*, 1994), the check of the wave model results is one of the best pieces of information to judge the quality of the wind fields. It follows that good final results are very good indicators of a high quality input wind. Therefore, fig. 30 implicitly validates the wind hindcast described in subsect. 8·3. The present result is much more significant than the validation at the tower *vs.* the locally recorded wind data. Waves are an integrated effect, in space and time, of the driving wind field, memorizing with their characteristics those of the input field. Hence good wave results at one location implicitly tell of good quality wind in space and time.

The long-term hindcast allows a full characterization of the climate in the Adriatic Sea. The basin is subjected to two dominant winds, the bora, a cold, gusty wind blowing from North-East, and sirocco, a south-easterly wind often associated to low pressure and cyclogenesis in the Tyrrhenian and Ligurian Sea. See Cavaleri *et al.* (1997b) for a full characterization of the basin. The bora can have two different origins. If associated to a high pressure zone located on Central Europe, the bora, enhanced also by the catabatic effect, brings cold, energetic air on the Northern Adriatic, and occasionally on the whole basin. It is called *bora chiara* (clear bora) because of the clear weather associated to it. On the contrary, when associated to the sirocco that turns to the left North of the Po River exit (see fig. 1a), it is called *bora scura* (dark bora) because often characterized by rainy conditions.

The different physics of the two kinds of storms is conveniently reflected into their different statistics. Table I shows the H_s, T_m combined distributions for bora and sirocco storms, respectively. To give the corresponding one-dimensional distribution and the overall summation, normalized to 1000, they need to be integrated on the corresponding variables. The clustering of the bora waves toward lower values, and the tendency of the sirocco ones toward longer waves is evident.

10·6. *Extreme wave heights in the Northern Adriatic Sea.* – The results from the long-term hindcast described in the previous section have been used for an estimate of the possible extreme values. Given their substantially different characteristics, different statistics have been evaluated for bora and sirocco. The two extreme distributions are shown in fig. 31. In the diagram each line indicates the probability, in percent, that H_s (horizontal) larger than a given value will appear within a specified number of years (vertical). For instance, the diagram indicates a 10% probability of encountering a sirocco storm with $H_s > 6$ m within about 40 years. Note that the distributions are not given for periods shorter than ten years. Bertotti *et al.* (1996) justifies this pointing out the climate variability within this range, and the consequent lack of reliability of estimation of extremes.

A different approach for a similar estimate of the extremes was followed by the Consorzio Venezia Nuova (New Venice, the official authority in charge of the extensive studies on the Venice lagoon). Following the typical wind distribution in the area, Hurdle *et al.* (1995) identified three main storm incoming directions, namely North-East (bora), East (levante), and South-East (sirocco). While for the first two directions the area of study extends till the opposite main land (see fig. 1), to avoid a large extension of the grid in the sirocco direction, this was cut at 100 km South of Venice. A typical sirocco storm is generated along the whole fetch of the basin.

TABLE I. – *Density combined distributions of H_s and T_m, for bora (upper panel) and sirocco (lower panel) storms ($\times 1000$). Numbers are approximated to the nearest integer (after Bertotti et al., 1996).*

T_m (s)	Significant wave height (m)											Σ
		0.5	1.0	1.5	2.0	2.5	3.0	3.5	4.0	4.5	5.0	
2	5	1	0	0	0	0	0	0	0	0	0	3
3	353	518	26	0	0	0	0	0	0	0	0	449
4	95	249	326	93	6	0	0	0	0	0	0	384
5	0	1	31	126	95	31	2	0	0	0	0	142
6	0	0	0	3	4	17	11	6	2	0	0	21
7	0	0	0	0	0	0	0	1	0	0	0	1
8	0	0	0	0	0	0	0	0	0	0	0	0
9	0	0	0	0	0	0	0	0	0	0	0	0
10	0	0	0	0	0	0	0	0	0	0	0	0
Σ	453	768	383	221	104	48	14	6	2	0	0	1000

T_m (s)	Significant wave height (m)											Σ
		0.5	1.0	1.5	2.0	2.5	3.0	3.5	4.0	4.5	5.0	
2	1	0	0	0	0	0	0	0	0	0	0	1
3	264	168	3	0	0	0	0	0	0	0	0	217
4	805	251	54	7	0	0	0	0	0	0	0	558
5	30	177	45	31	10	1	0	0	0	0	0	147
6	0	66	27	9	7	5	2	0	0	0	0	58
7	0	7	18	3	1	1	1	0	0	0	0	15
8	0	0	3	2	0	0	0	0	0	0	0	3
9	0	0	0	0	0	0	0	0	0	0	0	1
10	0	0	0	0	0	0	0	0	0	0	0	0
Σ	1099	669	149	53	18	7	3	0	1	0	0	1000

Consequently, suitable boundary conditions had to be evaluated. These were derived from an empirical relationship between the wind recorded at the tower and the wave data available for some years, more or less at the border of the grid, close to the Italian coast.

The surge level was similarly derived from a relationship between surge values and wave heights derived from joint probability analysis of the available data. For the extreme sirocco storm the surge was fixed at 1.60 m.

For the derivation of the extremes, Hurdle *et al.* (1995) made use of the HISWA model (Holthuijsen *et al.*, 1989), that was carefully calibrated on the base of the wind and wave data obtained from the tower. The extreme wind speed then used to derive the extreme wave heights (HISWA assumes full uniformity in space and stationarity in time) was obtained from 25 years of data from the Lido island, between the lagoon and the sea (see fig. 1b), calibrated on the base of four contemporary years of data from the tower. For bora storms the wind speed was increased of 10% with respect to the

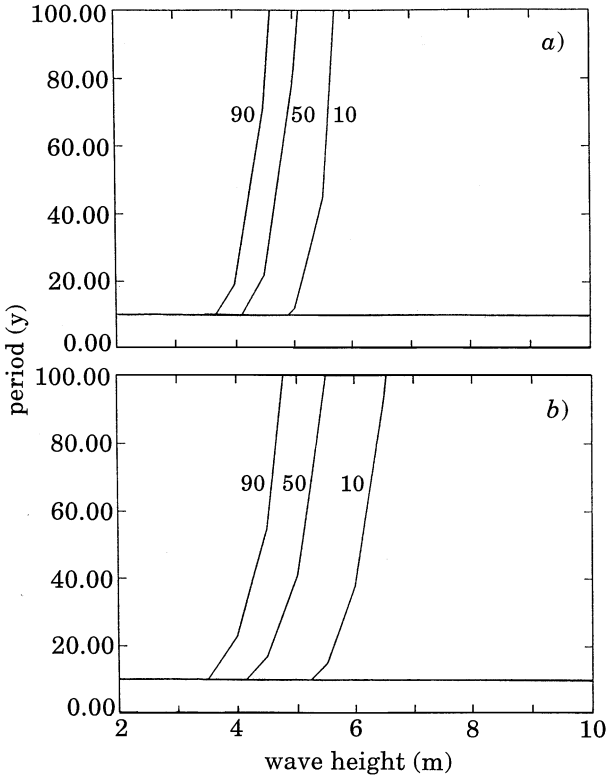

Fig. 31. – Statistical distribution of the peak wave height in bora (upper panel) and sirocco (lower panel) storms in the Northern Adriatic Sea. The lines show the relationship between wave height (m), exceedance probability (%, indicated close to each line) and considered period (years) (after Bertotti *et al.*, 1996).

nominal value to allow the extra growth due to instability, hence gustiness. Further discussion on the last subject is found in subsect. **10**˙10.

Besides the careful calibration of the HISWA model, an extensive study was done on the sensitivity of the results to the different parameters present in the model. This point is better discussed in subsect. **10**˙13.

The sirocco significant wave height with ten year return period turns out to be close to 4 m, growing to almost 5 for 100 years. These figures are remarkably similar to those derived from fig. 31 from Bertotti *et al.* (1996). It is certainly reassuring that two completely different approaches, one fully physical and without any tuning (the WAM model), the other deeply based on calibration (HISWA), provide more or less the same answer to the crucial question of the extreme wave height values.

However, it is somehow disturbing that, in contrast with the previous results, two major storms, 4 November 1966, 22 December 1979, with maximum H_s higher than 6 m (both from the hindcast, the latter also by the experimental evidence of the damages to the tower) occurred within the last 30 years. In the Gumbel extremal distribution for sirocco storms corresponding to fig. 31, these two extremes would appear as complete outliers. As such, they lead to very large confidence limits in the distribution (see

Borgman, 1983 and Efron, 1982, for their evaluation). If the two storms are neglected, the confidence limits, *e.g.* for 90% occurrence probability, narrow down to a much more limited range, of the order of 10% at 50 year elapsed time, a substantial indication of the self-consistency of the *reduced* data set. In this statistics, corresponding to what shown in fig. 31, the two outliers turn out to have a return time of the order of 200-300 years. This return time is consistent with the return time derived for the associated surges (see MAV, 1992, 1997).

However, I feel somehow uneasy with this conclusion. To accept it implies to accept that we happened to witness within 20–30 year period two events, whose single probability to occur within such a time interval is more or less 10%. In other words, based on the obtained distribution, we have witnessed a sequence of events with an overall 1% occurrence probability. I find this not easy to digest. I wonder if there is some physical process, some nonlinearity in the atmosphere, that we have not yet understood, and that in certain conditions can trigger a much larger event, that does not scale with the regular ones.

The question of how to deal with outliers in an extremal distribution is a classical one, and I do not have a general reply, if this exists at all. I would strongly appreciate any constructive comment by the readers on this point.

10·7. *Coupled models.* – While single models concerning tide, set-up or wave prediction, are regularly used, there is a growing tendency for a more complete approach to the problem. The reason is that the different processes, described by the various models, are not independent of each other. The interactions become more and more intense while we approach the shallow water zone and the shore. Consequently, if we want accurate predictions in these areas, we have to move to coupled models, *i.e.* the various processes must be modelled contemporarily, taking into consideration the reciprocal effects. A substantial step in this direction has been taken for the Adriatic Sea by Lionello (1995). He attacked the problem of fully characterizing the oceanographic conditions in front of the Venetian littoral, considering the effects of tide, set-up, circulation and wind waves. He started from the WAM wave model with $(1/6)^\circ$ resolution (Komen *et al.*, 1994; a compact description has been given in subsect. **10·5**) and a shallow water, primitive equations, free surface, barotropic hydrostatic circulation model (Simons, 1972) for the overall circulation and the evaluation of the storm surge. The model solves the two momentum and the continuity equations, providing the overall transport and the sea level at the knots of a grid covering the whole Adriatic Sea with $(1/12)^\circ$ resolution. There is hardly any effect of current on waves in deep water, the velocities being here too low to produce any appreciable refraction effect on the wave field. However, there is an evident influence of waves on the current field through their modulation of the driving surface stresses (Janssen 1989). While, according to the traditional approach, the surface drag coefficient C_D is kept constant, Janssen pointed out that the different stages of evolution of the wave spectrum correspond to different surface roughness, and consequently to different values of C_D. As the stresses that generate the waves are the same that drive the circulation, it is clear that the wave field with its presence affects the circulation, hence the storm surge. The input wind fields have been provided by the limited area meteorological model BOLAM (Buzzi *et al.*, 1994).

The results at the tower position, like sea level, circulation, and wave spectra, have been used as input to a complex coastal model, where the coastal current, the evolution of the wave field, the sea level profile are evaluated while approaching the coast.

The correctness of this input information has been verified *vs.* the data recorded at the tower. Figure 32 shows in the upper panel the comparison between the measured and the hindcast H_s at the tower. The bias is negligible, down at 5 cm. A similar comparison shows a 0.12 m bias for tide. Implicitly, these results validate also the input wind fields.

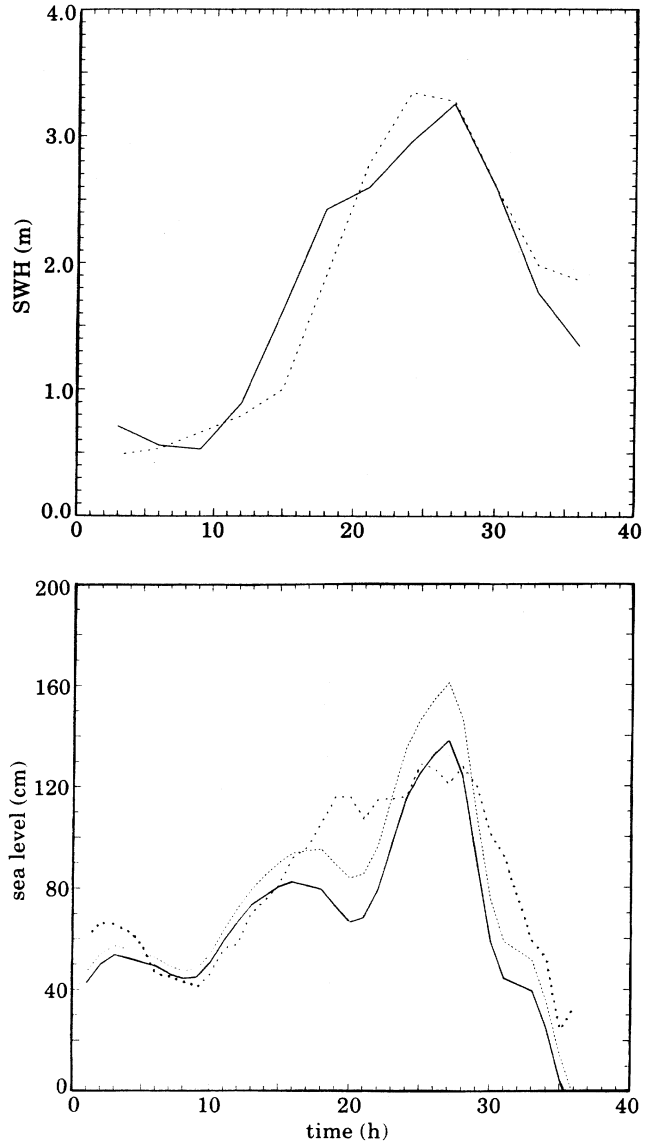

Fig. 32. – Upper panel: evolution of the significant wave height at the tower position (see fig. 1b) during the event of 9-10 December 1990. Time in hours is evaluated from the beginning of simulation. Continuous line = model results, dashed line = measured data. Lower panel: as above for tide at the Lido entrance; the dotted line shows model prediction at the shore (after Lionello, 1995).

The coastal model extends till 11 km offshore, assuming steady state and homogeneity in the cross shore direction. The sea level profile is evaluated as superposition of the storm surge and the set-up, whose effects become relevant when the waves begin to break because of limited depth. Its effect is made evident in the lower panel of fig. 32, showing the level at the end of the Lido jetty (recorded and hindcast) and the corresponding one at the shore. At the peak of the storm more than 20 cm differences are present between the two points. In this case the coastal set-up is not relevant for the tide in the lagoon (given the maximum H_s, the set-up begins inshore with respect to the entrance between the jetties). However, it is relevant for the coastal processes, *e.g.* the erosion of the beach.

A clear view of the overall situation is offered by fig. 33, showing how the various quantities, bottom profile, wave height, set-up, wave direction, long- and offshore current components, vary along a line perpendicolar to the shore. Note the increase of set-up, corresponding to the sudden decrease of wave height, and, in general, the dramatic changes that take place within the last two kilometers, when waves begin to break. It is worthwhile to point out that during the most severe storms this distance expands dramatically. We have reasons to believe that, during the historical storm

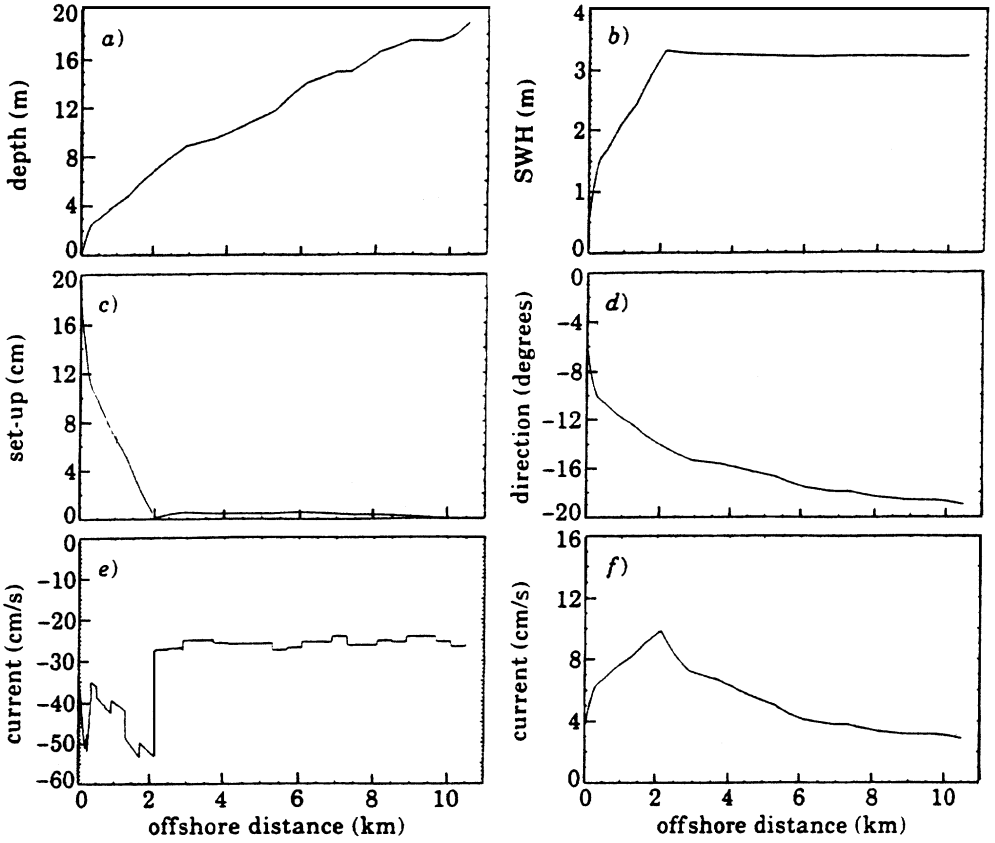

Fig. 33. – Coastal prediction in front of the Venetian littoral. a) bottom profile; b) wave height (m); c) set-up (cm); d) angle between cross-shore and mean wave direction (degrees); e) long-shore current (cm/s); f) offshore mean current (cm/s) (after Lionello, 1995).

of 22 December 1979, waves were such that the set-up was present already at the tower.

10·8. *Calibration of* ECMWF *wind.* – In subsect. 8·2 I have discussed the validation of the surface wind out of meteorological models on the base of wind data measured in the middle of the sea. In particular, the ECMWF wind was found to be on the average underestimated by about 50% at the tower position. However, I had pointed out that this is a local value, and that the corresponding figure was likely to change throughout the basin. A more general judgement on the quality of the overall wind fields can be obtained by using them to drive a reliable wave model, and comparing the results with measured wave data at different positions throughout the basin. As I have pointed out in subsect. **10**·5, waves are an integrated effect in space and time of the input wind fields. Using an advanced wave model, like WAM (Komen *et al.*, 1994), the quality of the results depends essentially on that of the input wind. Besides, contrarily to wind, the measured wave data are not affected by coastal effects, and we can use for our comparison also data taken close to coast. So doing, we can obtain an estimate of the overall quality, not specific for each location, but this is already a drastic step ahead.

Following this line of action, Cavaleri and Bertotti (1997) selected in the Adriatic Sea 15 storms of different types and hindcast them using as input the ECMWF wind at ten metre height U_{10}. The H_s results were compared to the data measured at three different points, the tower plus two WAVEC buoys located at Pescara and Monopoli, on the Italian coast, respectively in the central and southern part of the basin. The result is shown in fig. 34a) and clearly indicates a substantial underestimate by the model. The overall consistent result was that, using as input the ECMWF wind, the wave heights in the Adriatic Sea turn out to be low by about 50%. However, the interesting point (not shown in the figure) was that the directions were generally correct, which

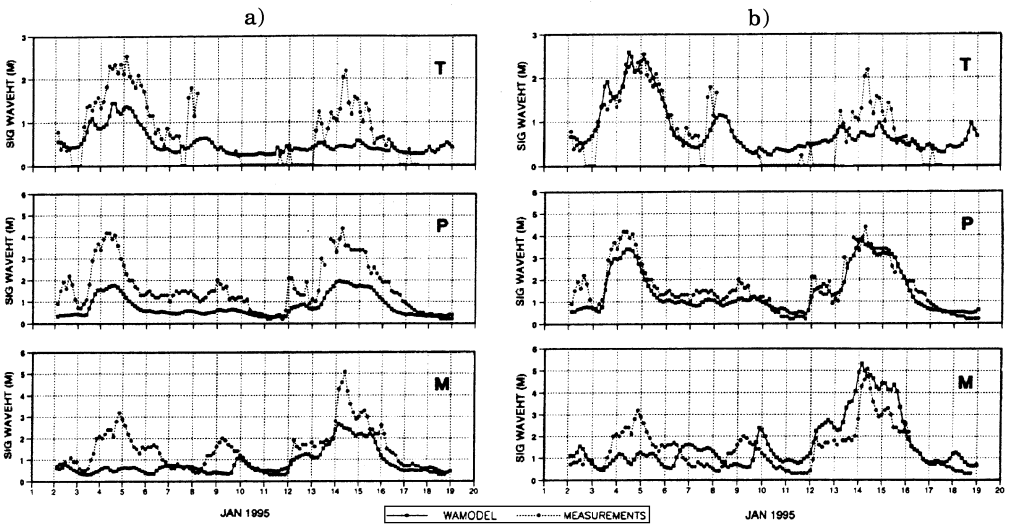

Fig. 34. – Comparison between measured (dotted) and modelled (continuous) wave height at the tower (T), Pescara (P) and Monopoli (M), respectively on the northern, central and southern Italian coast. a) using ECMWF wind; b) after calibration of the ECMWF wind (after Cavaleri and Bertotti, 1997).

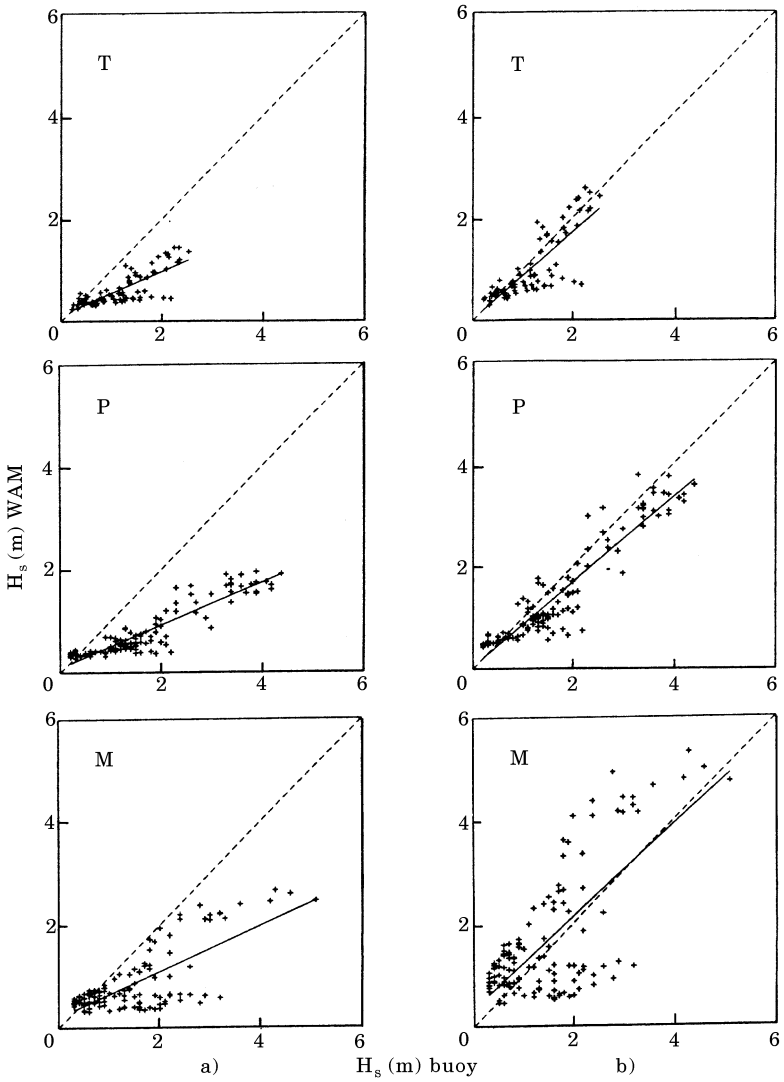

Fig. 35. – Scatter plots of the results obtained using the model wind a) without and b) with the wind enhancement (after Cavaleri and Bertotti, 1997).

suggests that the overall structure of the field was correct, but the modelled U_{10} were too low. This prompted a sequence of trials to find out if a suitable uniform wind enhancement α was enough to solve most of the problems. After some trials and errors α was determined as 1.5 (± 0.05). The derived results are shown in fig. 34b). The improvement with respect to the a) panel is evident. A better idea is obtained by considering the corresponding scatter diagrams in fig. 35. On the whole, the best fit slope of all the enhanced results has a slope of 0.99 with a rms value of 0.08.

A careful analysis of the results suggests that the enhancement factor should be a function of position and of the type of storm. However, Cavaleri and Bertotti (1997)

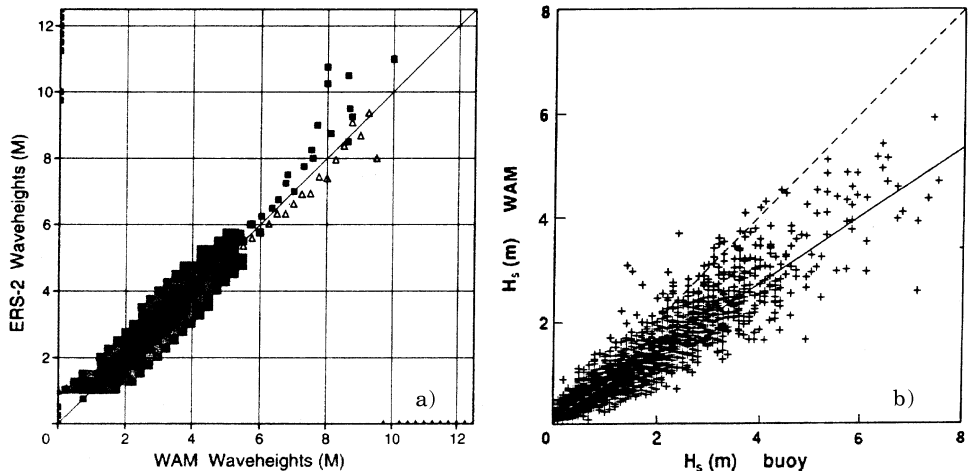

Fig. 36. – Scatter diagrams between modelled and measured wave heights. a) global; model on horizontal scale (after Janssen, 1997). b) Mediterranean Sea; model on vertical scale (after Pontes *et al.*, 1996). All the data are in metres.

point out the insufficiency of the present information for a more detailed analysis. Besides, they stress that $\alpha = 1.5$ is only a local value, at the scale of the basin, and it should not be used for other areas. However, there is substantial evidence that the quality of the surface winds from the global or large scale meteorological models seems to deteriorate when moving from the open oceans to the relatively small basins. So, while Janssen (1997) reports a bias of only 3 cm at the global scale with a best fit slope of 0.993 in the scatter diagram (see fig. 36), Pontes *et al.* (1996) report an understimate of the modelled H_s in the Mediterranean Sea varying from 10 to 30%, which suggests U_{10} to be low by 10-15%. A problem quantitatively similar to the Adriatic Sea is present in the Baltic Sea (personal communication by Kihmo Kahma).

On the whole, there is a strong indication that the quality of the surface wind deteriorates when we move to smaller basins. The problem is probably connected to the ratio between the dimensions of the basin and the grid resolution, and to border and orographic effects. In particular, a partial reason seems to be the smoothing of the surface fields associated to the horizontal diffusion introduced into the meteorological models for stability reasons. Cavaleri *et al.* (1997a) have clearly shown how its reduction enhances the peak of the fields. This is particularly true close to the coast, hence in the enclosed basins, because of the lowest wind speeds on land with respect to the sea.

Whichever the reason, a substantial underestimate of the wind speed seems to be the rule in the meteorological models, the smaller the basin the larger the underestimate. At present the only solution is to go to higher resolution, either with a limited area model focused on the area of interest, or, as expected to happen in the next few years, to drastically increase the resolution of the global models. The latter possibility should bring with it a drastic advance of the quality of the results in all the sub-basins of the world.

10·9. *Bottom friction.* – I have repeatedly mentioned in the previous sections extensive applications of the WAM wave model (Komen *et al.*, 1994) in the Adriatic Sea.

This model is built on a physical basis, *i.e.* the various processes that concur to the evolution of wind waves in the field are mathematically reproduced at the best of the present knowledge. According to different theories, different expressions may exist for the representation of a certain process.

While waves propagate in shallow water, the term representing the loss of energy by bottom friction becomes more and more important. The Northern Adriatic Sea, with its shallow bathymetry (the slope of the bottom is about 1/1000 for about 200 km towards South-East) and the availability of accurate wave measurements at the tower, offers a very good possibility for the verification of the bottom friction formulation in wave modelling. In WAM this is done following a linear approach derived from the JONSWAP experiment (Hasselmann *et al.*, 1973). Briefly mentioned, for each spectral component, specified in frequency and direction, the rate of loss of energy density F is expressed as

$$\frac{\partial F}{\partial t} = \alpha F \,, \tag{1}$$

where α is a coefficient that depends only on frequency and on the local depth. The basic assumption behind (1) is that the loss happens because of viscous dissipation in the laminar motion close to bottom. As in this case the loss scales linearly with velocity, also the derived expression is linear. In practice, in this respect the different wave components act independently of each other. The use of (1) provides results of different quality, with both under- and overprediction of the significant wave height H_s. In general, we find underprediction for low wave height, overprediction for large H_s; see, *e.g.*, Bows and Komen (1983).

The use of (1) is convenient for computer time and because, acting on a global scale, hence mostly in deep water, the bottom friction becomes a nonrelevant part of the physics. However, moving to shallow water, a more sound approach is required. The point is that the bottom boundary layer under a wave field is almost always turbulent, which implies that the loss should scale with the square of the velocity. In turn, this implies nonlinearity and that each wave component affects also the other ones. With respect to (1), two more sound approaches, based, respectively, on the nonlinear interactions and on eddy viscosity, have been proposed by Hasselmann and Collins (1968) and Weber (1989). Even if fundamentally different, these two approaches give similar results (Komen *et al.*, 1994).

Cavaleri and Lionello (1990) have done an extensive comparison between the linear and nonlinear approaches, comparing the results with the data recorded at the tower. A typical result is shown in fig. 37. It was a typical case of *bora scura* (see subsect. **10**˙3), with sirocco blowing along the Adriatic Sea, turning to bora in the northern part. On 1st December 1982 the wind dropped, leaving a long heavy swell moving towards the coast of Venice. The overprediction by the standard WAM formulation is evident. The reason for it is clarified in fig. 38, showing the rate of loss p according to linear (J) and nonlinear (N-L) approaches, as a function of depth and for two different wave periods. In practice, below a certain wave height J overestimates the loss, but it drastically underestimates it for heavy sea conditions. Of course, the opposite is true for the resulting wave height.

The physical explanation is connected to the average orbital velocity $\langle u \rangle$ at the bottom. The more shallow the water, the larger the wave height, and the larger becomes $\langle u \rangle$ with consequently stronger nonlinear effects. As shown in fig. 39, the

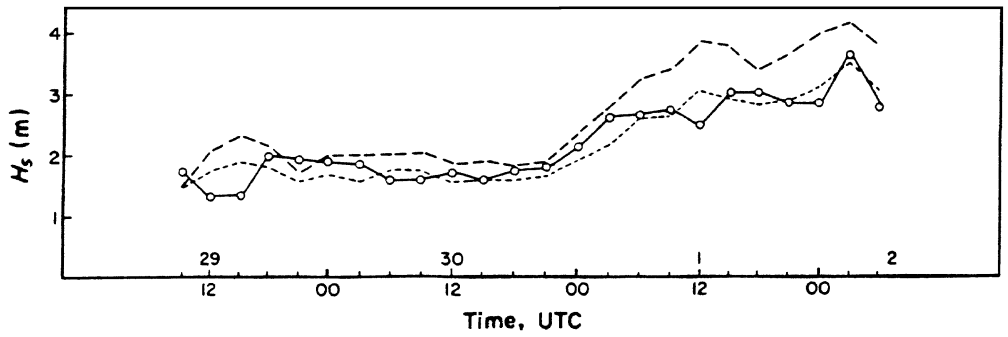

Fig. 37. – Time history of wave height H_s at the tower on 29 November–2 December 1982. Record (continuous line), standard WAM (broken), WAM with nonlinear H-C formulation for bottom friction (dotted) (after Cavaleri and Lionello, 1990).

consequences are felt more in the low frequency range, where, as in this case, there is a drastic loss of energy in the swell range (note the direction almost at cross angle with respect to the wind), while the remaining part of the spectrum maintains its energy, helped also by the local active generation.

The critical $\langle u \rangle$ value, for which the approaches are equivalent, varies between 14 and 18 cm/s, being weakly dependent on the directional distribution of energy in the spectrum.

10·10. *Wind gustiness—effects on ocean modelling.* – In subsect. 8·4, I have mentioned the wind gustiness and how different air-sea (in)stability conditions

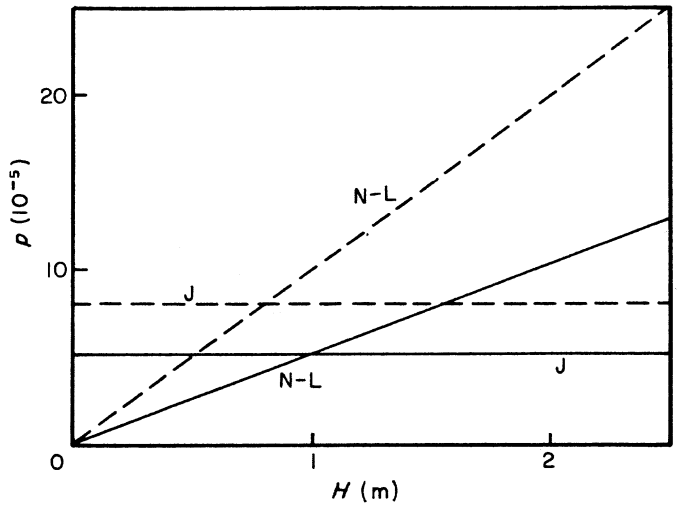

Fig. 38. – Dependence of fractional dissipation rate p on wave height H. Depth is 25 m. Swell period 9 (continuous) and 11 (broken line). Nonlinear (N-L) and linear (J) descriptions of bottom friction are considered (after Cavaleri and Lionello, 1990).

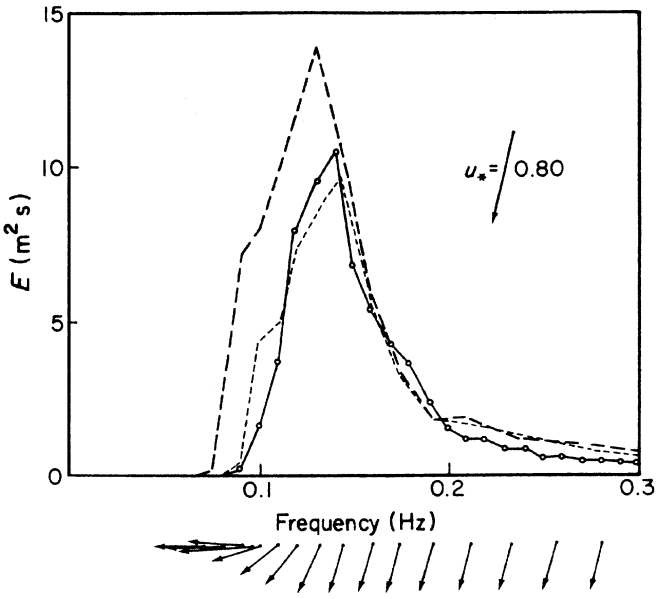

Fig. 39. – One-dimensional spectra at the tower (see fig. 1b for its position) at 15 UTC 1 December 1982. Measured data (continuous line), linear model (long dash), nonlinear model (short dash) (after Cavaleri *et al.*, 1989).

determine the level of turbulence in the lowest layers of the atmosphere. This has consequences on the wave fields.

During wave generation, the energy input by wind scales linearly with the friction velocity $U_\star$ (see Komen *et al.*, 1994). In turn, because of the direct effect of the wind on the surface drag coefficient, $U_\star$ scales with U_{10} with a power larger than 1. At the same time the analysis of high frequency wind records taken from the ISDGM oceanographic tower and during the HEXMAX experiment (Smith, 1988) have clearly shown a Gaussian distribution of the wind speed during each record taken with average speed U_{10}, the σ depending on the air-sea stability conditions. The combination of these two facts implies

$$\overline{S_{\mathrm{in}}(u)} > S_{\mathrm{in}}(\overline{u}), \tag{2}$$

i.e. in turbulent conditions the average energy input by wind is larger than with $\sigma = 0$.

A second, more effective process appears when the waves are well developed. At this stage their phase speed c approaches that of the wind. As the latter varies, there may be short periods during which $c > U_{10}$. Because the process opposite to generation, waves *pushing* the wind, is only marginally effective, the resulting rectification process implies again an incresed average input by wind with respect to the uniform wind conditions.

A detailed analysis of the above processes has been done by Cavaleri and Burgers (1992). The overall effect is shown in fig. 40, where the time evolution of the significant wave height H_{s} is represented as a function of time and of the σ level in the turbulent wind field. We see that a gustiness of 30% implies increases of H_{s} larger than 30%.

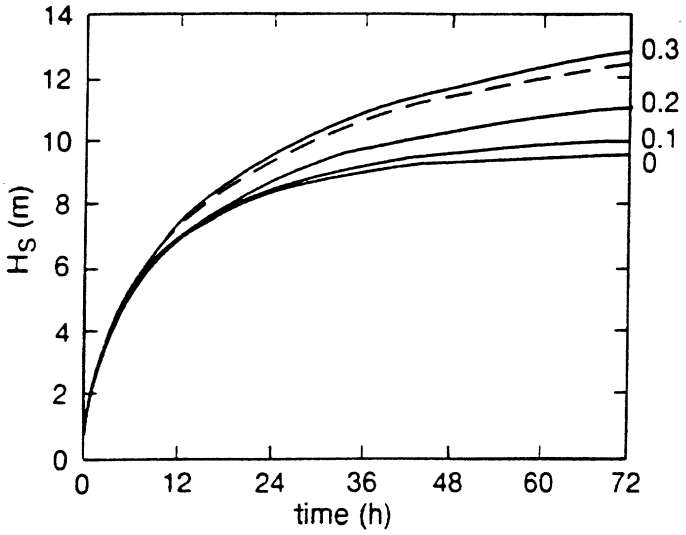

Fig. 40. – Growth curves of H_s under the same wind speed, but with different level of gustiness (after Komen *et al.*, 1994).

All this helps to explain why, in the standard applications of WAM using wind fields from the global meteorological models, we find a negative bias particularly in strong gusty storms. In the Northern Adriatic Sea, even using winds produced by limited area models and positively verified *vs.* the wind data from the tower, we have found a consistent underestimate of the obtained wave height. The underestimates are of the same order of magnitude as the enhancements shown in fig. 40. Similar conclusions have been reported for the Western Mediterranean Sea (Pontes *et al.*, 1996).

Evidence of the effect of gustiness has been supplied also by Komen *et al.* (1994) for a heavy Pacific storm affecting the Hawaii area, where a wave recording buoy was located. Figure 41 shows the comparison between model *vs.* recorded data without and with the introduction of wind gustiness in the WAM model. This has been obtained using a pseudo random variability of the input wind speed, the σ being determined from the air-sea stability conditions derived from the meteorological maps and a σ/air-sea stability relationship derived from the long-term measurements on the tower. The introduction of gustiness reduces the H_s bias of the model from $-$ 39 cm to 9 cm. The rms error is correspondingly reduced from 0.90 m to 0.70 m.

This limited reduction of the rms error follows the similar argument outlined for wind speed in subsect. 8·4. Even if with an attenuated response, the sea reacts to the turbulence in the wind field with similar oscillations. Consequently, because this wind variability is not present in the modelled input fields, the modelled time history of a storm is much smoother than the one we experience in the sea. It follows that the minimum rms we can aim to is simply the σ of the field, and there is no way we can go below this value.

The air-sea instability, hence gustiness, does not affect only the wave field, but also the storm surges. If we recall that the surface stresses that act on waves drive also the storm surge, it is obvious that gusty winds will lead to higher surges. The effect is here less evident because the surges in the Northern Adriatic Sea are associated to sirocco,

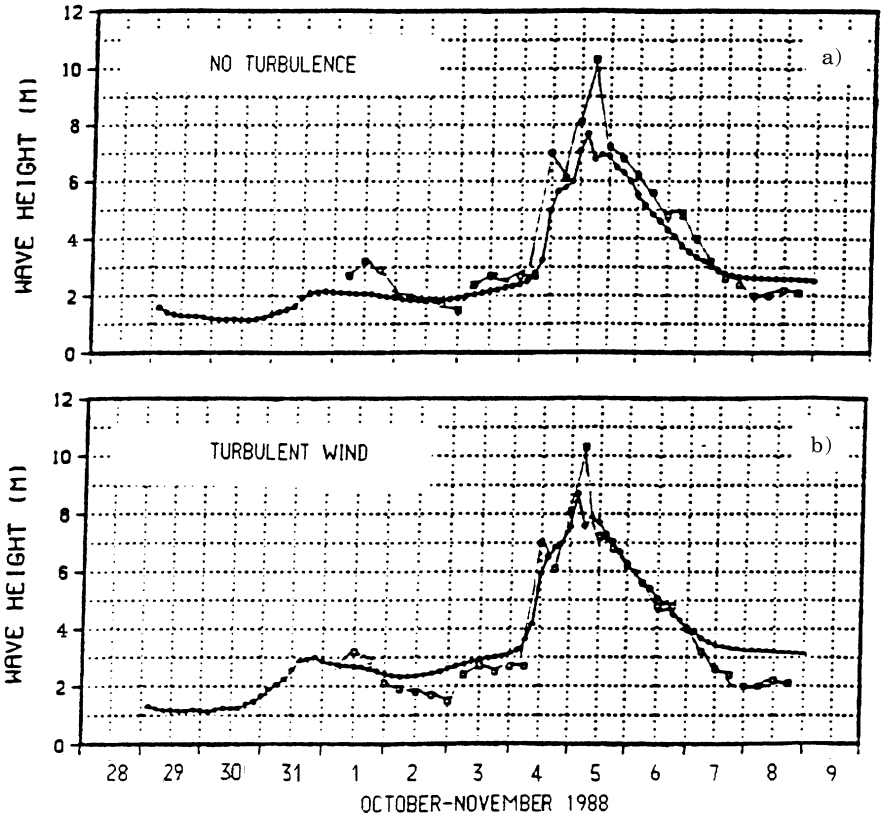

Fig. 41. – Comparison between measured (thin line) and hindcast (heavy line) significant wave heights close to Hawaii a) without and b) with gustiness taken into account (after Komen *et al.*, 1994).

that is for itself a rather stable wind (air warmer than water). However, this may not be the case in fall, when the sea is still warm and we experience the first storms of the cold season. As I have already discussed in subsect. 8·4, this can partly explain the skewness present in the distribution of the floods in Venice, notwithstanding that (see Camuffo, 1984) this is not justified by the statistics of the wind fields.

10·11. *Refraction modelling*

10·11.1. VENICE—a ray wave model. The extensive shallow water zone in front of the Venetian littoral (see fig. 44 below) implies that waves, while moving toward the coast, are subjected for quite a while to refraction effects. While in the area there are no dominant bottom features that can lead to spectacular local refraction effects, nevertheless the extension of the area can produce some remarkable focusing of energy at the coast. A good example has been given by Battiston and Malanotte Rizzoli (1972), who have shown how the extensive damage suffered by the *murazzi*, the artificial defences along the Venetian coast, during the big storm of November

1966 could be due to long distance focusing of long period waves from the South-East direction.

The relevance of the shallow water effects in the area prompted Cavaleri and Malanotte Rizzoli (1981) to develop a wave prediction model, VENICE, based on the refraction approach. Rather than considering the wave conditions on the whole area, the attention is here focused on a single point P. For each frequency f of the wave spectrum, all the possible incoming directions θ are considered, typically at 10 or 15 degree interval. For each (f, θ) couple the path potentially followed by the wave is traced back by refraction tecnique (see, *e.g.*, Collins, 1972) for a given maximum time or till when the wave ray ends at the facing coast. Given the linearity of the refraction laws, the same path will be followed in a toward P direction by the (f, θ) component during a storm. Cavaleri and Malanotte Rizzoli (1981) complemented the refraction with generation and dissipation processes, producing a model capable of evaluating, once the bathymetry and the input wind are specified, the wave conditions at a given time and at any specified location. This approach has the advantage of very limited computer requirements (very fast execution; the refraction paths are precalculated once forever) and of providing the results at the very spot of interest.

While the VENICE model was extensively applied also to other locations, the obvious point chosen for validation was the tower, where detailed wave records, including evaluation of the two-dimensional spectra, were available. The wind was evaluated with the first version of the ADRIAWIND model, described by Bergamasco *et al.* (1986).

The results of the hindcast of a bora storm are shown in fig. 42. There is a quite

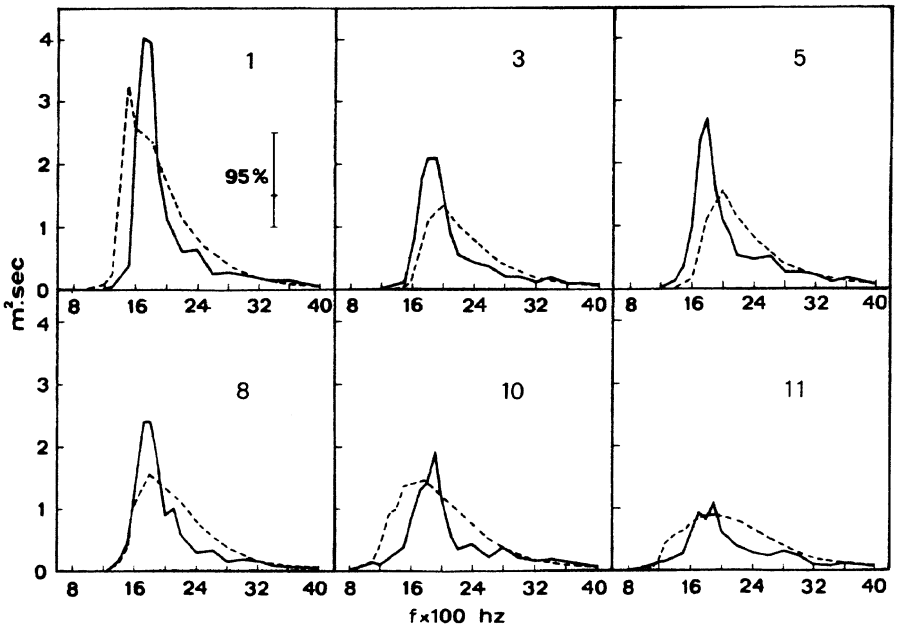

Fig. 42. – Spectra of six records taken during February 12, 1978. 95% confidence limits are shown aside spectrum of record number 1. The dashed line shows the hindcast of the model (after Cavaleri and Malanotte Rizzoli, 1981).

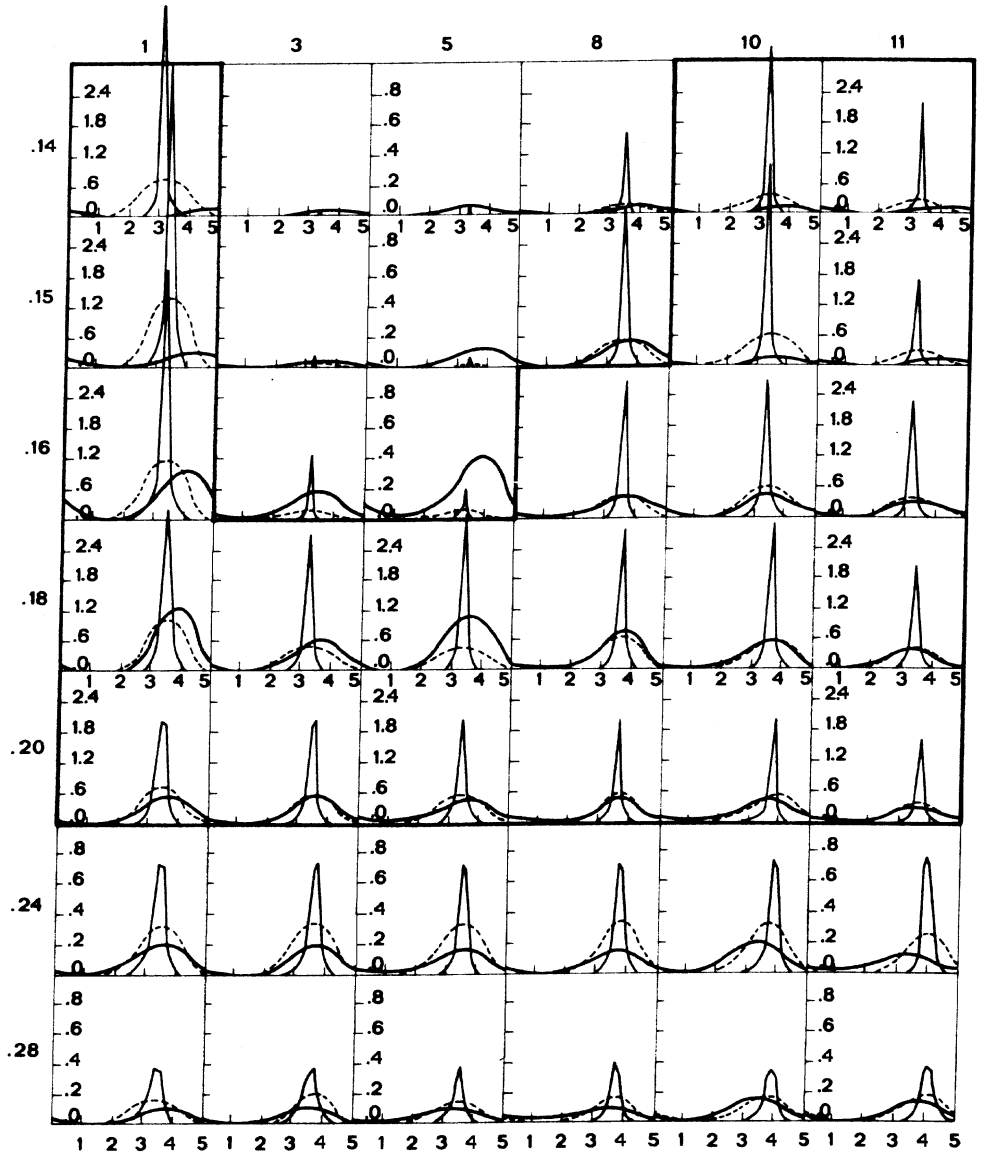

Fig. 43. – Directional energy distributions for seven frequencies of the six spectra of fig. 42. Thicker line, measure; thin line, model results; dashed line, filtered model results. The 2π interval is divided into five sections (after Cavaleri and Malanotte Rizzoli, 1981).

acceptable agreement between measured and model spectra. The comparison becomes more interesting when we consider the directional distribution of energy for each single frequency. This is a crucial test, because limited errors in H_s or in the spectrum can correspond to drastic differences in the circular distribution. The output in fig. 43 confirms the validity of the approach. Note that the analysis of the measured data done following Longuet-Higgins *et al.* (1963; see subsect. **10**·2) implies a smoothing of the

circular distribution. Therefore, for a meaningful comparison, also the directional distributions out of the model have been filtered by the same weighting function.

A relatively simple model like VENICE can produce remarkably good results. Its main limitation is the intrinsic lack of nonlinear processes. In practice, this limits its use to basins of limited dimensions ($L < 10^3$ km) and to not very complicated situations (*e.g.* hurricanes). However, used in the proper environment, it has a high pay-off with respect to the more complicated wave models.

10·11.2. Wave refraction in front of the Venetian littoral. Within the extensive effort for Venice, a wave measurement campaign was carried out during the period October 1993-March 1994. A complete report of the campaign and its findings is given by Viezzoli and Cavaleri (1996). Beside the permanent system at the tower, three more instruments were used: two wave measuring buoys (a Directional and a scalar Waverider), and an electromagnetic currentmeter plus a pressure transducer clamped to a bottom fixed pole. Their respective positions A, B, C, on depth of 15, 11, 6 m, are shown in fig. 44.

In principle, given the directional distribution of energy at point P (tower), A and C, a keen verification of the refraction procedure should have been possible. However, the

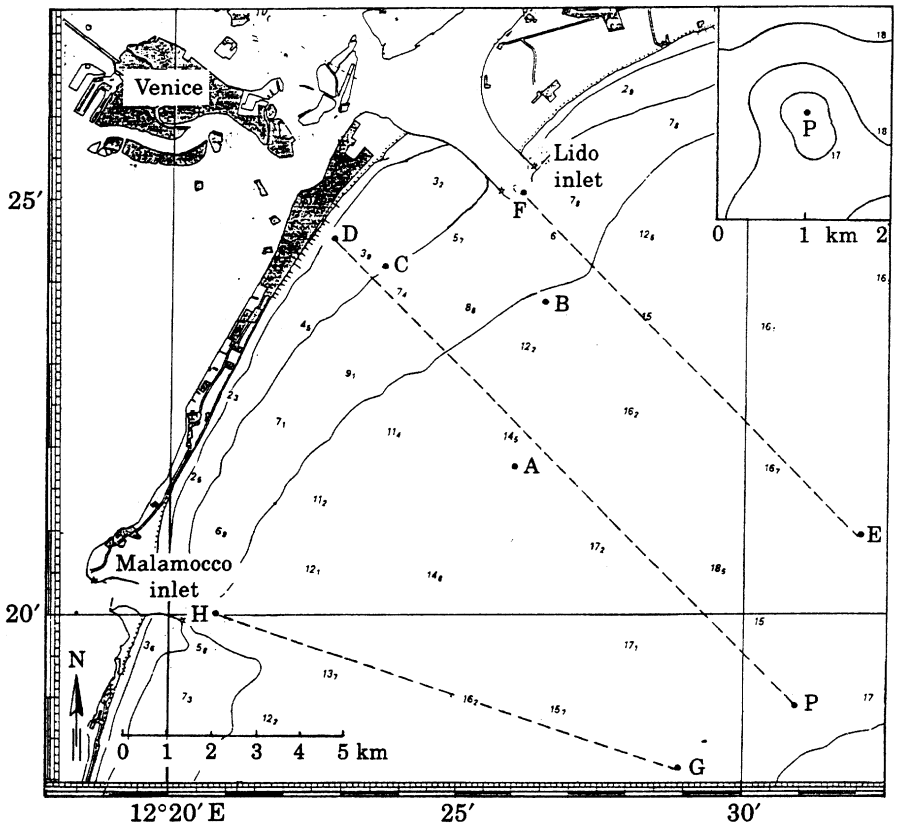

Fig. 44. – Investigation area with location of the wave gauges (points A, B, C). Isobaths in metres. The small rectangle shows in detail the bathymetry around the tower P (after Sclavo *et al.*, 1996).

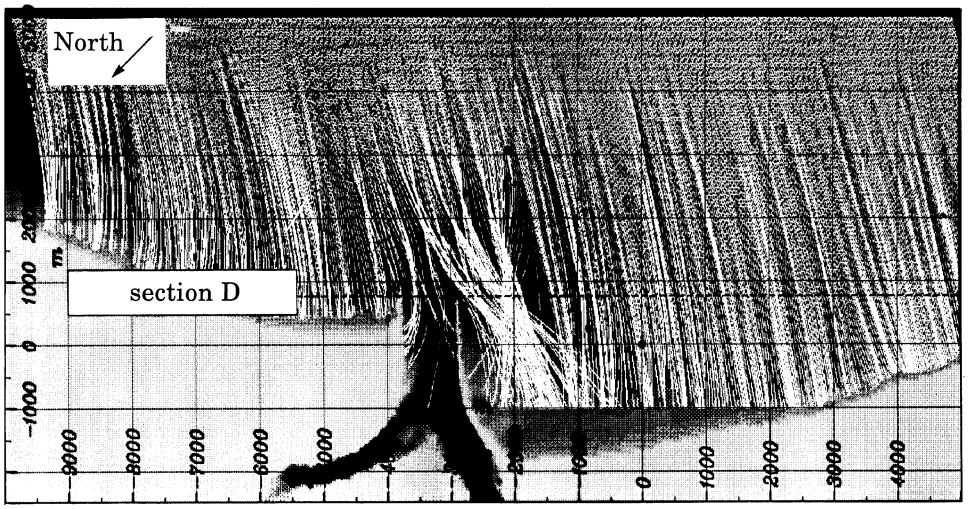

Fig. 45. – Refraction rays in the area of the Lido inlet. Input conditions $T = 7.1$ s, $\theta = 300$ degrees (after Viezzoli and Cavaleri, 1996).

area close to the shore is strongly affected by the tidal in- and outflow from the entrances to the lagoon. One of the aims of the campaign was to verify the influence of the current on the local wave refraction. At this aim, and to show better the eventual focusing-defocusing of wave energy, rather than the single point approach used in the model VENICE described in the previous subsubsection, a more classical frontal wave refraction model was used for 23 frequencies (from 0.08 to 0.30 Hz) and 66 directions (from 230 to 360 degrees, with two degree step size). Besides, three different water levels were considered, respectively 0.2, 0.6 and 1.2 m above the mean sea level.

On a qualitative basis the frontal approach produced some enlightening results. Figure 45 shows the refraction paths for a wave period of 7.1 s and a flow direction of 300 degrees. There is a strong focusing of wave energy to the West of the Lido entrance. This is connected to the more complex bathymetry present in this zone, as a result of the tidal flow in the inlet and of the littoral sediment transport. These conditions are typical of a severe bora storm, when the waves coming from East or North-East turn toward the shore because of refraction. The overall sediment transport, associated to the local wave climate (see subsect. **10**·5), lead to the asymmetrical distribution to the North and South of the Lido entrance visible in fig. 45. The average flow is from left to right in the figure, causing the bottom features that lead to the wave focusing. Note that the energy concentration to the South of the inlet helps in depriving of sand the local beach. The specific area of focusing moves around as a function of the characteristics (f, θ) of the considered component, but always remaining in the same area.

On a more quantitative basis, Viezzoli and Cavaleri (1996) considered the relationship between the spectra measured at the different points. The discrepancies they found were not only in the overall energy, lower than expected at the inner points, a fact clearly connected to dissipation, but also in the shape of the spectra. Two reasons were identified for this: coastal currents and variable bathymetry.

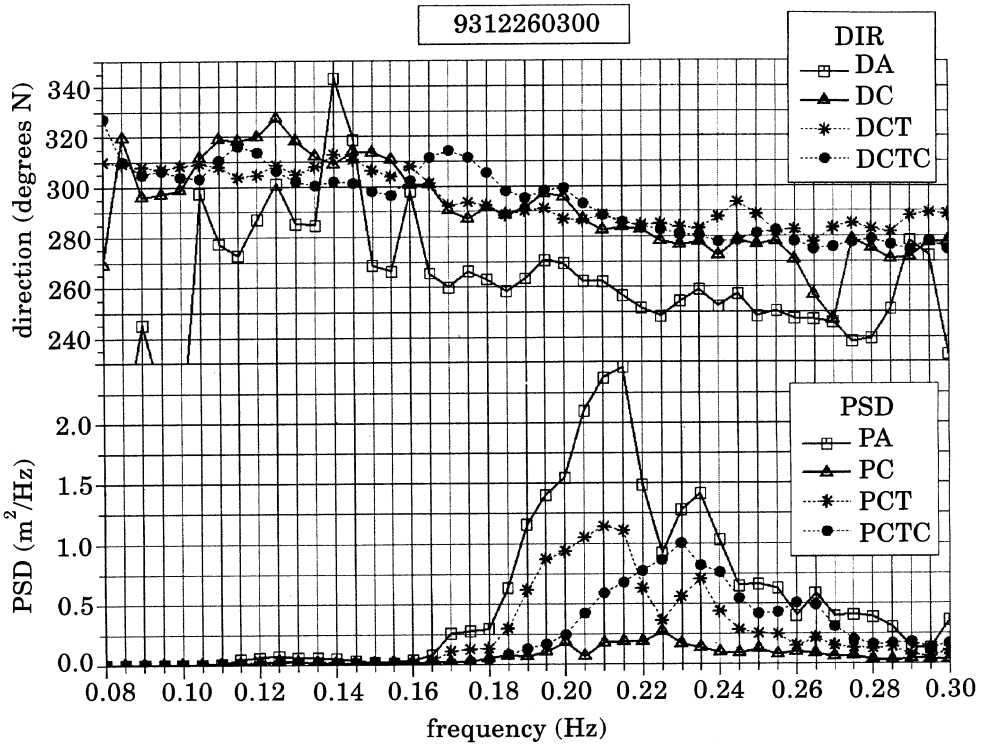

Fig. 46. – Comparison between the wave conditions: power spectrum densities (PSD) and directions at point A (PA, DA) and point C (locations shown in fig. 44). At C: PC, DC are recorded data, PCT, DCT computed including bottom refraction, PCTC, DCTC including also current refraction effects (after Viezzoli and Cavaleri, 1996).

Without a detailed operational description of the currents in the area no proper evaluation of their influence on waves could be attempted. Therefore, the opposite approach was followed. Under the strong hypothesis of uniform current conditions, and considering its effect on the wave fields (see, *e.g.*, Komen *et al.*, 1994), an estimate of its velocity U was reached by minimizing a cost function between the estimated and measured spectra at the inner points. An example is given in fig. 46. While, given the assumptions, the results are far from being fully satisfactory, they help in clarifying the role of currents in shaping the coastal wave spectra. For the case in the figure the estimated U was close to 0.80 m/s. While its actual distribution is certainly far from uniform, this figure demonstrates the relevant currents present in the area, particularly during bora storms. An overall approach to this problem, but necessarily less detailed in resolution and refraction, has been given by the work of Lionello (1995), described in subsect. **10·7**.

The second point of uncertainty is the actual bottom topography. Viezzoli and Cavaleri (1996) used a very detailed, but basically smooth, bathymetry. However, surveys in the area of the tower and along the line P-D in fig. 44 showed clearly how the bottom is characterized by continuous oscillations with amplitude up to one metre. Not only that. Repeated surveys on the same area, and direct evidence while diving at the

tower, showed also that at the same spot variations up to one metre within a few years are a real possibility. Incidentally, as this finding happened in the early years of existence of the tower, it was the main reason, together with the intense fishing activity with bottom nets, for giving up the idea of bringing AC power to the tower from the coast by a buried cable.

For our present interests this spatial and temporal variability introduces a sort of random noise on the measured data, known as *scintillation*. It can be studied by introducing a suitable noise on the distribution of depth. The implications for coastal engineers are not trivial. As mentioned at the beginning of this section, Battiston and Malanotte Rizzoli (1972) showed the potential effect of mild, but long distance focusing of wave energy on coastal defences. Because no permanent relevant bottom feature exists on the large scale, the focusing is the combined effect of minor disturbances on the bottom. As these change in the years, the same is true for focusing. This implies that the design wave conditions for a coastal defence must not be evaluated with respect to the *undisturbed* value of the maximum wave height, but with respect to the much higher conditions possible at any location, while the focusing point moves around as a consequence of the changes of bathymetry.

10˙12. *Evaluation of the wave conditions at the coast.* – Given the wave conditions at the tower, or more in general at an offshore position, it is obviously of interest to derive the corresponding conditions at the coast, at a specified location. This piece of information is essential for all the planned works along the Venetian littoral and at their inlets. Apart from the refraction modelling described in the previous subsection, two different approaches have been followed. In one case a relatively simple, but effective, wave model, HISWA (Holthuijsen *et al.*, 1989), has been used to explore the sensitivity of the results at the coast to the different physical processes that concur to the progressive modifications of the wave conditions. Then a highly nonlinear equation approach, based on the solution of the KdV and Boussinesq equations and on the nonlinear spectral analysis, has highlighted the effects of nonlinearity during shoaling. The results of these two different approaches are singularly described in the following sections. An exaustive study carried out for the specific design of the barrages proposed at the inlets of the lagoon is described in subsubsect. **10**˙13.1.

10˙12.1. Sensitivity of the wave conditions to the different physical processes. The HISWA wave model was developed by Holthuijsen *et al.* (1989) as a simplified version of the more sophisticated models, but suitable for accurate calculations in coastal areas, under the hypothesis of time stability. As such it is a very effective tool to verify how coastal wave conditions change as a function of variations in the input or along the way. Starting from the information available at the tower, Sclavo *et al.* (1996) have used this model to analyse the conditions at the shore. The area of study is the one shown in fig. 44.

Apart from refraction and shoaling, the evolution of the wave field while moving toward the shore is dominated by generation by wind (input), dissipation by bottom friction and breaking (output), and by the conservative wave-wave nonlinear interactions. The last process is not present in the HISWA model, and it was consequently not part of the study.

The sensitivity of the results at the coast and at intermediate distances was explored by alternatively switching on and off in the model the terms representing the different processes, and comparing the results to those of the *undisturbed* run. The

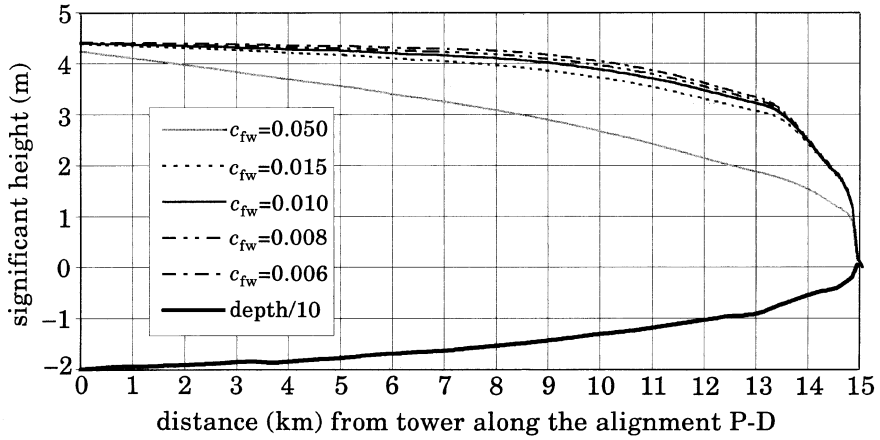

Fig. 47. – Variation of H_s *vs.* distance from the ISDGM tower along the alignment P-D in fig. 44 (after Sclavo *et al.*, 1996).

input information at the tower was provided by the hindcast with the WAM model (see subsect. **10**˙5) of a very severe event happened in January 1987.

Wave generation by wind (the results of the tests are summarized in fig. 47) was found of marginal importance on such a short distance (16 km). Its effect is simply to decrease of a few percents the wave height at intermediate depths, but with practically no effect at the coast. At intermediate distances the dominant process turns out to be the bottom friction, whose role becomes more and more relevant as we move to more shallow waters. Neglecting it increases the wave height H_s of more than 40 cm (10% of the local wave height) at intermediate depth. However, approaching the shore the dominant factor becomes the bottom induced breaking, in practice forcing H_s to be smaller than a given fraction of the local depth.

Tide and surges affect the wave conditions with the variations they introduce in the water depth. In principle a shift upward of the sea level should simply shift the whole pattern toward the shore. Two facts counteract this statement. The first one is the higher bottom steepness present in the shore area. The second one is the statistical aspect of the breaking, connected to the statistical distribution of the single wave heights in a storm. This implies that the adaptation of the wave conditions to the local depth requires some, short but still finite, time. Combined with the rapid decrease of depth at the shore, the overall effect of a positive surge is a substantial increase of the wave height at the shore. The quantification of this influence is given in fig. 48.

All the previous results have been obtained with the waves moving practically perpendicularly toward the shore. For bora storms, similarly to what shown in subsect. **10**˙11, there is a substantial influence of refraction. This is well represented in fig. 49. The single lines represent the directional distribution of energy at the various points in fig. 44. We see clearly how, parallel to the decrease of energy associated to the processes outlined above, there is a steady shift of the direction toward the perpendicular to the shore, more or less 300°. Note also how one effect of refraction is to narrow the directional distribution, as a consequence of the tendency of each single component to approach the perpendicular line.

Using the results of extreme statistics described in subsect. **10**˙6, Sclavo *et al.* (1996)

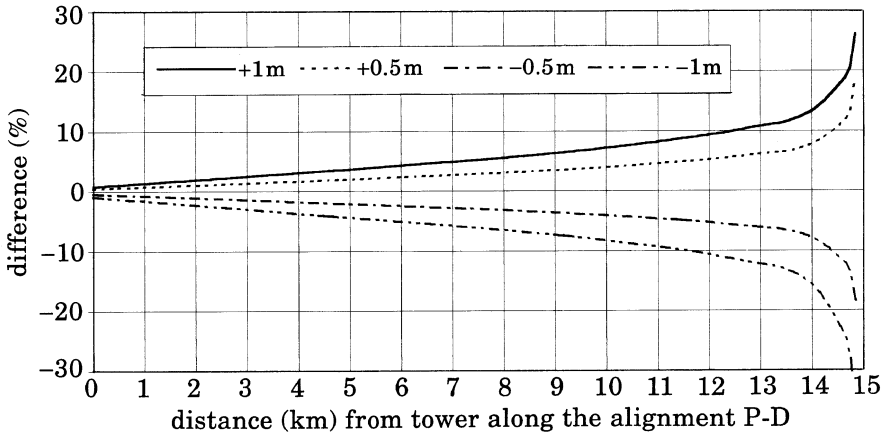

Fig. 48. – Effects of tide variation on H_s along the alignment P-D in fig. 44 (after Sclavo *et al.*, 1996).

have evaluated the possible extreme conditions in the area between the tower and the shore. Given an extreme H_s value at the tower, the corresponding two-dimensional spectrum has been estimated by similitude with the results of the hindcast of storms of the same type. Besides, for sirocco storms, considering the strong connections with the surges in the Northern Adriatic Sea, a 1.40 m surge has been considered. The results for the bora and sirocco storms are shown in fig. 50. Note the heavier wave conditions at the Malamocco inlet with respect to Lido (see fig. 44 for their location), associated to the larger depth in the former area.

Finally, the sensitivity of the extreme wave conditions at the coast to the input extreme at the tower was explored by sistematically varying the latter in both H_s and

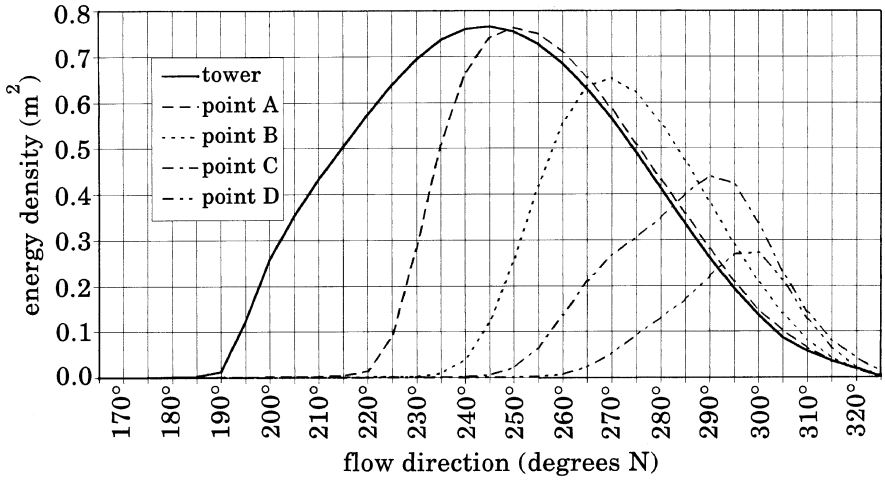

Fig. 49. – Evolution of the one-dimensional directional spectrum during a severe bora storm. See fig. 44 for the location of the points (after Sclavo *et al.*, 1996).

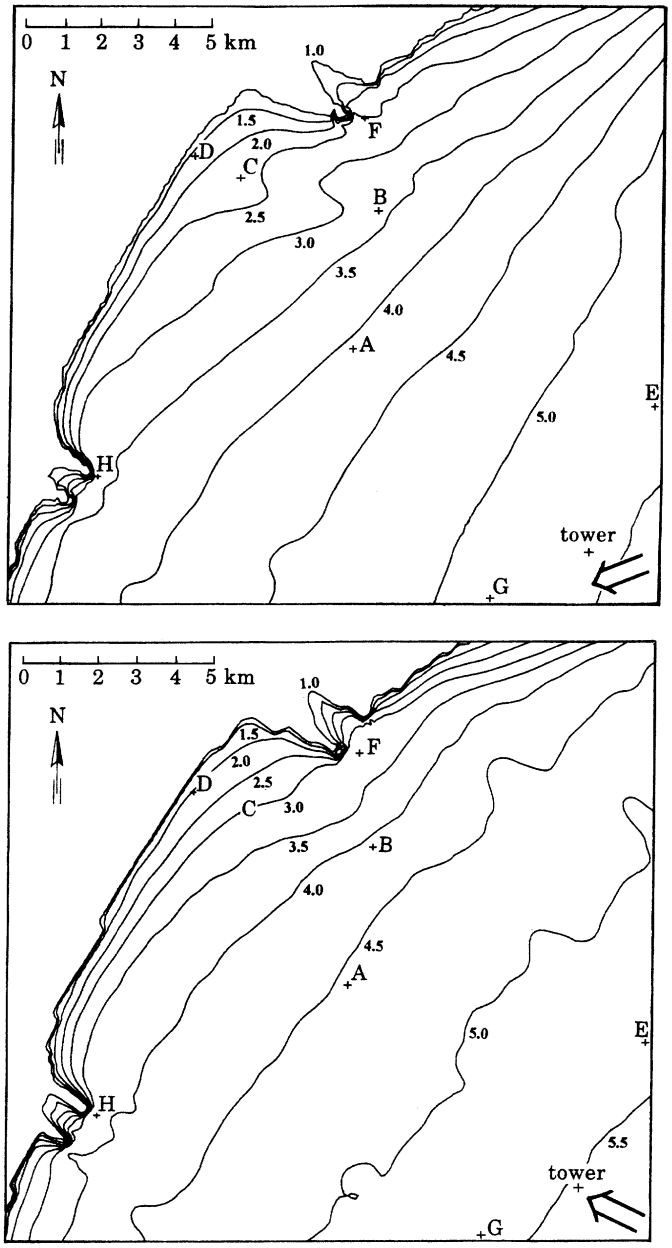

Fig. 50. – Isolines of significant wave height (m) for an extreme bora (upper) and sirocco storm (lower panel). The arrow in the lower right corners indicates the input wave direction (after Sclavo *et al.*, 1996).

T_m (mean period). The results at the Lido entrance (point F in fig. 44) are given in table II. There is an expected, but limited, increase of the wave height at F while increasing it at P. The physical meaning is that, while the bottom induced breaking

TABLE II. – *Significant wave height at point F in fig. 50 for different H_s and T_m conditions at point P during a sirocco storm (after Sclavo et al., 1996).*

H_s (m)	T_m (s)		
	9	10	11
5.0	3.30	3.28	3.17
5.5	3.45	3.40	3.35
6.0	3.50	3.45	3.40
6.5	3.53	3.50	3.45

puts an upper limit on the local H_s value, being the process statistical, it takes time. Hence, similarly to the just discussed case of a positive tide, a higher extreme wave height offshore implies a slightly higher H_s at the shore. The slight decrease with incresing T_m is associated to the larger amount of energy lost by bottom friction while approaching the shore.

10·12.2. Nonlinear shoaling. During the development of a wave field in deep water a dominant role is played by the conservative fourth order nonlinear wave-wave interactions, *i.e.* by the exchange of energy among the different components under certain resonance conditions of wavenumber and frequency (Hasselmann, 1962). Entering shallow water, hence with the change of the dispersion relationship, the same resonance conditions are no longer satisfied, and different kinds of nonlinear interactions appear. These interactions are rarely considered, and they appear only in the most recent wave modelling developments (see Booij *et al.*, 1996). The alternative approach is to carry out the direct numerical integration of the basic equations, that implicitly contain in their formulation all the nonlinear processes at work in an evolving wave field. The calculations are extremely difficult and computer demanding, which explains why this procedure has not been widely followed. Taking also advantage of the wave measurements available in front of the Venetian littoral, Osborne *et al.* (1996) have done a keen analysis of the measured data and of the nonlinear shoaling connected to them. The study has proceeded through different lines.

The first approach made use of the Korteweg-de Vries equation (KdV) to study the time and space evolution of the wave field, starting from the time series given at a certain position. In the present case the records used were those obtained during the heavy swell already described in subsubsect. **10**·2.2. The KdV considers the surface profile as a linear superposition of nonlinear hyperelliptic functions. The big advantage is that, in so doing, the nonlinear evolution and interactions of the functions are fully taken into account. This approach allows full integration of many highly nonlinear equations, the KdV having been the first example of this kind (see Zacharov *et al.*, 1980, and Ablowitz and Segur, 1981). An advantage of the KdV is that, being linear with respect to the hyperelliptic functions, and with no consideration of generation and dissipation, it can be integrated indifferently either forwards or backwards in time. Starting from one record at the tower, this has allowed the analysis of the wave conditions both inshore and offshore with respect to this position.

Rather than by the standard spectral analysis, the time series at the various points have been analysed with the so-called inverse scattering trasform (IST). IST (see

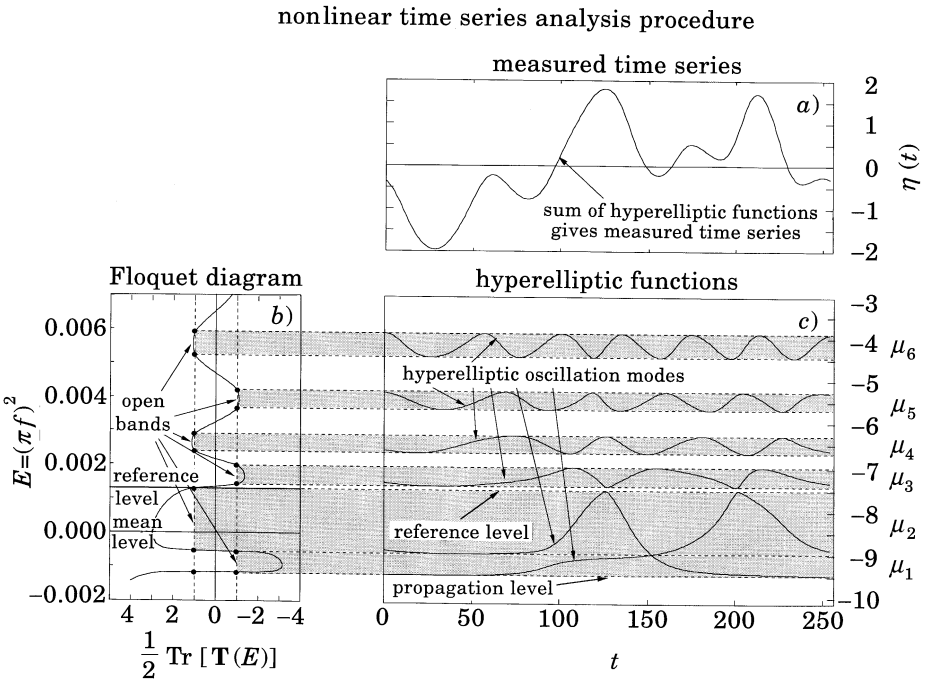

Fig. 51. – Schematic of the inverse scattering transform analysis in the hyperelliptic function representation. In panel a) is a typical wave train (time series) which is to be analysed with the inverse scattering transform. In panel b) the Floquet discriminant graph is shown as a function of squared frequency; note the presence of the "open band" (within which the hyperelliptic functions oscillate) and the references, mean and propagation levels. In panel c) the hyperelliptic functions themselves are shown. Note that they oscillate exactly within the open bands of panel b). The linear superposition of the hyperelliptic functions gives the wave train shown in panel a) (after Osborne *et al.*, 1996).

Osborne, 1991a,b) can be defined as a nonlinear Fourier transform of broad-banded nonlinear wave motion. Instead of sines and cosines, the single components are nonlinear hyperelliptic functions. In very short terms the original signal is represented as a linear superposition of nonlinear components. As such the IST is ideally suited for the analysis of the integration of nonlinear equations. An essential scheme of the procedure is represented in fig. 51. The procedure has been applied to a case of heavy swell (March 1979, quoted also in subsubsect. **10**˙2.2 on Reynolds stresses) for which detailed records are available. A key result of the IST analysis is the *spectral modulus* R, a parameter providing the degree of nonlinearity of the different spectral components. $R = 0$ means full linearity, $R = 1$ full nonlinearity. Figure 52 shows how the spectrum evolves while propagating towards the shore. The continuous line indicates the spectrum, the broken line the modulus. The *reference level* indicates a critical frequency, below which the single components behave like solitons. Above it the components are periodic, the level of interaction being given by the modulus R.

From the figure, showing six of the locations at which the calculations have been carried out, we see that till 20 m of depth the solitons are limited to the lowest

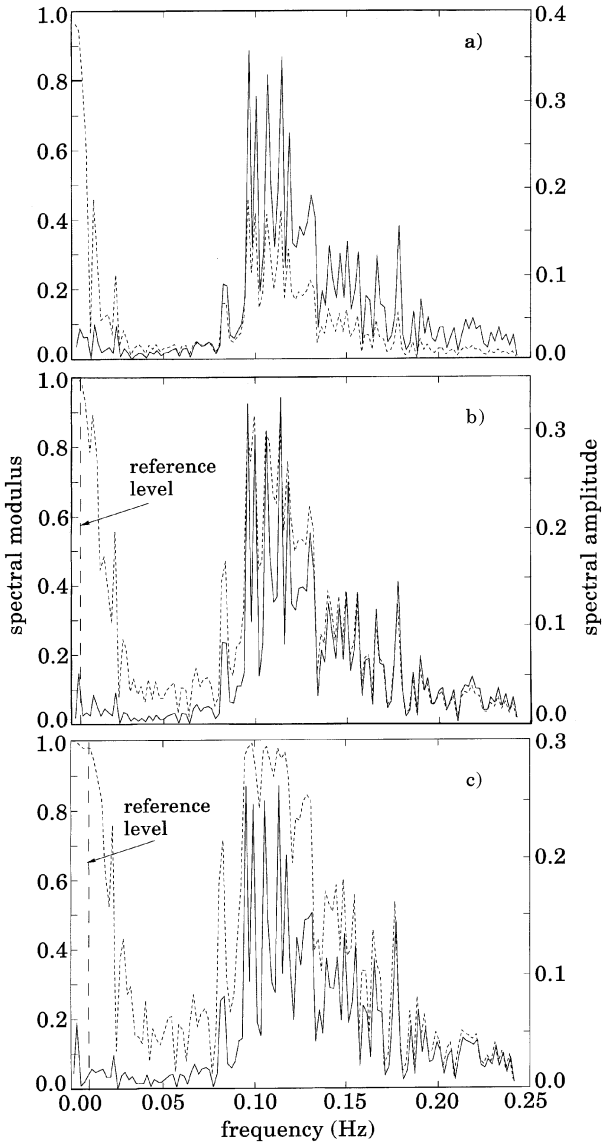

Fig. 52. – Inverse scattering transform spectra (continuous line) and nonlinear moduli (dotted) at a) 49, b) 28, c) 21 metres of depth. Wave components to the left of the reference level behave like solitons (after Osborne *et al.*, 1996).

frequency range, while in the periodic range the nonlinearity (R approaching 1) is limited to the area of the spectral peak. At the tower, where the depth is 16 m, the soliton range is larger, while the nonlinearity begins to dominate the periodic range. At the lowest depth all the low frequencies (below 0.05 Hz) behave like solitons, while the whole spectrum, with the exception of the still *deep water* components, is fully nonlinear.

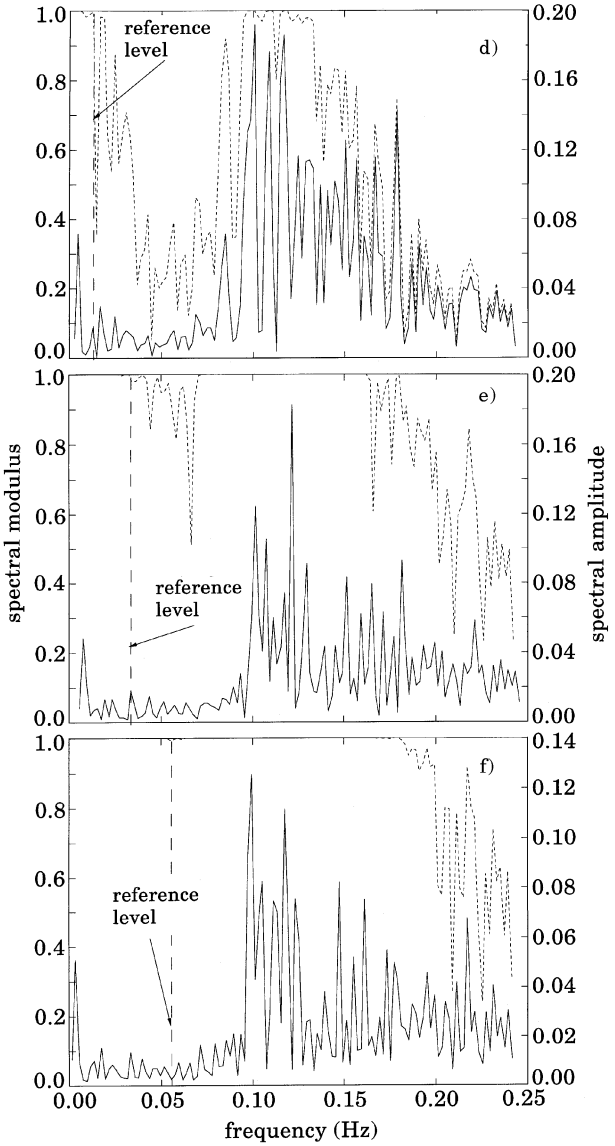

Fig. 52. – (*Continued*). Inverse scattering transform spectra (continuous line) and nonlinear moduli (dotted) at d) 16.5, e) 9 and f) 8 metres of depth. Wave components to the left of the reference level behave like solitons (after Osborne *et al.*, 1996).

In principle, the applicability of the KdV equation is limited to waves required to be *small, but finite-amplitude on constant depth on one dimension.* This could cast doubts on the previous results, obtained from waves that were certainly neither *small* ($H_s \simeq 2$ m), nor on *constant depth.* A verification was obtained by analysing with the same IST tecnique the data obtained during the devoted wave measuring campaign described in subsubsect. **10**˙11.2. The considered records were taken on 26 December

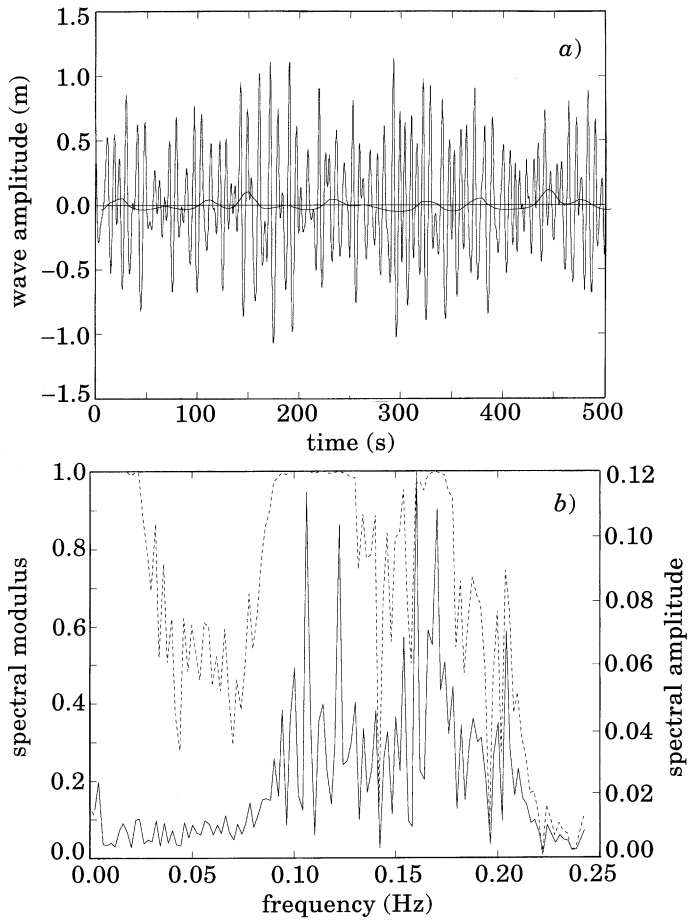

Fig. 53. – Analysis of data obtained by measurements at point B (depth $\simeq$10 m) in fig. 44. a) Time series with solitons highlighted. b) Inverse scattering transform spectrum of the data plus modulus of the spectral components. Record of 26 December 1993 (after Osborne *et al.*, 1996).

1993. With respect to the case of heavy swell, the wave heights were somehow smaller, and their respective timing is not ideal. Nevertheless, they provide a sequence of records taken at different positions, on different depths, throughout a storm.

The results are quite positive, the ones obtained from the analysis of the measured data being fully consistent with those derived by the direct integration of the KdV equation. One example is given in fig. 53, showing the output for data measured at point B (depth of about 10 m) in fig. 44. The details of the spectrum in panel b) are very similar to what shown in fig. 52, with the soliton range, and the high degree of nonlinearity around the peak of the periodic part. A nonlinear filtering has also been used to isolate the soliton components from the spectrum. These appear as the thin continuous line superimposed to the actual record in panel a). In a way this could be considered as a variation of the *mean* surface over which the other components oscillate.

The final verification was done numerically integrating, as with the KdV, the Boussinesq equation, but starting from the data of 26 December 1993. This approach is

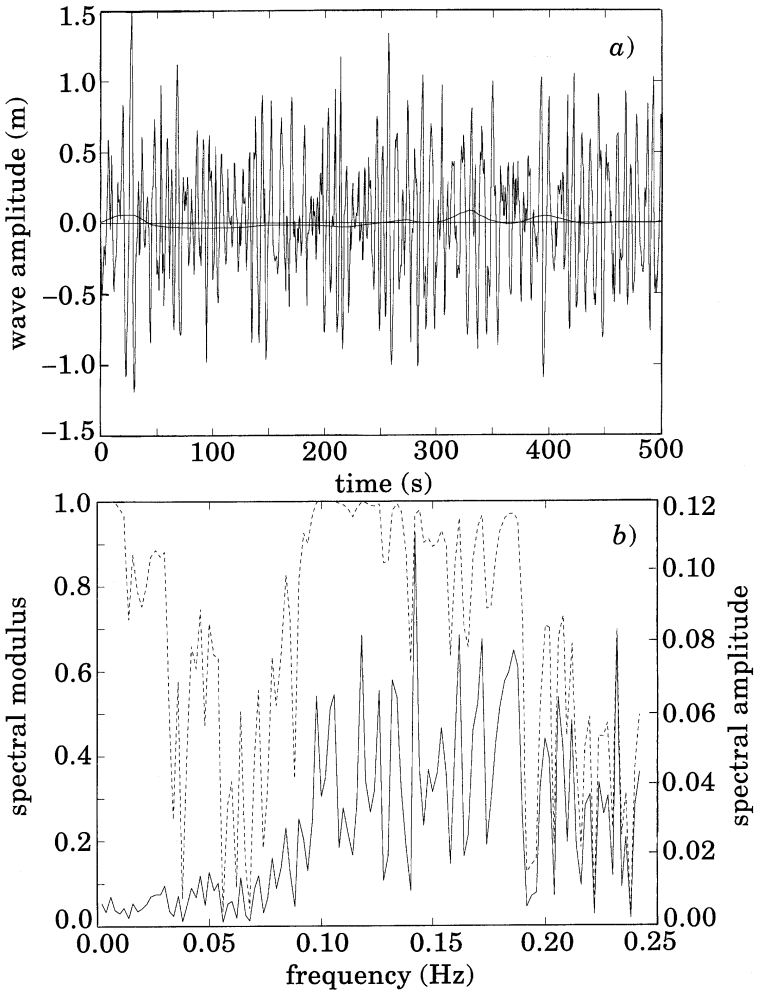

Fig. 54. – Inverse scattering transform analysis of computer simulations using the Boussinesq equation. The initial conditions are based on measured data from the tower (26 December 1993). Results have been integrated from the tower to point B (depth $\simeq$10 m). See fig. 44 for locations. a) Time series with filtered solitons highlighted. b) Inverse scattering transform spectrum of the data plus the modulus of the spectral components (after Osborne *et al.*, 1996).

far more complicated, but it has the strong theoretical advantage of embedding in itself all the nonlinearities that manifest themselves during the shoaling (see Brocchini *et al.*, 1994, for an extensive discussion on the subject). The results have been extracted at the same locations of the measurements, and again analysed with the IST tecnique. The output for point B, corresponding in space and time and in the specifications to that in fig. 53, is given in fig. 54. It is clear that the two figures show qualitatively the same characteristics, a further confirmation of the nonlinearities present in the field, and of the capability of the numerical methods of both identifying them in the records and simulating them with the integration of the nonlinear equations.

10˙13. *Design wave height at the barrages of the lagoon*

10˙13.1. Short waves. Within the extensive activities sponsored by the Italian Government for the studies on the lagoon and on the Venetian littoral, large attention was put on the design of the barrages proposed at the inlets of the lagoon. Their aim would obviously be to save the town from the frequent floods associated to the storm surges in the Northern Adriatic Sea. The authority in charge of the plan is the Consorzio Venezia Nuova (New Venice).

The cost of a marine structure is a rapidly growing function of the maximum wave height expected to impinge on the structure. The proposed location is inside the inlets, where the waves conditions are expectably less severe than at their ends, practically in the open sea. The design wave height at the expected positions was an obvious necessary piece of information. The problem was approached in two steps. The first was the evaluation of the offshore extremes, *i.e.* at the tower. This has been described in subsect. **10**˙6. The second one was to transfer the wave information to the coast and inside the harbour. At this aim different models were applied at different design phases (see De Girolamo *et al.*, 1993), a refraction-diffraction wave model, a model based on the mild slope equation, and a Boussinesq model. A sequence of nested grids was established, starting from the overall Northern Adriatic Sea, and focusing gradually on the area between the tower and the coast, and then on the inlets.

Given the wave extremes at the tower, the evaluation of the corresponding conditions at the inlet entrances was done with the HISWA model (Holthuijsen *et al.*, 1989). However, given the sensitivity of the results to the different physical processes parametrized into the model, a careful calibration of the relevant parameters was done using the multiple wave measurements that had been made available for this purpose in the area. Similarly to Sclavo *et al.* (1996), the most critical processes, hence calibration parameters, turned out to be the bottom friction and the bottom induced breaking. The variation of depth due to tide and storm surges has the effect already discussed in subsubsect. **10**˙12.1.

As expected, once the different parameters of the HISWA model were properly calibrated, the results at the various points between the tower and the coast were quite good, with average errors for H_s less than 10% at most of the stations. A problem specific to the procedure was the nonstationarity and nonhomogeneity of the meteorological conditions, because of the opposite basic assumptions of HISWA. As discussed in subsect. **10**˙10, some of the discrepancies are likely to be justified by the gustiness effects of the driving wind fields.

At the entrance of the Malamocco inlet (point H in fig. 44) the design wave height with a return period of 100, 300 and 1000 years was estimated, respectively, as 4.0, 4.2 and 4.3 m. Using conservative values for the bottom friction and breaking parameters with respect to those found with the calibration procedure, the value grows to 4.7 m for the 300 year period.

In subsect. **10**˙6, I had pointed out the reassuring fact that Sclavo *et al.* (1996) and Hurdle *et al.* (1995) had, with substantially different procedures, reached more or less the same estimate of the possible extremes at the tower. It is therefore disturbing that, starting with the same offshore values and using the same model, the two groups (see subsubsect. **10**˙12.1) reach different values of the design wave height at the entrances of the lagoon. The specific reason is that different coefficients have been used in the HISWA model, in one case the standard ones suggested by the literature, in the other one those derived from the local calibration. While the latter approach sounds locally

more reliable, there are possible doubts about the extrapolation to extreme storms of values of breaking and bottom friction derived from relatively mild storms.

The further step was the transfer of the information from the inlet entrances to the barrage positions. For this a careful study was done to analyse the sensitivity of the results to the basic wave processes. The three inlets are characterized by relatively shallow water with a central deeper channel for navigation. A preliminary analysis with the Boussinesq model indicated the relevance of the directional spreading of energy at the entrances. It turns out that the spreading leads to an increase of the wave height at the barrages, also in the case when the wave mean direction is aligned with the axis of the inlet. The explanation is associated to the refraction toward the inner side of the jetties due to the bathymetry in the channels, with a central channel bordered by two shallow zones. This is partly compensated by diffraction, and mainly by the lateral components of the directional distribution, also in connection to the large width of the inlets as compared to the distance between the inlet entrances and the position of the barrages.

At the time of the study no breaking was included in the Boussinesq model. To reach a quantitative estimate of its influence on the final results, De Girolamo *et al.* (1993) used a mild slope equation model, inclusive of breaking and directional spreading, the latter obtained using superposition. To consider the nonlinearity introduced by breaking in the process, an iterative approach was followed. The effect of the directional spreading on the so obtained results is even more spectacular. For waves with mean direction along the inlet axis, the wave height at the barrages increases up to three times, from 10% to 30% of the value offshore. Note that the worst conditions at the barriers happen for wave directions different from the axial one.

Besides the measurements off and close to coast, extensive wave measurements were done also inside the inlets. Figure 55 shows the scatter diagram of the wave heights recorded at the tower and inside the Malamocco inlet. The two lines represent the best fit, respectively for ebb and flood tide. The described calculations have been repeated for the different possible tidal conditions (flood, ebb and no flow conditions). The results of the simulations are shown in the figure, fitting well the lines derived from the measurements.

The result of the study is that at the barriers inside the three inlets the significant wave height does not exceed 3-3.7 metre for the 1000 year return period.

10˙13.2. Long waves. In subsubsect. **10**˙12.2, following the results by Osborne *et al.* (1996), I have pointed out how the nonlinearities acting in the wave field lead to the appearance of long waves, with period much longer than the wind waves that created them. Spectral analysis of very long records (lasting more than one hour), taken with the system described in subsect. **10**˙2 during stable wave conditions, have revealed the existence of low frequency components, with $T > 100$ s. These are just examples of a series of mechanisms that, starting from waves in the range of seconds, can shift part of their energy in the very low frequency range. These long period components are of interest for floating or movable structures, because of the resonance they can induce if the structure has a potential motion with period within their range.

Figure 56 shows the planned scheme for the Lido inlet. Basically the barrages close separately the two channels present where the inlet enters the lagoon. A refuge harbour for small vessels is located on the side of the northern jetty. The study on the effect of long waves inside the inlets has been carried out by Mattioli (1996). He used a finite element expansion tecnique to numerically solve on a suitable grid the mild-slope

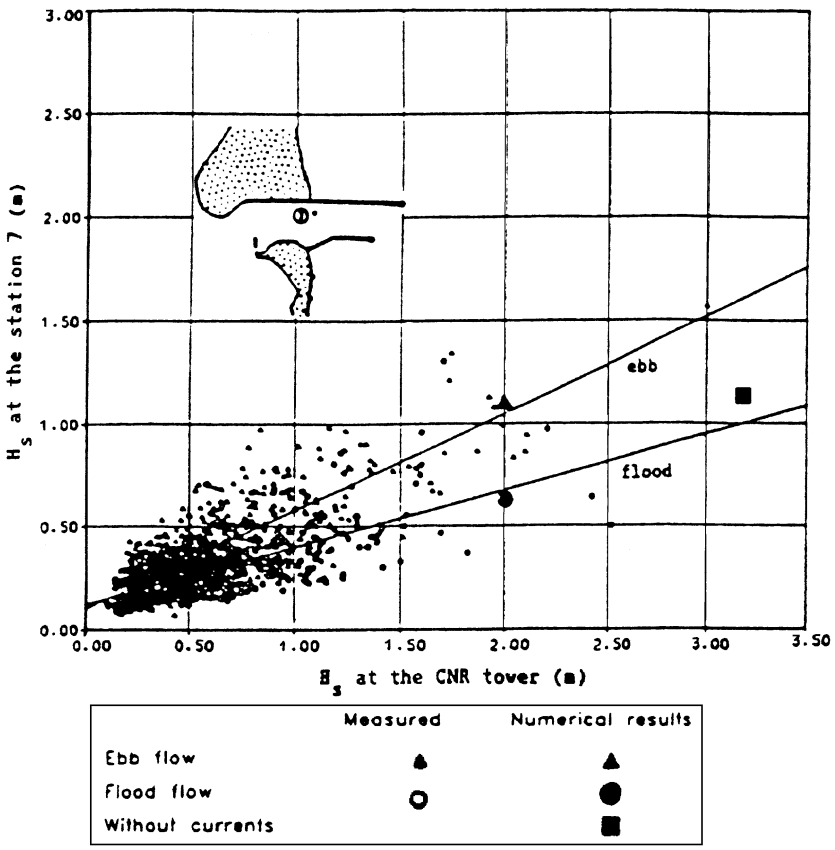

Fig. 55. – Scatter diagram of significant wave height at the tower and inside the Malamocco inlet (see insert and fig. 44 for position). Comparison between measurements and the numerical simulation obtained with the mild slope model (after De Girolamo *et al.*, 1993).

equation derived by Berkhoff (1972). He considered unidirectional monochromatic wave systems of different period, entering the inlet with different angles. While a systematic analysis of all the possible cases has not been carried out and this approach cannot provide a complete view of the possible situations, useful indications can be obtained with a limited effort on some general characteristics of the system. From this, general suggestions can be derived for an eventual deeper study of some special cases.

The Lido channel shows resonance at specific periods. One example is given in fig. 57, where a 215 s wave of unitary height enters the channel along its main axis. An area of strong wave activity is close to the northern jetty (note that the orientation is the opposite one with respect to fig. 56). This is basically due to refraction. Another area of strong motion is at the West barrier. A peculiar feature are the two nodal lines, indicating reflection of energy from the closed barriers. Opening the barriers changes dramatically the situation, with the expected disappearance of the nodal lines, and a more even distribution of energy between the two barriers.

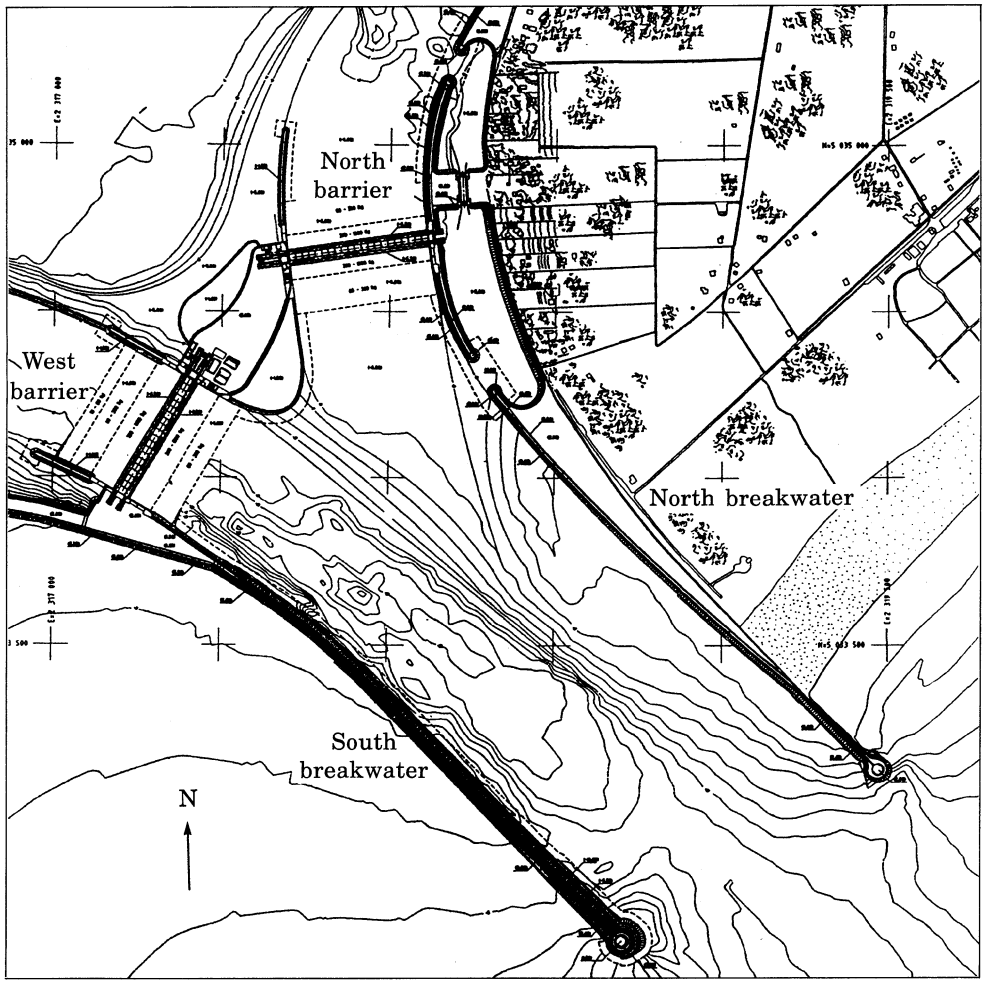

Fig. 56. – Scheme of the works planned for the Lido channel (after Mattioli, 1996).

The response can change completely from case to case. An interesting one is the reaction of the channel, with open barriers, to the forcing by a 150 s wave. The resulting pattern is shown in fig. 58. There are two focusing zones close to the northern jetty, the distance between them decreased with respect to the previous figure because of the shorter period, hence wavelength, of the forcing wave. However, the main feature is the strong excitation of the refuge harbour. This is critically dependent on the details of the field. In turn, its presence is crucial in determining what happens in the channel. Its exclusion cancels any particular wave activity, the whole field turning quite uniform and smooth.

Resonance conditions have been found also at 60 and 45 s. At 90 s there appears another effect worthy to mention. At this period the North entrance to the lagoon is affected by a strong transversal oscillation, both with the barriers open or closed. Thus

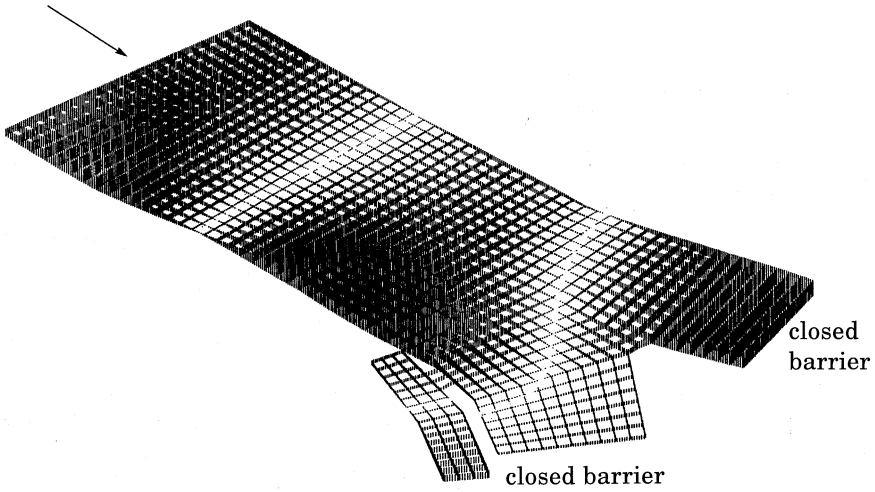

Fig. 57. – Response of the Lido channel to a 215 s wave forcing. Here the barriers are closed, so that the figure represents the resonance of a mode of oscillation with two nodal lines. In this case the West barrier is subject to a strong motion, while the North one is almost motionless (after Mattioli, 1996).

the barrier, when closed, is subjected to a nonuniform forcing. Given the structure of the barriers, made of a sequence of modules separated by short gaps, this could induce ample not-in-phase oscillations of the modules, with a decrease of efficiency of the barrier.

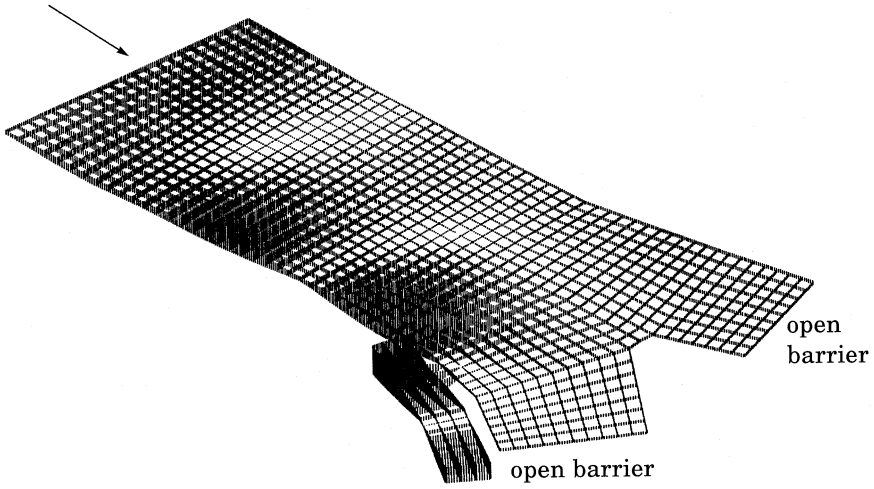

Fig. 58. – Response of the Lido channel to a 150 s wave forcing. Here the barriers are open. When the barriers are closed the modulation pattern of the wave field is enhanced, but maintains essentially the same structure (after Mattioli, 1996).

10·14. *Wave forecast in the Adriatic Sea.* – In a previous subsection (see **10**·8) I have mentioned that the quality of the surface wind out of a global model seems to decrease with the dimensions of the basin where we focus our attention. In particular, for the Adriatic Sea Cavaleri and Bertotti (1997) have found that the structure of the field is reasonably correct, but the wind speed needs to be enhanced, multiplying it times 1.5, to obtain then good wave results. They argue on the possible reasons for that, quoting a) the limited resolution of the model compared to the dimensions of the basin, b) the effect of the orography not sufficiently detailed, c) the lack of information from former Jugoslavia during part of the test period. The question is relevant particularly for forecast applications, because, if c) were the reason, it would affect the forecast fields to a lesser extent, due to their rapid adaptation to the local orography and their dependence on conditions formerly existing in areas with sufficient data availability. However, the extensive tests done by Cavaleri and Bertotti (1997) have shown that the underestimate of the wind speed characterizes at a similar extent also the forecast fields. In a way this is a good news, because, without choosing between possibilities a) and b), we know that, for an acceptable wave analysis and forecast, we can use the ECMWF wind simply multiplying the speed for the known enhancement factor.

One could argue why a similar procedure is not applied directly to the wave results. Unluckily, this is not possible, because of the nonlinearity intrinsic in the wave

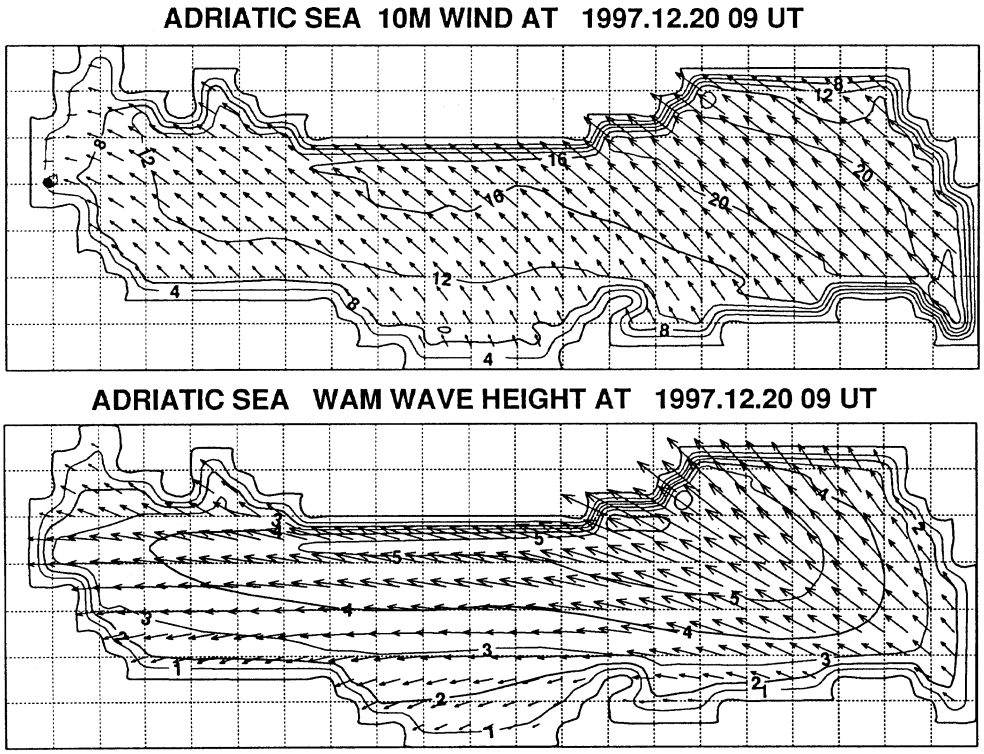

Fig. 59. – Wind and wave conditions in the Adriatic Sea at 09 UTC 20 Dec 1997. Wind speed in m/s, wave height in metres. The wind speed has been enhanced by 1.5. The dot shows the location of the ISDGM tower.

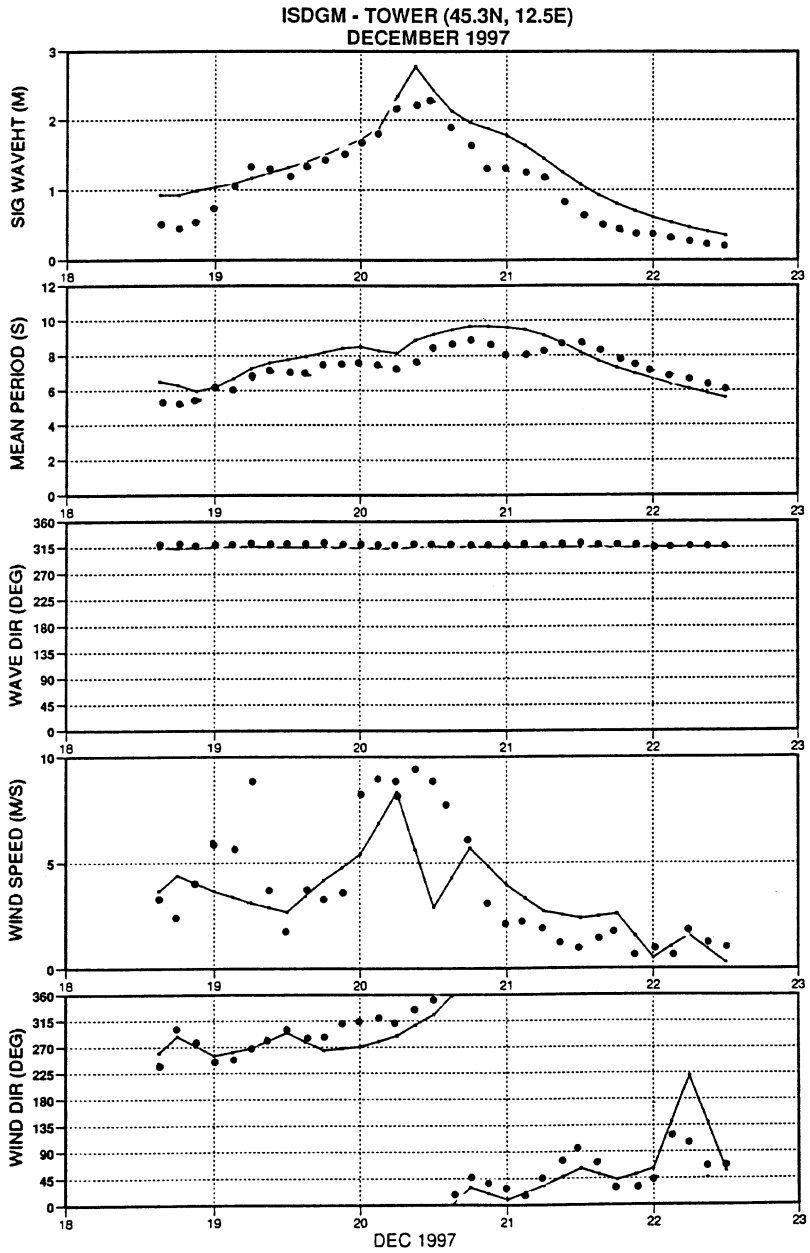

Fig. 60. – One-day analysis and three-day forecast at the tower position (see fig. 59). The continuous lines indicate model data. The dots show the results of the on board measurements.

generation process. It follows that the eventual calibration factor would depend on fetch, wind speed or the meteorological pattern, excluding any practical application. On the contrary, still within the range discussed by Cavaleri and Bertotti (1997), the wind

calibration factor is reasonably constant, allowing its effective use for operational applications.

Such a procedure has been implemented at ISDGM, in Venice, as a cooperative effort with ENEL (the National Electricity Company) and former Cray Research s.r.l., now Sylicon Graphics. Each day the last 24 hour analysis plus 72 hour forecast wind fields are received from ECMWF. Starting from the last wave analysis field of the previous day, after due enhancement of the wind velocities (see above), and using the WAM model (see Komen *et al.*, 1994), a new 24 hour wave analysis plus 72 hour forecast is produced. The grid used is the 20 km resolution one shown in fig. 59.

The compact output for a given location, in this case the tower, is shown in fig. 60. It shows (continuous lines) the time evolution of the significant wave height H_s, the mean period T_m, the mean direction θ_m, the wind speed and direction U, θ_U. The quality of the forecast is derived by comparison with the measured data, reported as dots in the figure. It is interesting to note the large scatter in the comparison of U, but how this does not substantially affect the overall performance of the wave model. The reason, as already pointed out in subsect. **10**˙8, is that the wave conditions at the tower depend on the overall wind fields, in space and time. So, while the wind conditions at the tower may be particularly difficult to represent in the model (note that the depression minimum passed in this area), the overall storm is well defined, leading to the good wave results. This is shown very clearly by the rotation of the wind direction round the full circle during the three-day forecast, while the waves, determined by the overall field, maintain their well defined sirocco direction.

A good idea of the quality of the forecast at different time extents is given by fig. 61, by comparing the wave analysis results at the tower *vs.* the corresponding one-, two- and three-day forecasts. The close-to-45° best-fit lines show that, on the average, the forecast waves, and hence the winds, equal the analysis ones. However, the increasing spreading with the extent of the forecast indicates clearly the decreasing accuracy in terms of *what* and *when*, stressing the limited reliability after 72 hours.

For obvious practical reasons, but also because it is the only one of the three stations mentioned in subsect. **10**˙8 whose data are available in real time, the results at the tower have received much attention. A comparison between model and measured wave height indicate a negative bias of 0.10 m out of 0.8 average value, with a scatter index equal to 0.66. This relatively large scatter is justified by the mentioned difficulty to properly represent the local wind fields. 80% of the wave heights recorded at the tower are smaller than 0.5 m. Apart from the case of swell, these waves are locally generated, and consequently poorly represented by the model. However, the main interest lies on the stormy events, in which cases the overall pattern of the wind fields, and consequently the wave conditions, are well defined and properly hind- and forecast.

A similar wave forecasting system for the Adriatic Sea has been implemented at ARPA, of Regional Meteorological Service of Regione Emilia-Romagna (Bologna, Italy), as a cooperation with ISDGM and CINECA (Bologna). In this case a higher quality wind is used, derived from the limited area model LAMBO (see Paccagnella *et al.*, 1992). In this case the WAM model has been implemented on a geographical grid with (1/12) degree resolution. The forecast is issued daily for the next 72 hours. The average bias at the tower is -0.21 m, with a rms error growing from 0.41 m at one-day to 0.52 m at three-day forecast. Note that, notwithstanding the use of a limited area model (LAM), the length of the forecast cannot be usefully extended beyond the three-day span. Because the system works in pure forecast mode, and the LAM boundary

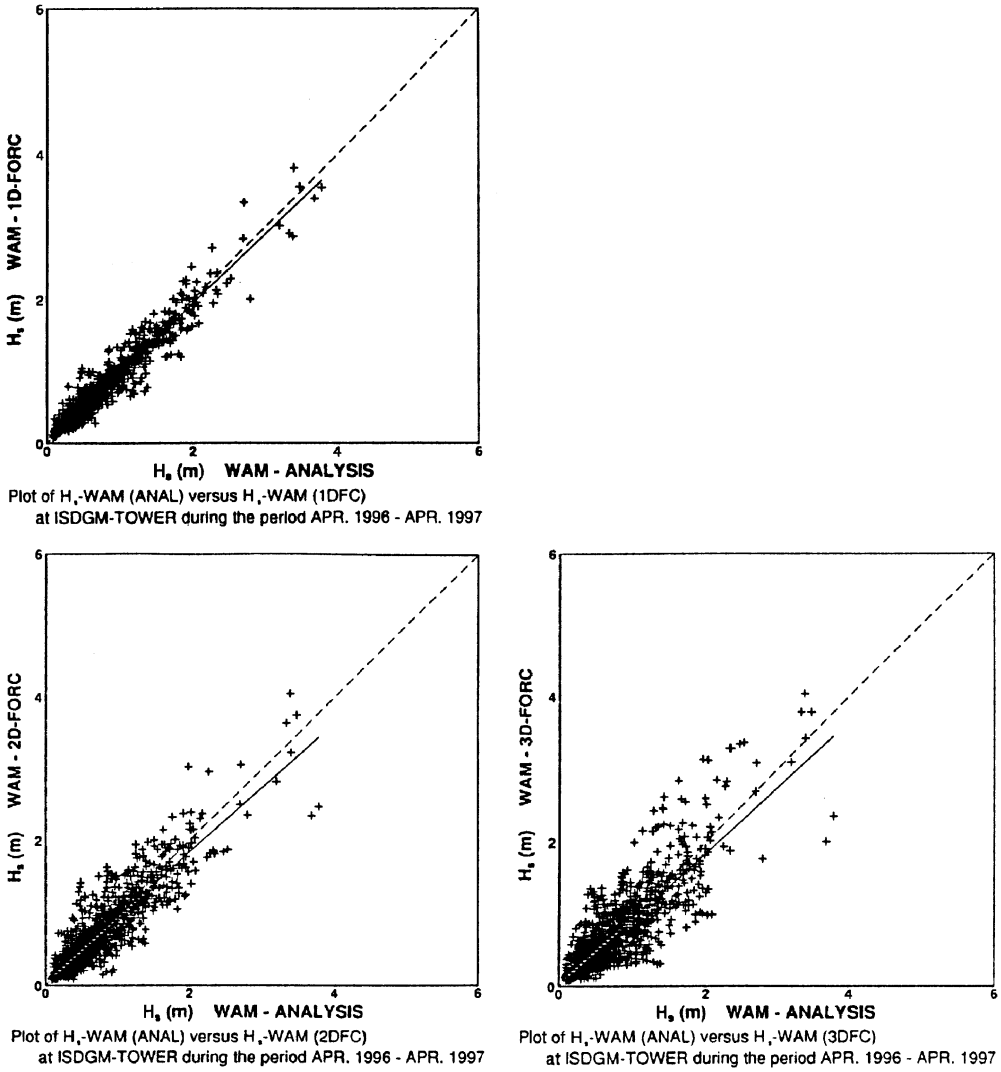

Fig. 61. – Comparison between analysis wave height and corresponding one- (top), two- (bottom left), and three-day forecasts (bottom right).

conditions are taken from the global ECMWF analysis, after a couple of days the system is subjected to the same limitations of the global model.

11. – Sediment transport

I have repeatedly mentioned along the paper the stirring of the bottom sediments by wave action. As a matter of fact, the active local wave conditions, together with the extensive area of shallow water in front of the Venetian littoral (see fig. 44) and

TABLE III. – *Maximum water velocity expected at the bottom, with the indicated yearly frequency, on different depths in front of the Venetian littoral. The last column refers to the estimated conditions during the storm of 4 November 1966 (after Stefanon, 1984).*

depth (m)	velocity at bottom (cm/s)							
12	38	50	63	75	88	125	160	132
14	33	45	56	67	78	111	143	127
16	30	39	49	59	69	99	125	123
18	26	35	43	52	61	87	112	119
20	23	30	38	45	53	76	98	116
22	20	26	33	40	46	66	87	112
24	17	23	29	34	40	57	74	108
26	15	20	25	30	35	50	60	104
28	13	18	21	26	30	43	55	100
30	11	16	18	22	27	37	48	97
likely yearly frequency	20	10	6	4	2	0,5	0,1	4/11 1966

the unconsolidated fine sediments on the bottom, form the ideal combination for an energetic suspension and motion of the bottom sediments.

The sediments in the area are a mixture of sand and silt, with an alternative areal predominance in the different zones. At the tower the bottom is a mixture of the two elements, but the conditions can change on the scale of hundreds of metres.

Waves can stir the bottom down to a surprising depth. Cavaleri and Stefanon (1980) have found evidence of storm action 30 miles off the coast, at a depth between 27 and 29 metres. In general terms, table III shows an estimate of the maximum orbital velocities that can be expected, with the indicated frequency of occurrence, at the bottom in different depths. The table has been obtained on the base of the results available at the time. The last column refers to the peak conditions estimated during the big storm of 4 November 1966, the same one that caused the record flood of Venice. It is evident from the table that stirring of sediments also down to twenty or thirty metres of depth is not an uncommon event. The ensemble of the data recorded in the following years is consistent with the above figures.

A good example of the motion of sediments, and of the consequent mobility of the geometric bottom features, is given by the tower itself. In fig. 2, showing how the tower was put into position, we can see the lowest horizontal beam of the structure touching the bottom. In the first following years the four beams (one for each side of the tower) were gradually covered by sediments, not originated from the tower. Then a phase of erosion began, after which it was possible for a diver to pass between the beams and the bottom. In the latest years this space has gradually filled up, and presently the bottom is again at the level of the beams.

A monitoring of the sediments in suspension in the area of the tower, and of their relationship with the carbon cycle in the water column, has been described in sect. **6**. In the following subsection I describe a nourishment programme carried out for the beaches of Cavallino and Pellestrina, and their following monitoring and management on the base of the wave data recorded at the tower.

11·1. *Coastal transport.* – I have repeatedly mentioned along the paper the potential motion of sediments at different depths. The gradually shoaling bottom while

approaching the shore implies a more energetic stirring by waves, hence a more frequent suspension and transport by local currents. The peak is reached at the shore, where the breaking waves have the double effect of a strong suspension of sediments and an active coastal current. Together with their motion in the direction perpendicular to the shore, this leads to the relatively fast changes that we experience on the shoreline and on the beach profiles.

The shoreline in the Venice area is characterized by long stretches of sandy beaches, with intermediate areas where artificial defenses have been built to separate the lagoon from the sea. The sand was supplied by the various rivers pouring their water into the Adriatic Sea, North and South of the Venice lagoon. Actually, some rivers were discharging their sediments directly in the lagoon itself, but they were diverted outside in the past centuries to avoid the siltation and the consequent disappearance of the lagoon (see Miozzi, 1957, for a full account of the various hydrodynamical works done for this purpose, or Gatto and Carbognin, 1981, for a more compact summary of the main works).

The sediment transport along the coast is determined by the local wave regime. In general terms (see subsects. **8**·3 and **10**·6 for wind and wave statistics in the Northern Adriatic Sea) the area is characterized by the bora storms, blowing from North-East, and the sirocco ones from South-East. Combined with the orientation of the coast (see fig. 1) and the availability of sediments at the river exits, this implies that the sediments transport is toward the lower left direction along the sea border of the lagoon and to the North of it, and in the opposite direction more to the South.

The construction of the jetties at the inlets and the control of the river flows, with a consequent drastic decrease of the supply of sediments, has led to a distributed erosion of the beaches, with eventual accumulation on the jetty on the up-wind side of the inlet. The most evident example is on the North side of the Lido entrance (see fig. 44, where the shoreline has advanced more than one kilometer with respect to its original position.

With the purpose of restoring the eroded beaches to their original conditions, and consequently of a better protection of the narrow separations between the sea and the lagoon, the Consorzio Venezia Nuova (see sect. **3**) has undergone and just completed an extensive nourishment programme that involved $2 \times 10^6\,m^3$ of sand at Cavallino (the area to the North of the Lido entrance), and $4 \times 10^6\,m^3$ at Pellestrina, just South of the area shown in fig. 44, where the width of the island separating the sea and the lagoon reduces practically to zero and artificial defenses, the *murazzi* (see subsub-sect. **10**·11.1), have been built. The contemporary availability of a nourishment programme and of continuous wave measurements at the tower offered the chance for an extended validation, and application, of numerical models for sediment transport, with the further aim of monitoring the beach evolution, and the consequent management of the situation. The nourishment programme is described by Noli *et al.* (1993). The monitoring activity is described by De Girolamo *et al.* (1998).

Instead of using a complicated approach, and given the relatively simple geometry of the coastline, the simplifying assumption was taken of a full independence between the longitudinal and transversal sediment transports. In general terms, the longitudinal motion of sediments is connected to the wave climate and to the long-term changes, while the transversal motion, determining the beach profile, acts with the seasonal cycle, possibly within the duration of a single storm. From the economical point of view the latter one deserves more consideration, because it implies the eventual loss of sand toward the offshore zone.

The Aries model used for the long-term evolution is similar to the one developed by

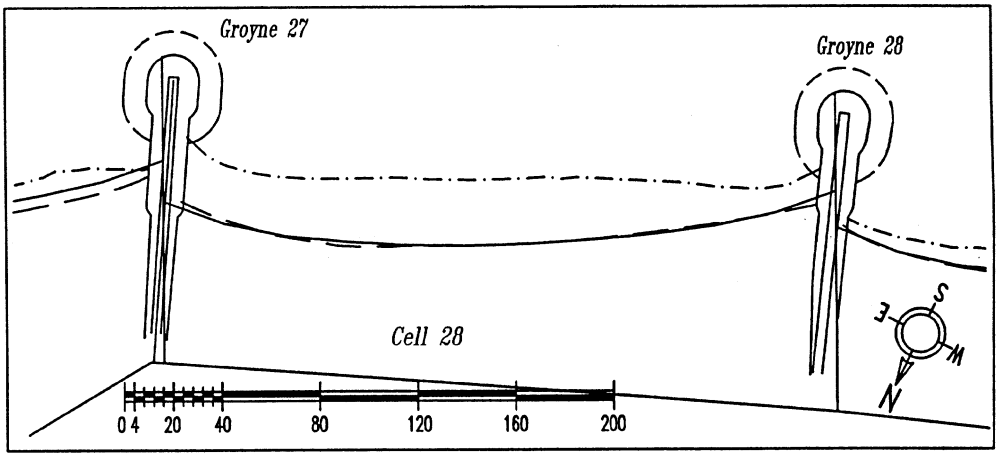

Fig. 62. – Cavallino beach: monitored shoreline evolution and simulation carried out by the one-line model (after De Girolamo *et al.*, 1998).

H R Wallingford (1992a,b). It is based on the calibration of a large number of parameters characterizing the beach and the wave conditions acting on it. Once a sufficiently long time series of these parameters is available, the model can be used to estimate (to forecast) its evolution on the base of the measured wave conditions (expected wave regime). The wave data recorded at the tower position are transferred first to the ten metre depth level, and then to the shore, by means of the ray tecnique (see, *e.g.*, Dorrestein, 1960, Collins, 1972). Dense surveys of the beach coastline and profile were done at the start of the project, after the construction of a system of groins, after the nourishment (April 1995) and at one year distance (August 1996). The following considerations concern the variations occurred between the last two surveys.

Figure 62 shows the evolution of the coastline within one of the cells in the Cavallino area. It is clear from the fit between the expected and the occurred variations that, once properly tuned to specific location and conditions, the model works rather well. In the present case this can have been helped by having been the wave history statistically similar to that of the calibration period. The evident retreat of the shoreline is due to the transversal readjustment of the sand distribution, forced by the local wave regime. This is evident in fig. 63, where we see the typical formation of an offshore bar at the position where storm waves break.

The interesting question is which is the time required for the final adjustement of the beach to the new conditions. As seen in the figure, the original beach was characterized by a double layer bar system. Besides, confrontation of the depth of the bar crest with the distance from the shoreline X_c (see Silvester, 1993) reveals they are still off the relationship

$$h_c = 0.111 X_c^{0.575}$$

(measures in metres) reported as common for beaches of this kind. All this suggests that after more than one year (one winter) the profile is still approaching its

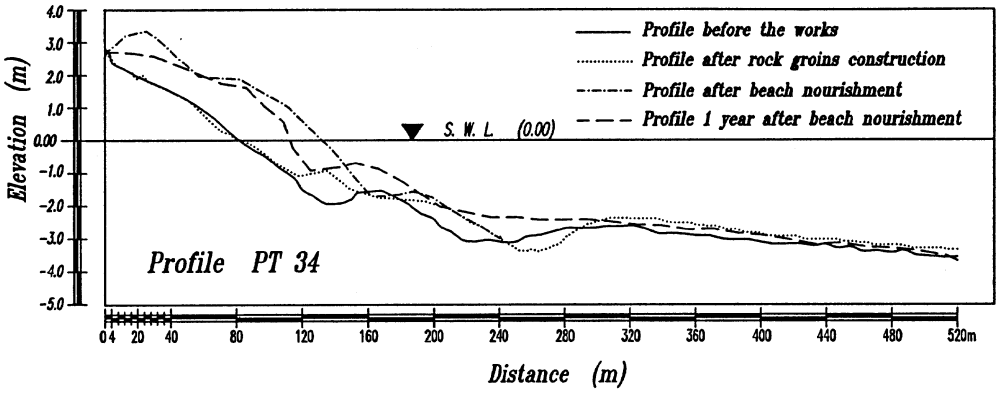

Fig. 63. – Four beach profiles measured for a cross-section at Cavallino (after De Girolamo *et al.*, 1998).

equilibrium conditions. The lack of the second bar is expectably related to the non-occurrence of exceptional storms during the period elapsed after the nourishment.

A frequent monitoring, coupled with the expectations derived from the numerical model, is essential for a proper management of the beach. Because this has been enlarged for the protection of the background zone, the key parameter to consider is the risk R_t that a flood due to a T-year return period storm happens within a specified period t. In economical terms, and following an approach commonly applied for rivers, R is evaluated as

$$R_t = EVt/T \,,$$

where E is the economical value of the properties exposed to flooding, V is their dimensionless vulnerability, $0 < V < 1$. In practice, T is taken as the return period of the "weakest" storm, strong enough to cause damage, while t, the "exposure period", is the time required for a saltuary nourishment intervention. Once R has been established on the base of social, political and economical considerations, using the results from the survey or the expectations derived from the model, it is possible to decide where to act and the volume of sand required to restore the desired conditions.

12. – Remote sensing

The last twenty years have witnessed the globalization of the measuring systems, following a similar trend both in the physical approach to the problems of the planet as in a political and social perspective. Point measurements, however valid they are for a not n-small number of reasons (I am obviously stressing this view in the present paper), cannot supply the worldwide amount of data required. This task has been taken over by the satellites, whose sophistication and capabilities keep growing at a fast rate.

There is a close link between satellite and ground based measurements. Satellite instruments need calibration, ground truth, reference points, etc. An instrumented

point in the middle of the sea is an ideal location for this kind of activity. Consequently, the tower has been involved in a number of projects in connection with different satellite missions. In the following sections I describe the activities related to a) the calibration of optical measurements, b) the absolute calibration of the ERS-1 radar altimeter, c) the measurements of surface wind by scatterometer, and d) the detection of surface wind stresses by SAR images.

12·1. *The calibration of optical measurements.* – Initially, the attention of the satellite marine instruments was focused on the deep sea waters. Being confronted with basic problems of satellite measurements, researchers had an obvious tendency to keep their applications off the coastal zone, where the possible interaction with the coastline and the shallow waters would introduce additional problems. However, with the refinement of the techniques and the extension of practical interests toward the coastal zone, attention has gradually moved to this area.

The complications arising from the influence of the bottom on the characteristics of the above layers imply the extensive use of the calibration/validation tecnique, *i.e.* of devoted campaigns aimed at measuring the sea truth allowing the calibration of the satellite sensors.

One advantage of operating in shallow waters is the possibility of making use of fixed structures, allowing more continuous, extended and possibly more accurate campaigns with respect to the use of oceanographic ships.

The "Adria 84" campaign was devoted to the calibration of radiometer data in the sea, and an extensive series of measurements was carried out (Maracci *et al.*, 1984). Besides the tower, "Adria 84" involved a number of ships and an aircraft. The aim was to repeat the measurements in all the possible conditions, to fully understand the influence of the various parameters on the final results. While all the ships involved in the experiment employed the same EOS underwater radiometer, only at the tower was the different RSI radiometer available. The Research Support Instruments (RSI) was a five channel underwater radiometer, expecially designed to be compatible with the Nimbus-7 colour scanner. It included an optical-mechanical package, an integrated detector with a photomultiplier tube detector, a tilt sensor, pressure and temperature transducers, a computer for instrument control and data collection. The radiometer had four spectral channels, 443, 520, 550 and 670 nm, and one channel to measure dark current. Both downwelling and upwelling radiation could be measured.

The use of the RSI radiometer requires particular attention because of its nonlinear response after a certain irradiance threshold. Careful calibration in the laboratory, followed by a series of accurate measurements, provided a clear characterization of the conditions typical at the tower. The variation of irradiance with depth is typically represented as

$$I_{\mathrm{U,D}}(\lambda, z) = I_{\mathrm{U,D}}(\lambda, 0)\, e^{-k_{\mathrm{U,D}}(\lambda) z},$$

where $I(\lambda, 0)$ is the surface extrapolated value for the irradiance, $k(\lambda)$ is the diffusive attenuation coefficient, z is the depth, U, D indicate up- and downwelling respectively.

Table IV shows the result of some typical measurements, reporting the parameter $k_{\mathrm{U,D}}(\lambda)$ and $I_{\mathrm{U,D}}(\lambda, 0)$ that have been obtained from the underwater profiles, the derived values of the ratios $R(\lambda, 0) = I_{\mathrm{U}}(\lambda, 0)/I_{\mathrm{D}}(\lambda, 0)$ to be used for the inter-

TABLE IV. – *Sea optical parameters at the CNR platform during the "Adria 84" campaign (after Maracci et al., 1984).*

λ (nm)	$K_{U,D}(\lambda)$ $I_{U,D}(\lambda,0)$ $R(\lambda,0)$	29.8.84 12.40	30.8.84 12.15	31.8.84 13.00	UNITS sun time
439	K_U	.315	.216±.011	.208	
	K_D	.297	.18±.009	.167	
	I_U	2.36	2.56±.18	2.07	mw/cm^2 μm
	I_D	62.43	65.04±4.55	58.85	mw/cm^2 μm
	R_{439}	.0378	.0394±.0039	.0352	
520	K_U	.197	.120±.006	.116	
	K_D	.187	.110±.006	.116	
	I_U	3.41	2.61±.18	2.24	mw/cm^2 μm
	I_D	64.97	62.5±4.37	63.5	mw/cm^2 μm
	R_{520}	.0525	.0417±.0041	.0353	
550	K_U	.184	.103±.005	.100	
	K_D	.158	.100±.005	.105	
	I_U	3.74	2.24±.16	2.00	mw/cm^2 μm
	I_D	60.76	57.63±4.03	47.97	mw/cm^2 μm
	R_{550}	.0616	.0389±.0039	.0345	
670	K_U	.30	.44±.044	.35	
	K_D	.55	.49±.025	.49	
	I_U	.38	.22±.02	.14	mw/cm^2 μm
	I_D	49.03	54.87±3.84	54.93	mw/cm^2 μm
	R_{670}	.0064	.0040±.0005	.0025	
$\frac{R_{439}}{R_{550}}$		.61	1.01±.15	1.02	
$\frac{R_{520}}{R_{550}}$		.85	1.07±.15	1.02	
Secchi disk		5.5	8.5	8	m

pretation algorithms of the sea colour, and the measured values of the Secchi disk depth.

Typical vertical profiles of up- and downwelling irradiance are given in fig. 64. Note the drastically different attenuation with depth at the different wavelengths.

The approach followed by Maracci *et al.* (1984) in "Adria 84" is clearly based on the use of data measured in the field to derive empirical laws to be then applied on a routine basis. The experience and knowledge acquired in the intermediate years have shifted the procedure towards a more sound approach. Nowadays the basic idea is to measure in detail all the physical parameters (Inherent Optical Properties) affecting the optical measurements, to be able to derive or verify their effect on the final results.

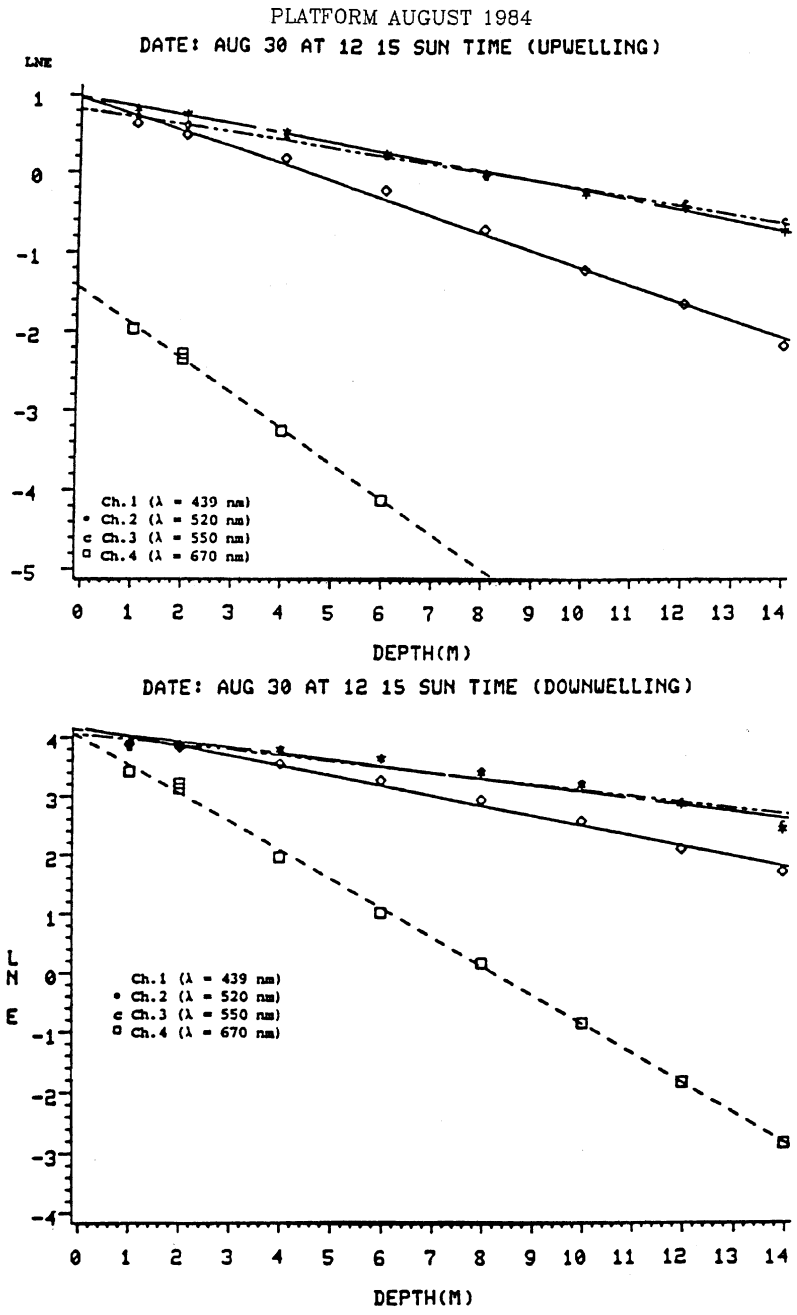

Fig. 64. – Example of underwater irradiance profiles for upwelling (above) and downwelling (below) (after Maracci *et al.*, 1984).

A large project, CoASTS, managed by the Joint Research Center and ISDGM, and better described in sect. **13** on the ongoing activities, is making use of the tower for the calibration of the presently flying optical instruments devoted to ocean colour.

The advantage of a physical approach is that, once the physics of the process is sufficiently understood, the results can be used on a worldwide basis. In this respect, and to fully exploit the potential of each calibration facility, it is clearly essential to establish a protocol, so that measurements taken at different positions with different instruments can be intercompared, and a single recommended conclusion is derived. CEVEx (Concertation of European Validation EXperiments for coastal/shelf water remote sensing) is a Concerted Action between CoASTS and PlyMBODy (Plymouth Marine Bio-Optical buoy), a project managed by the Oceanography Department of the University of Southampton, and based on a buoy equipped with authomated optical instruments, operative in the Western English Channel. The aim is a full definition and unification of the calibration procedures, in practice the creation of a protocol (see CEVEx group, 1997).

Following CoASTS and CEVEx, the ISDGM tower and the PlyMBODy buoy have been chosen by NASA as two of the three worldwide existing calibration points for ocean colour satellite instruments (the third one is a devoted buoy in the area of Hawaii). In the case of the tower the specific aim is the evaluation of the disturbance introduced in the measurements by close-by structures, and therefore a series of recommendations to be followed during the practical phase of the measurement campaigns.

12˙2. *The calibration of the* ERS-1 *radar altimeter*. – The ERS-1 satellite was launched in July 1991. It was a very successful mission, the satellite lasting much longer than expected and with a wealth of results that had, and still have, a profound impact on the applied meteorology and oceanography. The satellite is still usable, but kept in a dormant stage, with saltuary brief active interruptions for routine checking. It was substituted in active operations by its follow-up ERS-2.

The ERS-1 hosts a synthetic aperture radar (SAR), a scatterometer for the remote measurements of the wind on the sea surface, a radar altimeter and a radiometer. The altimeter is used for two different purposes: measuring the distance between the satellite and the surface, and for an estimate of the wave weight and wind speed on the satellite nadir. All the calibrations in connections with meteo-oceanographic parameters were done off the coast of Norway. The absolute calibration, *i.e.* the one connected to the distance between the satellite and the sea surface, was done on the oceanographic tower of ISDGM.

This required quite a concerted action by a number of institutes. The basic reference for it is given by ESA (1993). For the benefit of the description of the campaign, the actions involved can be logically split into two parts: the pre-launch activities, related to the accurate positioning of the tower and the obvious logistics, and the actual operations during the passes of ERS-1. These activities are described in the two following subsubsections.

12˙2.1. The tower position. The basic idea after the calibration of the radar altimeter (explained in the following subsubsection) required the accurate positioning (at the centimeter level) of the tower with respect to a known large scale network, in particular with respect to the radar stations expected to track the satellite when this overflew the tower. This was obtained first by linking the tower by the Global Positioning System (GPS) to a regional network, with dimensions 100×80 km, This network included also Monte Venda, close to Padua, 64 km West of the tower, a location chosen as basis for a devoted tracking laser during the altimeter calibration. The

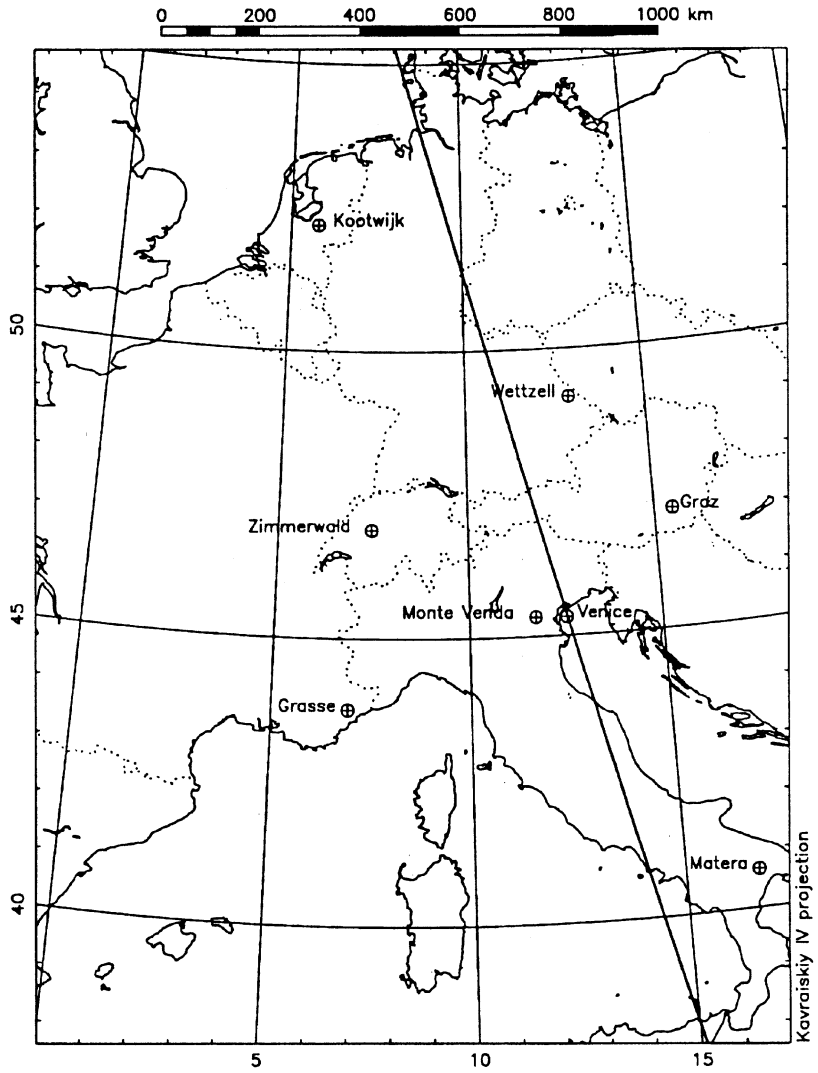

Fig. 65. – Sites occupied by GPS receivers for the "large" campaign in 1990. The straight line indicates the "Calibration Orbit" of ERS-1 overhead the *Acqua Alta* tower (after ESA, 1993).

position of the tower was obtained by a sequence of devoted campaigns in 1988, 1990 and 1991, see Caporali *et al.* (1988) and ESA (1993).

The availability of two well positioned points, the tower and Monte Venda, allowed to connect the regional network, hence the two locations, to a "large" network (see fig. 65), including all the stations to be used for tracking the ERS-1 during the calibration phase. To increase the accuracy and to cross-check the results, the analysis of the data was done by different groups with different sofwares, using also different instruments in the two campaigns of 1990 and 1991.

The results of the parallel calibration are reported in table V. Once accounting for the local eccentricity, they clearly show that the measurements satisfy the required

TABLE V. – *The position of the tower* (VT WM90) *and Monte Venda* (MV 7542) *with respect to the global network, as derived by different institutes with different softwares* (*after* ESA, *1993*).

Year	Obs	Proc	Station	x (m)	y (m)	z (m)	h (m)
1990	GPS	AIUB	MV 7542	4399363.527	910506.391	4512940.815	523.186
1990	GPS	DUT	MV 7542	4399363.582	910506.368	4512940.800	523.210
1991	GPS	AIUB	MV 7542	4399363.564	910506.408	4512940.772	523.183
1991	SLR	DUT	MV 7542	4399363.543	910506.419	4512940.880	523.248
1990	GPS	AIUB	VT WM90	4386229.603	973073.288	4512012.437	55.634
1990	GPS	DUT	VT WM90	4386229.670	973073.271	4512012.435	55.677
1991	GPS	AIUB	VT WM90	4386229.651	973073.347	4512012.393	55.645

accuracy. Formal errors, repeatability and comparison between the 1990 and 1991 data suggest an accuracy of the height difference between Monte Venda and the tower of the order of 2 centimeters, therefore easily meeting the requirements for the calibration of the radar altimeter.

12'2.2. The absolute calibration. The aim of the radar altimeter (RA) on board of ERS-1 is to measure the distance between the satellite (its devoted antenna) and the sea surface. Continuous monitoring, in space and time, of this distance, together with that of the satellite orbit, provides an accurate description of the geometry of the sea surface, a key information for the monitoring and modelling of mean sea level, tide and circulation.

The declared accuracy to aim to was 5 cm. The difficulty of the task becomes readily apparent when we think of the height of the orbit, about 715 km. The required relative accuracy is better than $1 : 10^7$.

The calibration of the RA measurements implied the comparison of the altimeter output with an independent evaluation of the distance between the ERS-1 and the sea surface. The basic idea is sketched in fig. 66. While flying along the orbit on the vertical of the tower, the ERS-1 was tracked from the stations indicated in fig. 65. Therefore its position is accurately known. Also the tower position is known within the same network (see the previous subsubsection). Knowing the tidal level at the tower at the time of the pass, it is then possible to intercompare the RA measure with the corresponding one derived from the geometry of the system. The problem (see fig. 67) is to link the instantaneous mean sea surface to the reference position (the GPS antenna) on the tower.

The GPS antenna was located on the extension of the West corner of the tower, visible on the upper-left of the structure in fig. 3. The extension was specifically built to track ERS-1 with PRARE, an additional locally passive tracking system. As no obstacle had to be along the line of sight between the PRARE and the satellite, the terrace was built extending horizontally from the main structure to put the PRARE in the right position. Incidentally, this system was not used because of the failure of the corresponding active part on board of ERS-1.

The task on board of the tower was to link the tidal level to the GPS antenna. The basic requirement was an accurate and fast tide gauge, without the delay typical of the

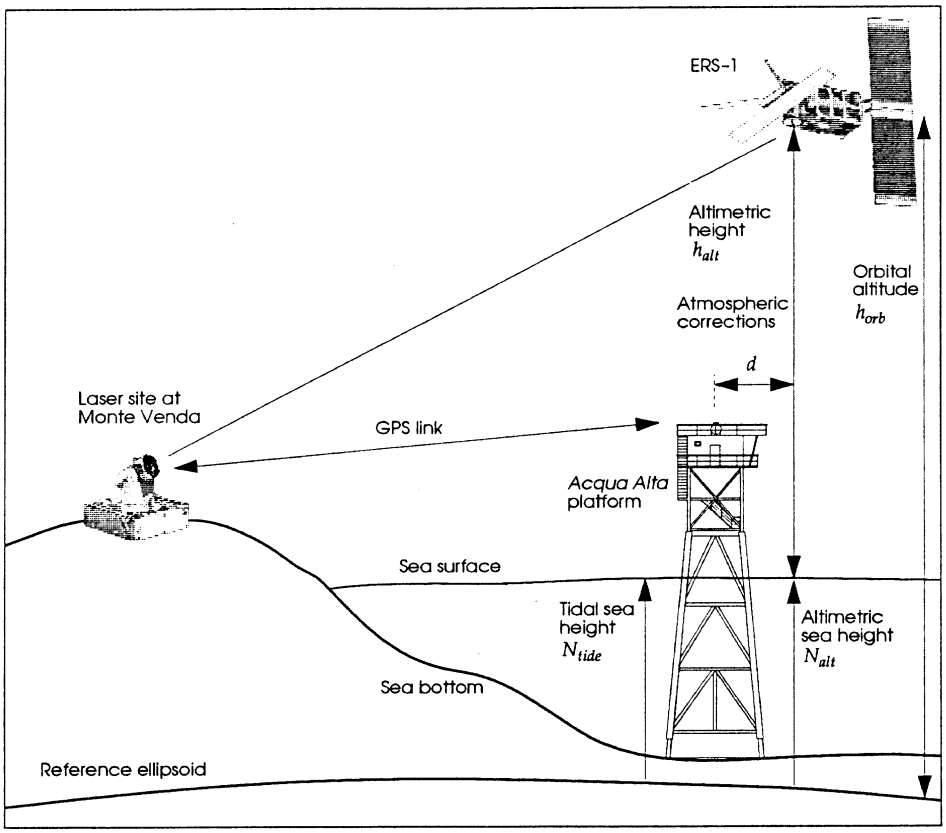

Fig. 66. – Schematic illustration of the calibration tecnique (after ESA, 1993).

tidal wells. This was already available, and has been described in subsect. **9**˙1. There remained the link with the antenna to be dealt with. The scheme is summarized in fig. 68. A small reference mark T was welded to the tower, approximately, but not necessarily, at the mean sea level. Checking the tide on a calm, still water, day, the level l was marked on the tidal record when the water was at the T level. Then, by geometrical calibration, the vertical distance between the GPS antenna and T was established, passing through the intermediate points O, on the vertical of T, and MO. At the time of the pass the tide would be at a generic level t. Inspection of the difference $d = t - l$ allowed the evaluation of $b = c - d$ (see figure), hence the link of the tidal level to the GPS antenna. In turn, see again figs. 67 and 66, this allowed the geometrical evaluation of the distance between the satellite and the sea surface, hence the calibration of the radar altimeter.

The difficulties of the overall procedure cannot be overestimated. A large number of elements must be considered for the accuracy of the final measure. A full account is given in ESA (1993). As far as the tower is concerned, two more points were taken into account. The first one was the microwave radiometer, located on top of the tower. The radiometer, supported by the data from the on board meteorological measurements (air pressure and temperature, relative humidity), provided an estimate of the wet content

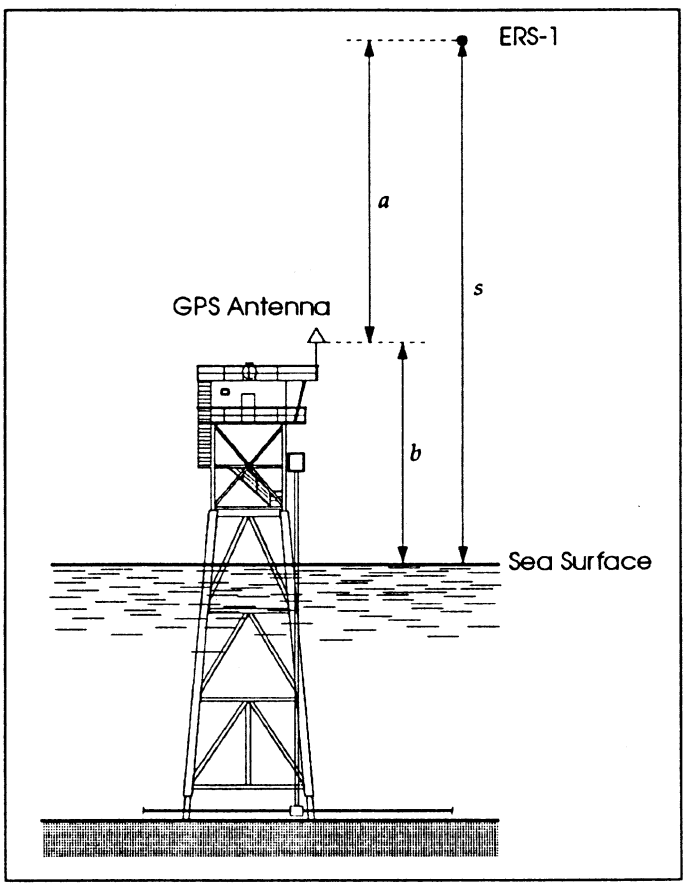

Fig. 67. – Schematic illustration of the calibration of the ERS-1 radar altimeter. The satellite range s is the sum of the range to the GPS antenna, a, and the distance b from the GPS antenna to the sea surface (after ESA, 1993).

of the atmosphere. This is required to estimate with sufficient accuracy the time delay of the altimeter signal due to atmospheric delay and refraction effects (ESA, 1993, pp. 80-89).

The second point concerns the thermal expansion of the tower as a consequence of the daily thermal cycle, particularly of the sun radiation (most of the tower is painted black, so reflection is kept to a minimum). An expansion would affect the distance b (see fig. 67), hence the calibration. Independently of any simple calculation, a series of devoted measurements was done suspending from the terrace a long INVAR wire (dimensions not changing with temperature), ending with a weight pointing to a reference mark. The expansion (see Cavaleri *et al.*, 1987) was found even smaller than expected, less than 1 mm, because of the high thermal conductivity of the steel that, immersed in the sea, cools down the structure even during the hot hours of the day.

During the calibration campaign ten useful passes, with the suitable conditions and all the instruments working properly, were obtained. The final result derives from these ten data sets. The output of a typical pass is shown in fig. 69.

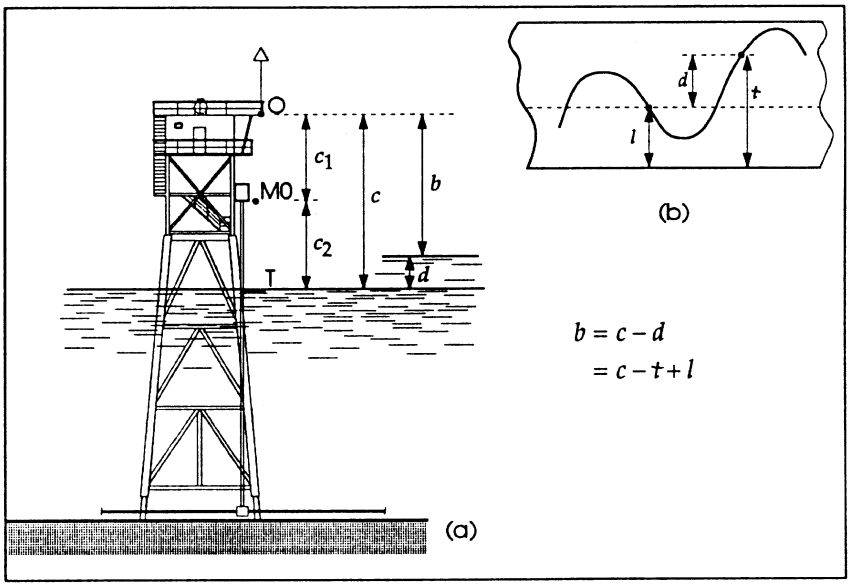

Fig. 68. – Scheme for the determination of the distance b (GPS antenna-sea surface) on the tower (after ESA, 1993).

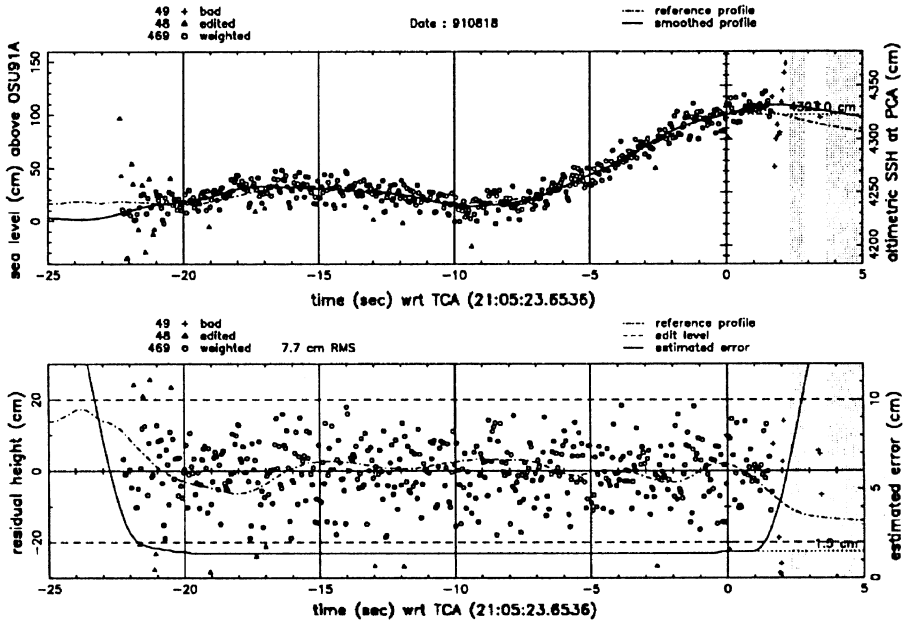

Fig. 69. – Smoothing and interpolation of the relative sea surface height derived from the ERS-1 20-per-second altimeter samples from the Venice pass of 18 August 1991. The upper panel shows the smoothed altimetric sea surface height, and the lower panel the estimated error (after ESA, 1993).

TABLE VI. – *Estimated errors of the various entities building up the bias estimate per pass, in centimeters* (*after* ESA, *1993*).

Entity	Method	Static Error
Recorded sea level	Analogue tide gauge	0.0
Height of the zero tide level wrt GPS marker WM90	Local survey	2.0
Height of the GPS marker WM90	GPS	2.0
Local solid Earth tide	Love Model	1.0
Station coordinates	ERS90B coordinate set	1.0
CM correction	Geometry	0.1
Bias estimate per pass	RSS	3.2

The errors which occur in the final value of the bias calibration are of two types. Static errors (also called systematic, or bias errors) are errors that are always present, for every pass. They are, for example, caused by wrong measurements in static position or by errors in models. The other type of errors is the nonstatic (or random, or noise) error. These are different from pass to pass and can be reduced by increasing the number of calibration passes.

The contribution of errors in the measurements and models is given in table VI. The overall uncertainty is 3.2 cm. The estimate of the nonstatic error, as estimated from the output of the ten passes, is ± 2.0 cm.

On the whole the final result for the bias estimation, and total uncertainty, in the RA height measurement was

$$-41.5 \pm 5.2 \text{ cm}.$$

12'3. *Wind measurement by scatterometer.* – The basic idea behind the measurement of surface wind speed with an air-borne scatterometer is the reflection by Bragg effect of short electromagnetic waves by the surface waves with half the radar wavelength (< 30 cm). From the practical point of view, such short waves react instantly to variations of the wind speed. This allows to establish a direct relationship between the radar backscatter and the surface wind.

The investigation of the sea surface roughness using radar backscattering tecniques is a complicated problem. The sea surface roughness corresponds to the fine structure of the waves travelling at the sea surface. It is the result of many physical interactions occurring at the boundary layer between air and sea, including wind turbulence and wave generation. To understand the physics of these processes it is necessary to perform accurate measurements of the involved parameters.

The methods of computing the wind speed from satellite backscattering data rely, at present, on empirical models. These relate the radar backscatter, expressed in terms of the normalized radar cross-section σ_0, directly to the wind speed at neutral conditions ($T_{\text{air}} = T_{\text{sea}}$) through functions depending on the radar incident angle. In this way they neglect the influence of all the other parameters that may influence σ_0, namely the sea surface temperature, the air-sea temperature difference, the quality of the water surface (clean or polluted), and the age of the wave system. To understand the nature and the importance of these possible influences, Zecchetto and Trivero

(1993) carried out a series of experiments aimed at measuring the high frequency spectra under different oceanographic conditions.

The basic experiments were carried out on the ISDGM oceanographic tower during a series of devoted campaigns. Three kinds of instruments were used: radar, anemometers and wave gauges. The two scatterometer radars used coherent pulses at, respectively, C band (5.4 GHz) and at L, S, C bands (1.35, 2.7, 5.4 GHz). These correspond to wavelengths of about 23, 11 and 5.5 cm. The output was a 150 Hz bandwidth complex signal. The absolute calibration was carried out by pointing the radars towards a certified metal sphere of known cross-section. The scatterometers were located on top of the tower, at its East corner, facing the two main incoming wind directions. The support used for the instruments is visible at the upper-right corner of the tower in fig. 3.

The wave gauge is a 10 GHz microwave interferometer radar. It is based on conveying the electromagnetic waves on a teflon coated wire stretched vertically into the sea (Goubau line), and measuring the sea surface elevation after detection of the phase of the reflected wave short circuited by the water (Fiscella *et al.*, 1982). The wave gauge was located at the outer end of the horizontally protruding platform visible in fig. 3, and parallel to the vertically tensed wires used as guide to the cart.

On the vertical of the Goubau line two K-Gill propeller and a Kaijo-Denki ultrasonic anemometers allowed three-dimensional high frequency sampling of the air motion.

The measurements aimed at clarifying the role of the overall wind field and of the underlying wind waves on the value of σ_0 measured by the satellite scatterometer. The basic results are summarized in fig. 70, showing the amplitude spectra of a) σ_0 and b) the sea surface Doppler frequency consequent to the water orbital motion with respect to the scatterometer. Panel a) shows two distinct peaks, around 0.01 and 0.18 Hz. The coincidence of the latter with the one in panel b) suggests clearly the modulation of the radar signal by the dominant waves. This interpretation is supported also by the coherence between the two signals. The explanation is connected to the interactions among the different wave components and the stretching of the surface connected to the alternative orbital motion that forces the small short waves in the area just ahead of

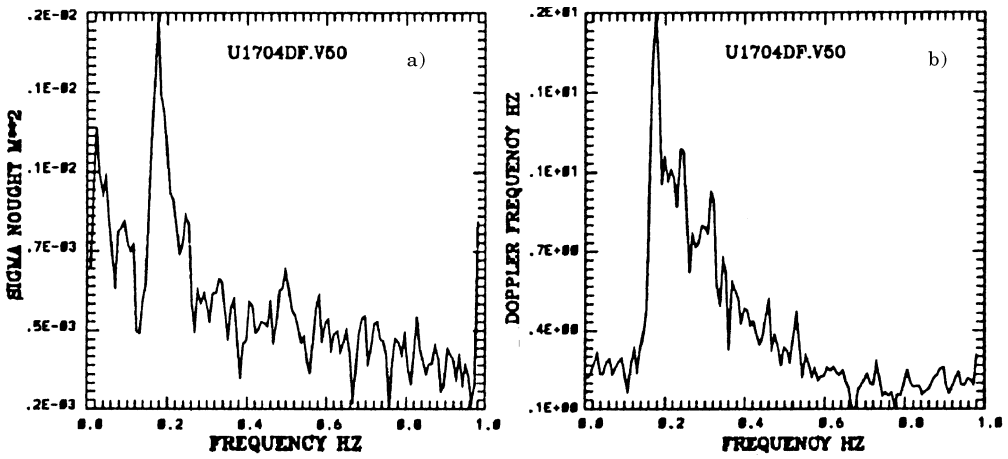

Fig. 70. – Amplitude spectrum of a) σ_0 and b) sea surface Doppler frequency (after Zecchetto, 1993).

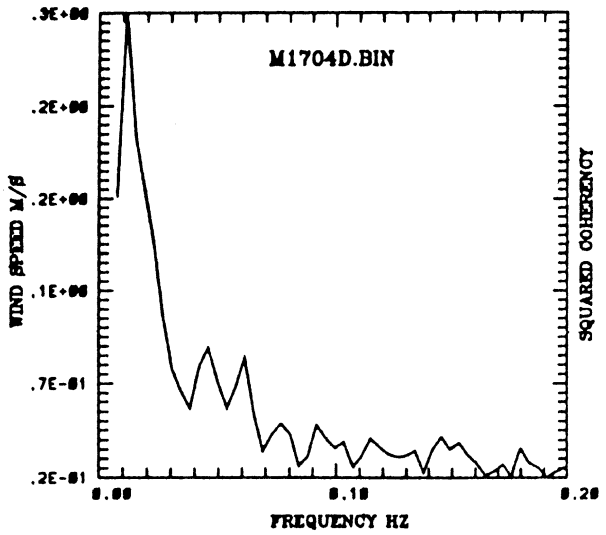

Fig. 71. – Amplitude spectrum of wind speed (after Zecchetto, 1993).

the leading crests. Therefore the signal of the scatterometer is characterized by a sequence of peaks in connection to the passage of the wave crests. The phase analysis confirms the position of the wavelets on the wave profile.

The 0.01 Hz peak in the scatterometer signal has a quite different origin. As I have discussed in subsect. 8·4, a wind field is not uniform, but it shows oscillations in space and time, whose amplitude and scale depend basically on the air-sea stability conditions. The record from which the spectra in fig. 70 have been derived was taken under bora conditions, the cold and gusty North-East wind. Figure 71 shows the corresponding wind speed spectrum, with a well defined peak at low frequency, corresponding to the one in the scatterometer signal. In practice, in a turbulent wind field the radar return signal is not constant, but it varies with the instantaneous wind speed, hence with the energy level of the generated wavelets.

This has implications for satellite measurements. The area looked at by the flying scatterometer is typically $25 \times 25\ \mathrm{km}^2$. The algorithm relating the return signal, *i.e.* σ_0, to the wind speed does not take air-sea stability into account, and it assumes implicitly uniformity in space. As we have seen in fig. 71, this may not be the case. The problem is that the relationship between σ_0 and U is exponential in type (*i.e.* $\sigma_0 \propto U^\gamma$). Therefore the average σ_0 derived from the observed area does not correspond to the average wind speed, *i.e.*

$$\overline{\sigma_0(U)} \neq \sigma_0(\overline{U})\,.$$

The difference increases with the level of gustiness in the field. Therefore the present algorithm relating σ_0 and U is likely to depend on the specific location where the calibration was carried out and on the conditions present during the campaign. Zecchetto (1993) stresses the importance of considering wind gustiness, as possibly derived from meteo-oceanographic models, for a correct retrieval of the surface wind speed.

Fig. 72. – SAR image of the area around the tower (dark spot up-right of the centre). Dimensions $4.4 \times 4.4\ \mathrm{km}^2$. The wind is blowing from left to the right (after Zecchetto *et al.*, 1996).

12·4. *Surface stresses derived from* SAR *images.* – The spatial variability mentioned in the previous section is well detected also by the Synthetic Aperture Radar (SAR). As a matter of fact, SAR has the notable capability of providing a synoptic view of the situation. Images as the one in fig. 72 give a fairly good idea of the turbulence present in the field.

Zecchetto *et al.* (1996, 1998) stress the amount of information contained in this

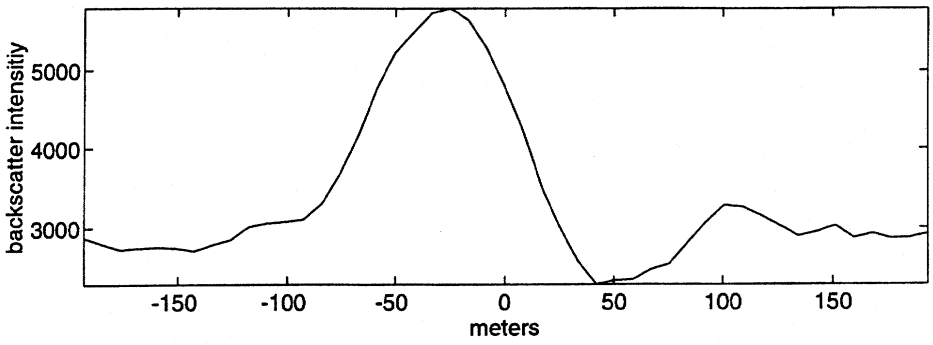

Fig. 73. – The ensemble average of the SAR backscatter of the image of fig. 72. The abscissae represent the distance from the maximum variance of the structure set at $x = 0$. Positive distances indicate downwind direction. The front of the structure is located right of the maximum of the curve (after Zecchetto *et al.*, 1998).

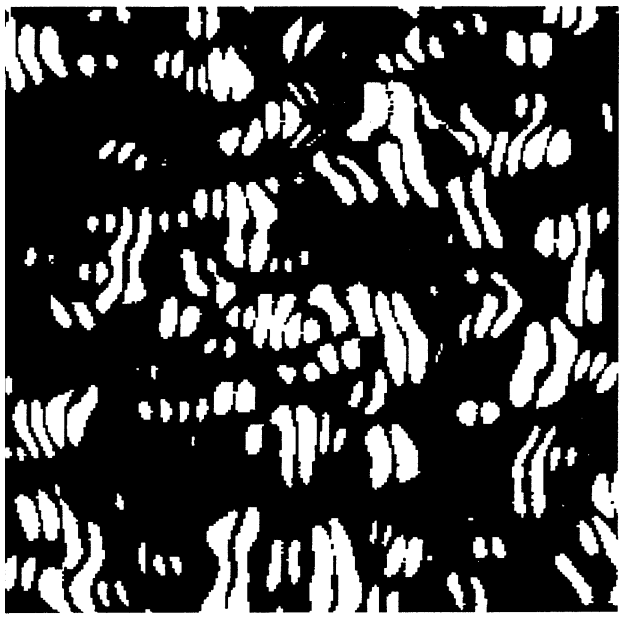

Fig. 74. – The image of the normalised short interval variance computed from a 2.2×2.2 km^2 area of fig. 72. The pairs of white patches represent the rise and decay of the backscattering structures (after Zecchetto *et al.*, 1998).

image. This was obtained with an air-borne SAR, working at the C and X bands (5.3 and 9.4 GHz, respectively, corresponding to 5.7 and 3.2 cm). They point out that at these wavelengths the signal represents the surface wind stress, or, in other words, the downward flux of horizontal momentum from the atmosphere to the sea.

A quantitative analysis of the image requires the proper interpretation of the single details. This was obtained by contemporarily measuring the three-dimensional wind vector from the tower (see the previous section for the details of the instruments), and analysing the pattern of variability of the stresses. Granted that these appear in sequential distinct bursts, the structure of the single burst is shown in fig. 73, with the structure moving to the right, *i.e.* the time flowing from the right to the left. There is a sharp increase of the backscatter signal, *i.e.* of the stress, followed by a slower return to the background value. Zecchetto *et al.* (1998) interpret the signal growth as associated to the actual stress, while the decay is associated to the time required for the dissipation of the surface wavelets, after the passage of the atmospheric burst.

The interpretation of fig. 72 on this basis is given in fig. 74, showing all the microfronts present in the area, where the strong interaction between the atmosphere and the sea is concentrated. Note that each front is divided into two parts, the front (to the right), where the flux of momentum takes place, and the tail. The shape of each front appears elongated in the transversal direction, the wind blowing from left to the right. These atmospheric structures occupy 13% of the total area.

Such a study shows clearly the possibilities offered by the SAR in the investigation of the marine atmospheric surface layer.

13. – Ongoing activities

The activity on board of the tower is never halted. Its permanent sets of instruments keep recording, providing a steady and regular flux of data. This includes the meteo-oceanographic station, plus the multiple measurements of wind, waves and tide. In particular, the directional wave recording system of ISDGM has just concluded its second decade of continuous use.

A long-term measurement of wind and waves has by now been collected also by the Consorzio Venezia Nuova. Besides the routine collection of data, the monitoring is finalized to the management of the extensive nourishment programme of a 20 km stretch of the Venetian littoral. Coupled with detailed bathymetric maps, upgraded after each heavy storm, the data collected are used to calibrate a littoral transport model. This model is then going to be used for the optimization, in terms of costs and risks, of the successive nourishment stages. The reference person is Dr. Giovanni Cecconi, Consorzio Venezia Nuova, S. Marco 2803, 30124 Venezia, Italy, e-mail: cecconi@gpnet.it.

Wind and tide are measured by the Centro Previsioni e Segnalazioni Maree (Tidal Forecast and Warning Centre) of Venice Municipality. The reference person is Dr. Paolo Canestrelli, Centro Previsioni e Segnalazioni Maree, Palazzo Cavalli 4090, 30124 Venezia, Italy, e-mail: pcanestr@tin.it.

In connection with the vertical flux of particulate discussed in sect. **6**, an extended experiment on sediment transport is under way in the vicinity of the tower. An Anderaa RCM-7 currentmeter is coupled to the sediment traps placed two metres off the bottom. The aim of connecting particulate flux with current and wave orbital motion is evident. The reference person is Dr. Sandro Rabitti, Istituto di Biologia del Mare, Castello 1364/a, 30122 Venezia, Italy, e-mail: rabitti@ibm.ve.cnr.it.

The wave data from the tower are presently used for a measurement campaign of the flux of organic matter off the exit of the Adige River, about 20 km South of the tower. Suspended organic matter is collected by a sediment trap, placed on a depth of 19.5 m. Evaluation of stirring of the bottom on the base of the recorded wave conditions in the area helps in distinguishing between the three possible sources, namely the local production, the fluvial contribution, and the resuspension of the already deposited material. The reference person is Dr. Michele Giani, ICRAM, viale della Stazione 5, 30015 Chioggia (VE), Italy, e-mail: icramve@uxd.unipd.it.

The fouling, and in particular the mussels, keep growing, providing both problems to the submerged instruments and source of information for the biological studies.

There is an ever growing activity in the field of ocean colour. A number of satellites equipped with advanced colour sensors are already flying (SeaWiFS, OCTS) or are expected to be launched in a short while (MERIS, MODIS at the time of writing). These sensors exhibit steady progresses with respect to the previous generation, and new algorithms are regularly proposed to make use of the wealth of high quality data they provide. In turn this require an ever more accurate calibration to fully exploit the potential of the remotely sensed data.

CoASTS (Coastal Atmosphere and Sea Time Series) is a project led by the Joint Research Centre of Ispra, Italy, and ISDGM, with the aim of providing atmospheric/marine optical data taken on a continuous basis by authomatic instrumentation installed on the ISDGM tower. A representative sketch of the campaign is given in fig. 75. Water samples, for water quality analysis, are monthly collected for one week to ensure the availability of bio-geo-chemical data complementary to the continuous optical measurements.

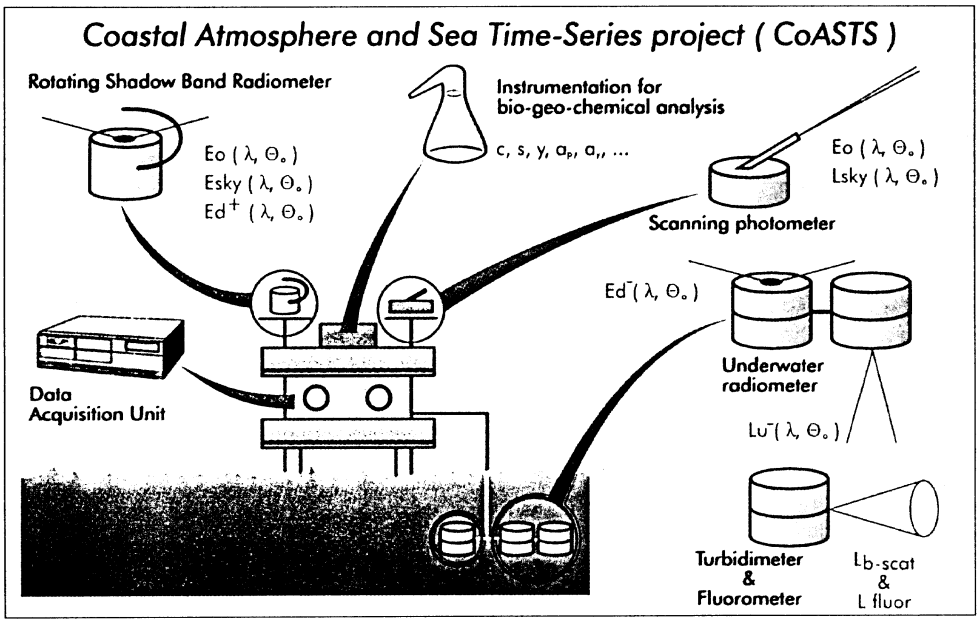

Fig. 75. – Coastal Atmosphere and Sea Time Series (CoASTS) project; offshore platform instrumentation set-up and measurements.

TABLE VII. – *Measurements collected at the* ISDGM *tower for the* CoASTS *project.*

(continuous)	global and diffuse irradiance at the surface at 415, 500, 610, 665 862 and 960 nm
	direct sun irradiance at 440, 670, 870, 936, 940 and 1020 nm
	sky radiance in sun plane and almucantar at 440, 670, 870 and 1020 nm
(periodic)	underwater upwelling radiance at 412, 443, 490, 510, 555, 620, 685 nm
	underwater downwelling irradiance at 412, 443, 490, 510, 555, 620, 665, 685 nm
	water turbidity and fluorometry
	wind speed and direction, temperature , humidity, pressure
	phytoplankton pigments by High Pressure Liquid Chromatography
	pigment and dissolved organic matter absorption,
	sediment concentration;
	marine particle size distribution
	salinity.

CoASTS has an expected life of five years, and was initiated in 1995. The list of the instruments used for continuous and periodic measurements is given in table VII.

Following the success of the Concerted Action CEVEx (see subsect. 12·1), a new project was recently initiated. COLORS (COastal region LOng-term measurements for colour Remote Sensing development and validation) is making heavy use of the

results of CEVEx, and aims at improving them, including also another station in the North Sea to better cover the possible environments of the European waters.

14. – Management

The volume of activity on board has been steadily growing during the last twenty years. At present, the tower has users on board on the average three weeks out of four. While this is a large figure itself, requiring a careful planning for the different projects, there is still room for improvement and further activities.

The tower is managed by an external contractor, who is in charge, under the supervision of ISDGM, of the transfers to and from land, maitenance, fuelling, power supply, logistics, including food and lodging. This provides the researcher with the possibility of concentrating on his work, without logistical problems.

The yearly overall management cost is about 250 kUS$/year. The users are charged for the use of the structure at 450 US$/day, plus 45 US$ for each person on board (prices at the time of writing). A typical transport from Venice (about 1 hour 20 minutes from our institute in the centre of the town, or 30 minutes from the exit of the lagoon) costs 250 US$.

The tower is also available for permanent instruments by external institutes or companies, the cost depending on the space and facilities required.

The structure offers a large panorama of possibilities for measurements and activities. However, working on a tower, with limited space and always subjected to rapidly changing atmospheric and sea conditions, requires a different attitude than on land. Any activity requires more time than in a standard laboratory. On the other hand, the advantage of being on the hot spot, in the middle of the developing event, is invaluable for the experience and perception it provides. I have spent some of my best hours watching a heavy storm and trying to understand what was going on under my eyes.

The structure is holding very well. The checks of the submerged part have not revealed any appreciable deterioration. A good construction and a careful maintenance have been the essential ingredients to a prolongued life. The projects are good and extend well into the future.

* * *

An efficient oceanographic tower can only be the product of a dedicated group of persons, too large to be singularly mentioned. However, a person deserves a special mention. Our first director, Dr. ROBERTO FRASSETTO, conceived the tower, had it realized, and guided a young group of scientists through the early phases of management and improvement. In more recent years, Dr. GIANFRANCO DALLAPORTA, director of ISDGM for more than ten years, has always been a valid support.

SILVESTRO CURIOTTO has been available since the start with his mechanical skill and technical capability.

Finally, ARMANDO PENZO and NARCISO ZENNARO, long-term members of the on board personnel, have been a key element in keeping the system going, made with their help many of the measurements possible, and helped in making the tower a lively and pleasant place to stay.

REFERENCES

Ablowitz M. J. and Segur H., *Solitons and the Inverse Scattering Transform*, *Series in Applied Mathematics* (Society for Industrial and Applied Mathematics, SIAM, Philadelphia) 1981, pp. 65.

Ansa Dossier, *Venice 1966-1996 - 30 years of protection as covered by the press*, year **52**, 1996, supplement to No. 292, pp. 160.

Battiston L. and Malanotte Rizzoli P., *The influence of refraction due to bottom topography on the distribution of wave energy along the coastline of the lagoon of Venice, Union des Oceanographes de France*, **3** (1972) 7-12.

Bergamasco A., Cavaleri L. and Sguazzero P., *Physical and mathematical analysis of a wind model, Nuovo Cimento C*, **9** (1986) 1-16.

Berkhoff J. C. W., *Computation of combined refraction-diffraction*, in *Proceedings of the XIII ICCE Conference, Vancouver*, Vol. **1** (ASCE, New York) 1972, pp. 471-490.

Bertotti L. and Cavaleri L., *Coastal set-up and wave breaking, Oceanologica Acta*, 8, No. 2 (1985) 237-242.

Bertotti L., Cavaleri L. and Tescaro N., *Long term wave hindcast in the Adriatic Sea, Nuovo Cimento C*, **19**, N. 1 (1996) 91-108.

Boldrin A., *Vertical flux of sedimentary particulate and associated C, N and P, in Prisma1 Project, task "Bio-geo-chemical cycles"*, Final report, edited by M. Giani and A. Puddu (1998) pp. 12.

Booij N., Holthuijsen L. H. and Ris R. C., *The "SWAN" wave model for shallow water, Proceedings of the 25th International Conference on Coastal Engineering* (ASCE, Orlando, Fla.) 1996, pp. 668-676.

Borgman L. E., *Feasibility for quantitative assessment of available margins inherent in flood protection of nuclear plants - final report.* A report to the Wave Dynamics Division, U.S. Army Waterways Experimental Station, Vicksburg, Mississipi, 1983.

Bouws E. and Komen G. J., *On the balance between growth and dissipation in an extreme depth-limited wind-sea in the southern North Sea*, *J. Phys. Oceanogr.*, **13** (1983) 1653-1658.

Box C.E.P. and Jenkins G. M., *Time Series Analysis, Forecasting and Control* (Holden Day, S. Francisco) 1970, pp. 368.

Brocchini M., Drago M. and Iovenitti L., *The modelling of short waves in shallow waters and in the surf zone*, *Nuovo Cimento C*, **17** (1994) 519.

Burns K. A., *Hydrocarbon metabolism in the intertidal fiddler crab Uca pugnax*, *Mar. Biol.*, **36** (1976) 5-11.

Buzzi A., Fantini M., Malguzzi P. and Nerozzi F., *Validation of a limited area model in cases of Mediterranean cyclogenesis: surface fields and precipitation scores, Meteorol. Atmos. Phys.*, **53** (1994) 53-67.

Camuffo D., *Fluctuations in wind direction at Venice, related to the origin of the air masses, Atmos. Environ.*, **15**, No. 9 (1981) 1543-1551.

Camuffo D., *Analysis of the series of precipation at Padova, Italy, Climate Change*, **6** (1984) 57-77.

Camuffo D., Tampieri F. and Zambon G., *Local mesoscale circulation over Venice as a result of the mountain-sea interaction, Boundary Layer Meteor.*, **16** (1979) 83-92.

Canestrelli P., Pastore F. and Tomasin A., *Development of an operational tide forecast model at Venice and revision of the relevant cases* (in Italian) (Venice Municipality, Section of Public Transport and Services) 1986, pp. 20.

Canestrelli P. and Pastore F., *Stocastic models for the forecast of the tidal level at Venice* (in Italian) (Istituto Veneto di Scienze, Lettere ed Arti, Venice, Italy) 1997, pp. 18.

Caporali A., Dallaporta G., Marzari F., Rusconi A., Curiotto S., Facchinelli F., Zambon G., Gatta A. and Tombolini L., *Localizzazione di precisione della piattaforma oceanografica del C.N.R. con i satelliti del GPS*, ISDGM, TR 146, 1988, pp. 21.

CAVALERI L., *Wave measurement using a pressure transducer, Oceanologica Acta*, **3**, No. 3 (1980) 339-346.

CAVALERI L. and CURIOTTO S., *A fast response shallow water tide gauge, Nuovo Cimento C*, **2** (1979) 273-287.

CAVALERI L. and STEFANON A., *Bottom features due to extreme meteorological events in the Northern Adriatic Sea, Marine Geology*, **36** (1980) 49-64.

CAVALERI L. and MALANOTTE RIZZOLI P., *Wind wave prediction in shallow water - theory and applications, J. Geophys. Res. C*, **86** (1981) 10961-10973.

CAVALERI L., PIANTÀ P. and IUSO G., *Influence of a sea structure on the surrounding wind field, Nuovo Cimento C*, **7**, No. 4 (1985) 440-446.

CAVALERI L. and ZECCHETTO S., *Reynolds stresses under wind waves, J. Geophys. Res. C*, **92**, No. 4 (1987) 3894-3904.

CAVALERI L., CURIOTTO S. and LIONELLO P., *Thermal expansion of a rig, Nuovo Cimento C*, **10**, No. 5 (1987) 573-576.

CAVALERI L., BERTOTTI L. and LIONELLO P., *Shallow water application of the third generation WAM wave model, J. Geophys. Res. C*, **94**, No. 6 (1989) 8111-8124.

CAVALERI L. and LIONELLO P., *Linear and nonlinear approaches to bottom friction in wave motion: a critical intercomparison, Estuarine, Coastal and Shelf Science*, **30** (1990) 355-367.

CAVALERI L. and LIONELLO P., *Possible mechanisms for wave breaking, IUTAM Symposium on Breaking Waves, Sydney, 15-19 July 1991*, edited by M. L. BANNER and R. H. J. GRIMSHAW (Springer-Verlag) 1991, pp. 175-179.

CAVALERI L., BERTOTTI L. and LIONELLO P., *Extreme storms in the Adriatic Sea, Proceedings of the 22nd International Conference on Coastal Engineering, Delft, The Netherlands, 2-6 July 1990*, edited by B. L. EDGE (Publ. ASCE) 1991, pp. 218-226.

CAVALERI L. and BURGERS G. J. H., *Wind gustiness and wave growth, KNMI Afdeling Oceanografisch Onderzoek memo*, 00-92-18 (De Bilt) 1992, pp. 38.

CAVALERI L., BERTOTTI L., PEDULLI L., TIBALDI S. and TOSI E., *Wind evaluation in the Adriatic Sea, Nuovo Cimento C*, **19**, No. 1 (1996a) 51-66.

CAVALERI L., BERTOTTI L. and TESCARO N., *Long term wind hindcast in the Adriatic Sea, Nuovo Cimento C*, **19**, No. 1 (1996b) 67-89.

CAVALERI L., CURIOTTO S., MAZZOLDI A. and PAVANATI M., *Long term directional wave recording in the Adriatic Sea, Nuovo Cimento C*, **20**, No. 1 (1996c) 103-110.

CAVALERI L. and BERTOTTI L., *In search of the correct wind and wave fields in a minor basin, Mon. Weather Rev.*, **125**, No. 8 (1997) 1964-1975.

CAVALERI L., BERTOTTI L., HORTAL K. and MILLER M., *Effects of reduced diffusion on surface wind fields, Mont. Weather Rev.*, **125** No. 11 (1997a) 3024-3029.

CAVALERI L., BERTOTTI L. and TESCARO N., *The modelled wind climatology of the Adriatic Sea, Theoretical and Applied Climatology*, **56**, No. 3-4 (1997b) 231-254.

CECCONI G., DI DONATO M. and CANESTRELLI P., *The forecast of the floods in the Venice lagoon* (in Italian), *XXV Convegno di Idraulica e Costruzioni Idrauliche, Turin, Italy, September 1996*, pp. 8-18.

CERADINI S. and MELONI L., *Evaluation of the flux of green house effect gases at the air-sea interface. Activity during 1994*, CISE, Report CISE-SAQ-94-54, 1994, pp. 35 (in Italian).

CERADINI S. and GAROFALO E., *Evaluation of the flux of green house effect gases at the air-sea interface. Activity during 1995*, CISE, Report CISE-SQS-95-29 (1995), pp. 39 (in Italian).

CEVEX GROUP, *Concertation on European Validation Experiments for coastal/shelf water remote sensing*, Work programme to Climate and Environment, DG XII, Brussel (1997), pp. 14.

COLLINS J. I., *Prediction of shallow water spectra, J. Geophys. Res.*, **77** (1972) 2693-2702.

DALLA VENEZIA L. *Size composition of a North-Adriatic mytilus population at different water depths, Archo Oceanogr. Limnol.*, **18**, Suppl. 3 (1976) 257-259.

DALLA VENEZIA L., *First observations on the settling of Mytilus sp. on the artificial barriers at Conero (Ancona), National Scientific Workshop on "Oceanografia e Fondi marini", Rome, 5-7 March 1979* (CNR) 1979, in Italian.

DALLA VENEZIA L., *Comparative study of populations of Mytilus galloprovincialis on artificial barriers, Quad. Lab. Tecnol. Pesca*, **3** (Suppl. 1) (1981) 631-633.

DALLA VENEZIA L., FOSSATO V. U. and SCARPI S., *First observations and behavioural response of Mytilus Galloprovincialis tp PCB Aroclor 1254 pollution, VI Journées Étud. Pollutions, Cannes* (C.I.E.S.M.) 1982, 669-675.

DALLA VENEZIA L., STRADELLA S., MENETTO A. and CAMPESAN G., *Fine structure of the gills of Mytilus sp. and damage due to LAS and cadmium pollution* (in Italian), *Biol. Mar. Mediterranea*, **1** (1994) 387-388.

DAUBECHIES I., *10 lectures on wavelets, Series in Applied Mathematics*, No. 61 (Society for Industrial and Applied Mathematics, SIAM, Philadelphia) 1992, pp. 357.

DE GIROLAMO P., PASSACANTANDO G., HURDLE D. and NOLI A., *Evaluation of design waves along the coast and at the inlets of the Venice lagoon, Proceedings of the 23rd International Conference on Coastal Engineering, 4-9 October 1992, Venice, Italy*, edited by B. L. EDGE (Pubbl. ASCE) 1993, pp. 1851-1864.

DE GIROLAMO P., CECCONI G., MARETTO G. P. and CONTINI P., *Monitoring of the Cavallino beach (Venice - Italy), Proceedings of International Conference on Coastlines, Structures and Breakwaters '98, Maritime Board and Institution of Civil Engineers, London, U.K.*, 1998.

DORRESTEIN R., *Simplified method of determining refraction coefficients for sea waves, J. Geophys. Res.*, No. 2, **65** (1960) 637-642.

DUNN B. P. and STICH H. F., *Release of the carcinogen benzo(a)pyrene from environmentally contaminated mussels, Bull. Environ. Contam. Toxicol.*, **15** (1976) 308-401.

EFRON B., *The jackknife, the bootstrap and other resampling plans, Reg. Conf. Ser. in Applied Math.* (Philadelphia, Penn.) 1982, pp. 93.

ESA - FRANCIS R., CAPORALI A., CAVALERI L., CENCI A., CIOTTI P., CIRAOLO L., GUNTHER W., MASSMAN F. H., DEL ROSSO D., SHARROO R., SPALLA P. and VERMAAT E., *The calibration of the ERS-1 radar altimeter*, ESA Report ER-RP-ESA-RA-0257, ESA/ESTEC (Noordwijk, The Netherlands) 1993, pp. 272.

FISCELLA B., LOMBARDINI P. P. and PAVESE P., *Interferential microwave probe for measuring sea ripples, Nuovo Cimento C*, **5** (1982) 247-262.

FOSSATO V. U. and SIVIERO E., *Oil pollution monitoring in the lagoon of Venice using the mussel Mytilus galloprovincialis, Mar. Biol.*, **25** (1974) 1-6.

FOSSATO V. U. and DOLCI F., *Hydrocarbon pollution in the northern part of the Venice lagoon* (in Italian), *Archo Oceanogr. Limnol.*, **18** (Suppl.) (1976) 73-82.

FOSSATO V. U. and DOLCI F., *Hydrocarbon pollution in the central and southern part of the Venice lagoon* (in Italian), *Archo Oceanogr. Limnol.*, **19** (1977) 47-54.

FOSSATO V. U., NASCI C. and DOLCI F., 3,4-*benzopyrene and perylene in mussels, Mytilus sp., from the Venice lagoon, Northern Italy, Mar. Environ. Res.*, **2** (1979) 47-53.

GATTO P. and CARBOGNIN L., *The lagoon of Venice, natural environmental trend and man-induced modification, Hydr. Sci. Bull.*, **26**, No. 4 (1981) 379-391.

GIANI M., ALBERIGHI L., BACCI C., BOLDRIN A., PUDDU A. and RABITTI S., *A preliminary approach to carbon cycling in the Northern Adriatic*, submitted to *J. Mar. Systems*, 1998.

HASSELMANN K., *On the non-linear energy transfer in a gravity-wave spectrum, part 1: general theory, J. Fluid Mech.*, **12** (1962) 481.

HASSELMANN K., *On the spectral dissipation of ocean waves due to whitecapping, Boundary Layer Meteorol.*, **6** (1974) 107-127.

HASSELMANN K. and COLLINS J. I., *Spectral dissipation of finite-depth gravity waves due to turbulent bottom friction, J. Mar. Res.*, **26** (1968) 1-12.

HASSELMANN K., BARNETT T. P., BOUWS E., CARLSON H., CARTWRIGHT D. E., ENKE K., EWING J. A., GIENAPP H., HASSELMANN D. E., KRUSEMAN P., MEERBURG A., MÜLLER P., OLBERS D. J., RICHTER K., SELL W. and WALDEN H., *Measurements of wind-wave growth and swell decay during the Joint North Sea Wave Project (JONSWAP), Dtsch. Hydrogr. Z. Suppl. A*, 8 (1973) 95.

HOLTHUIJSEN L. H., BOOIJ N. and HERBERS T. H. C., *A prediction model for stationary short-crested waves in shallow water in ambient currents, Coastal Engin.*, **13** (1989) 23-54.

HR WALLINGFORD, *Venice lagoon study B7.2/3rd phase: model tests for the Pellestrina littoral*, HR Wallingford, Report EX 2524, UK, 1992a.

HR WALLINGFORD, *Venice lagoon study B7.2/4th phase: model tests for the Cavallino littoral*, HR Wallingford, Report EX 2661, U.K., 1992b.

HURDLE D., DE GIROLAMO P. and PELLEGRINI G., *Evaluation of design waves along the Adriatic coast of the Venice lagoon, Coastal Engin.*, **25** (1995) 109-133.

JANSSEN P. A. E. M., *Wave-induced stress and the drag of air flow over sea waves, J. Phys. Oceanogr.*, **21** (1989) 745-754.

JANSSEN P. A. E. M., *Operational implementation of the high resolution Ocean Wave model, ECMWF Newsletter*, No. 74 (1997) 9-12.

KOMEN G. J., CAVALERI L., DONELAN M., HASSELMANN K., HASSELMANN S. and JANSSEN P. A. E. M., *Dynamics and Modelling of Ocean Waves* (Cambridge University Press) 1994, pp. 532.

KONDO J., *Air-sea bulk transfer coefficients in diabatic conditions, Boundary Layer Meteorol.*, **9** (1975) 91-112.

KOORNWINDER T. H., *Wavelets: an elementary treatment of theory and applications* (World Scientific) 1993, pp. 225.

KUIK A. J., VAN VLEDDER G. PH. and HOLTHUIJSEN L., *A method for the routine analysis of pitch-and-roll buoy wave data, J. Phys. Oceanogr.*, **18** (1988) 1020-1034.

LAVAGNINI A., MARTORELLI S. and CAVALERI L., *The wind climatology of the Adriatic Sea deduced from coastal stations*, *Nuovo Cimento C*, **19**, No. 1 (1996) 37-50.

LAZIC I. and TELENTA B., *Documentation of the UM/NMC eta model*, WMO/TMRP Technical Report 40, 1990.

LEE R. F., SAUERHEBER R. and BENSON A. A., *Petroleum hydrocarbons: uptake and discharge by the marine mussel Mytilus edulis*, *Science*, **177** (1972a) 344-346.

LEE R. F., SAUERHEBER R. and BENSON A. A., *Uptake, metabolism and discharge of polycyclic aromatic hydrocarbons by marine fish, Mar. Biol.*, **17** (1972b) 201-208.

LIONELLO P., *Oceanographic prediction for the Venetian littoral, Nuovo Cimento C*, **18**, No. 3 (1995) 245-268.

LIVINGSTONE D. R., LEMAIRE P., MATTHEWS A., PETERS L. D., PORTE C., FITZPATRICK P. J., FÖRLIN L., NASCI C., FOSSATO V., WOOTTON N. and GOLDFARB P., *Assessment of the impact of organic pollutants on Goby (Zosterisessor ophiocephalus) and mussel (Mytilus Gallo-provincialis) from the Venice lagoon, Italy: biochemical studies, Mar. Environ. Res.*, **39** (1995) 235-240.

LONG R. B. and HASSELMANN K., *A variational tecnique for extracting directional spectra from multi-component wave data, J. Phys. Oceanogr.*, **9** (1979) 373-381.

LONGUET-HIGGINS M. S., CARTWRIGHT D. E. and SMITH N. H., *Observations of the directional spectrum of sea waves using the motions of a floating buoy, Proceedings of Ocean Wave Spectra* (Englewood Cliffs, New York), 1963, pp. 11-136.

MALANOTTE RIZZOLI P. and BERGAMASCO A., *The dynamics of coastal regions in the Northern Adriatic Sea, J. Phys. Oceanogr.*, **13**, No. 7 (1983) 1105-1130.

MARACCI G., HOSGOOD B. and GRASSI P., *Underwater irradiance measurements from the Oceanographic platform "Acqua Alta" , ADRIA 84, Data Catalogue*, edited by P. M. SCHLITTENHARDT (EC Ispra, Italy), pp. 3.4.3-3.4.12.

MATTIOLI F., *Dynamic response of the Lido channel to wave motion in the presence of movable barriers, Nuovo Cimento C*, **19**, No. 1 (1996) 177-194.

MAV, MAGISTRATO ALLE ACQUE DI VENEZIA, *Actions at the inlets of the lagoon for the control of tidal flux - General Project*, Consorzio Venezia Nuova, 1992, Venice, Italy (in Italian).

MAV, MAGISTRATO ALLE ACQUE DI VENEZIA *Actions at the inlets of the lagoon for the control of tidal flux - Study on the environmental impact (SIA) of the General Project*, Consorzio Venezia Nuova, 1997, Venice, Italy (in Italian).

MIOZZI E., *Venezia nei secoli*, Vol.I-IV (Ed. Libeccio, Venezia) 1957, in Italian.

MONTANARI M., BARGIACCHI S., RISMONDI A. and RELINI G., *Fouling off the coast of Venice, 22nd Workshop of Società Italiana di Biologia Marina, Cagliari, Italy, 20-24 May 1991*, 1991, pp. 373-374 (in Italian).

MORISIERI M., *Variazioni della fauna a foraminiferi bentonici in una stazione dell'Adriatico Settentrionale e correlazioni con i parametri ambientali*, Tesi di Laurea, Facoltà di Scienze MM.FF.NN., Università di Padova, 1997, pp. 135 (in Italian).

NASCI C., CAMPESAN G., FOSSATO V. U., DOLCI F. and MENETTO A., *Hydrocarbon content and microsomal BPH and reductase activity in mussel, Mytilus sp., from the Venice area, North-East Italy, Mar. Environ. Res.*, **28** (1989) 109-112.

NOLI A., GALANTE F. and SILVA P., *Il progetto di ripascimento dei litorali veneziani eseguito dal Concessionario dello Stato sotto il controllo dell'ufficio G.C.OO.MM. di Venezia, Giornate Italiane di Ingegneria Costiera, Genova, Italy, 1993* (in Italian).

NOVO A. and BELGIOVINE N., *Trend analysis of wet deposition samples from the ENEL network, DSR/CRAM and DCO/LP stations*, ENEL/CRAM, Report 19660058, 1996, pp. 110.

OSBORNE A. R., *Nonlinear Fourier analysis*, in *Nonlinear Topics in Ocean Physics*, edited by A. R. OSBORNE (North-Holland, Amsterdam) 1991a, pp. 669-700.

OSBORNE A. R., *Nonlinear Fourier analysis for the infinite-interval Korteweg-de Vries equation I: An algorithm for the direct scattering transform, J. Comput. Phys.*, **94** (1991b) 284.

OSBORNE A. R., BERGAMASCO L., SERIO M., BIANCO L., CAVALERI L., DRAGO M., IOVENITTI L. and VIEZZOLI D., *Nonlinear shoaling of shallow water waves: perspective in terms of the inverse scattering transform, Nuovo Cimento C*, **19**, No. 1 (1976) 151-176.

PACCAGNELLA T., TIBALDI S., BUIZZA R. and SCOCCIANTI S., *High resolution numerical modelling of convective precipitation over Northern Italy, Meteor. Atmos. Phys.*, **50** (1992) 143.

PIPE R. K., COLES J. A., THOMAS M. E., FOSSATO V. U. and PULSFORD A. L., *Evidence for environmentally derived immunomodulation in mussels from the Venice lagoon, Aquatic Toxicol.*, **32** (1995) 59-73.

PONTES T., AGUIAR R., DEBETTENCOURT J., ATHANASSOULIS G. A., TSOULOS L., NAKOS B., SKARSOULIS E., STEFANAKOS C. N., SKOPELITI A., CAVALERI L., BERTOTTI L., MOLLISON D., LEWIS T., HOLMES B., OLIVEIRA-PIRES H., BARSTOW S. and CHRISTOPOULOS S., *WERATLAS - Atlas of Wave Energy Resource in Europe*, EU Contract N. JOU2-CT93-0390, Final Technical Report, 1996, pp. 136.

REITER E., *Digest of selected weather problems of the Mediterranean, Navy Research Facility*, Technical Paper no. 9-71, 1971, pp. 2199.

RIGET F., JOHANSEN P. and ASMUNT G., *Uptake and release of lead and zinc by Blue Mussels - Experience from transplantation experiments in Greenland, Mar. Poll. Bull.*, **34** (1997) 805-815.

SCLAVO M., LIBERATORE G. and RIDOLFO R., *Waves in front of the Venetian littoral, Nuovo Cimento C*, **19**, No. 1 (1996) 125-150.

SILVESTER R. and HSU J. R. C., *Coastal stabilization* (Prentice-Hall, Inc.) 1993.

SIMMONS A., *Development of the operational 31-level T213 version of the ECMWF forecast model, ECMWF Newslett.*, **56** (1991) 3-13.

SIMONS T. J., *Development of a numerical model for lake Ontario, Proceedings of the XIV Conference on Great Lakes*, 1972, pp. 654.

SMITH S., *Coefficients for surface stress, heat flux and wind profiles as a function of wind speed and temperature, J. Geophys. Res. C*, **93**, No. 12 (1988) 15467-15472.

STEFANON A., *Sedimentologia del Mare Adriatico: rapporti tra erosione e sedimentazione olocenica, Boll. Oceanolog. Teor. Applic.*, **2** (1984) 281-312 (in Italian).

STURARO G., *Dynamics of air-sea interface - interactions between long and short gravity waves*, Tesi di Dottorato, Università di Padova, 1994, pp. 219 (in Italian).

TIOZZO A., *Mytilus galloprovincialis come tester della disponibilità di metallo nelle acque della Laguna di Venezia*, Tesi di Laurea, Università di Modena, Dipartimento di Biologia Animale, 1998, pp. 77.

TOLMAN H. L., *A third-generation model for wind waves on slowly varying, unsteady and inhomogeneous depths and currents, J. Phys. Oceanogr.*, **21**, 6 (1991) 782-797.

TROEN I. and PETERSEN E. L., *Wind atlas for Europe*, Commission of European Communities DSG XII, ISBN 87-550-1639-1, 1988.

VIEZZOLI D. and CAVALERI L., *Wave observations and refraction modelling in intermediate water depths off the lagoon of Venice, Nuovo Cimento C*, **19**, No. 1 (1996) 109-123.

WAMDI GROUP: HASSELMANN S., HASSELMANN K., BAUER E., JANSSEN P. A. E. M., KOMEN G. J., BERTOTTI L., LIONELLO P., GUILLAUME A., CARDONE V. C., GREENWOOD J. A., REISTAD M., ZAMBRESKY L. and EWING J. A., *The WAM model - a third generation ocean wave prediction model, J. Phys. Oceanogr.*, **18** (1988) 1775-1810.

WEBER S. L., *Eddy-viscosity and drag-law models for random ocean wave dissipation, J. Fluid Mech.*, **232** (1991) 73-98.

WEIBULL W., *A statistical distribution function of wide applicability, J. Appl. Mech.*, **18** (1961) 293.

WEISSMAN M. A., ATAKTURK S. S. and KATSAROS K. B., *Detection of breaking events in a wind-generated wave field, J. Phys. Oceanogr.*, **14** (1984) 1608-1619.

WIDDOWS J. and NASCI C., *Venice Lagoon Ecosystem Project*, edited by P. LASSERRE and A. MARZOLLO (Unesco-Murst) 1998.

ZACHAROV V., MANAKOV S. V., NOVIKOV S. P. and PITAYEVSKY M. P., *The Method of the Inverse Scattering Transform* (Nauka, Moscow), 1980, pp. 224 (in Russian).

ZECCHETTO S., *Effects of modulation of σ_0 with implications for physical scatterometer modelling, Proceedings of the Air-Sea Interface - Radio and Acoustic Sensing, Turbulence and Wave Dynamics*, edited by M. A. DONELAN, W. H. HUI and W. J. PLANT (University of Miami, Miami) 1993, pp. 785.

ZECCHETTO S. and TRIVERO P., *Experimental ocean active microwave remote sensing, Proceedings of Satellite Remote Sensing of the Oceanic Environment*, edited by I. S. F. JONES, Y. SUGIMORI and R. W. STEWART (Seibutsu Kenkyusha) 1993, pp. 528.

ZECCHETTO S., TRIVERO P., FISCELLA B. and PAVESE P., *The spatial structure of the downward momentum flux on sea derived from a SAR image, Phys. Chem. Earth*, **21**, No. 5-6 (1996) 389-392.

ZECCHETTO S., TRIVERO P., FISCELLA B. and PAVESE P., *Wind stress structure in the unstable marine surface layer detected by SAR, Boundary Layer Meteor.*, **86** (1998) 1-28.